Scuola di Dottorato di Ricerca in Scienze Biochimiche

Dottorato di Ricerca in Scienze Biochimiche - XXXI Ciclo

UNIVERSITÀ DEGLI STUDI DI MILANO

DIPARTIMENTO DI SCIENZE BIOMEDICHE
E CLINICHE "LUIGI SACCO"

REGULATING HYDROLASES OF THE ENDOCANNABINOID SYSTEM: NOVEL PHOTOMETRIC ASSAYS FOR DRUG DISCOVERY

Candidato: Matteo MICELI

Matricola: R11417

Tutor: Prof.ssa Pierangela CIUFFREDA

Direttore: Prof. Sandro SONNINO

Anno Accademico 2017/2018

Abbreviations used

2-AG – 2- Arachidonoylglycerol
ABHD6 – α/β-Hydrolase domain containing 6
ABHD12 – α/β-Hydrolase domain containing 12
APS – Ammonium persulfate
BIS - N,N'-methylen-bis-acrilamide
BL - Bioluminescence
BSA – Bovine serum albumine
cAMP – cyclic adenosine monophospate
CB – Cannabinoid receptor
CL - Chemiluminescence
CHRM4 - Muscarinic acetylcholine receptor M4
CNS – Central nervous system
DCC – *N,N′*-Dicyclohexylcarbodiimide
DEA - Docosatetraenylethanol amide
DMAP - 4-Dimethylaminopyridine
DTT – Dithiothreithol ((2*S*,3*S*)-1,4-Bis(sulfanyl)butane-2,3-diol)
ERK – Extracellular signal-regulated kinase
EC – Endocannabinoid
ES – Endocannabinoid system
FAAH – Fatty acid amide hydrolase
FABP – Fatty acid binding protein
GPCR – G-protein coupled receptor
GPR119 - G-protein coupled receptor 119
IPTG - Isopropyl β-D-1-thiogalactopyranoside
IMAC – Immobilized metal affinity chromatography
LB – Lysogeny broth (Bertani, 2004)
LH_2 – D-luciferin
MAD – Multiple ascending dose
MAGL – Monoacylglycerol lipase
MAPK – Mitogen-activated protein kinase
NADA - N-arachidonoyl dopamine
NAPE - N-arachidonoylphosphatidylethanolamine
NAPE-PLD - N-acylphosphatidylethanolamine-hydrolyzing phospholipase D
NAT – N-acyltransferase
OD – Optical density
OEA - Oleoylethanolamide
o/n – overnight (a time period of about 14 hours)
PBS – Phosphate buffer saline
PCB – Protease cleavage buffer
PE- Phosphatidilethanolamine
PEA - Palmitoylethanolamide
PHARC - polyneuropathy, hearing loss, ataxia, retinitis pigmentosa, and cataract
PKA – cAMP-dependent protein kinase
PMSF - phenylmethylsulfonyl fluoride
PPAR-α – Peroxisome proliferator-activated receptor
PTX – Pertussis toxin

RFU – Relative fluorescence units
RLU - Relative luminescence units
RT – Room temperature
SD – Standard deviation
SDS - Sodium dodecyl sulfate
SDS-PAGE – Sodium dodecyl sulfate–polyacrylamide gel electrophoresis
TBS – Tris-buffered saline
TGS – Tris, glycine, SDS
TE – Tris and EDTA
TEMED – Tetramethylenediamine
THC - (−)-*trans*-Δ^9-tetrahydrocannabinol
TLC – Thin layer chromatography
TRPV1 - transient receptor potential cation channel subfamily V member 1

1. INTRODUCTION

1.1 The hidden system

"System" is a word that evokes unmistakable concepts: didactic schemes of the respiratory, circulatory and nervous systems, all come to the mind when a non-specialist (and possibly even a specialist) thinks about a "system" of the human body.

The endocannabinoid system (ES), however, is not so easy to describe: it actually has no organs, tissues, nor even cells of its own: its only constituents are molecules. The whole system is "embedded" into other, "proper" systems: its components can be found at the surface of immune cells, as well as at the neuronal synapses, and across a lot of other different systems, throughout the whole body. On top of this, *it does not even have a function of its own*: it just modulates the activities of other, "truer" systems. The picture, then, may look quite discomforting: the system we're considering has no organs, no specific anatomical location, nor function, of its own. Actually, the very definition of "system" is debatable, when referring to the ES. All it does is *to enhance or reduce the effects of other*, "truer" *systems*, from imprecise localizations in the body.

And yet, after a deeper insight into it, it immediately becomes evident that its peculiarities, which at first make it look obscure at best, are also what makes the ES so special and interesting. The lack of a precise anatomical district of its own, so that it can be brilliantly described as being "here, there, and everywhere" (Vettor, Pagotto, Pagano, & Pasquali, 2008), allows the ES to exert its functions on a huge variety of tissues and body districts, which greatly differ from one another. The other peculiarity of the ES, that of not having a specific function of its own, further enhances this versatility: since it does nothing but modulate an array of activities coming from other, specialised systems, its activity is exerted on *a lot* of different functions. These can be briefly, and incompletely, summed up as:

Target organ or system	ES localisation and function
Nervous system	Synapses and glial cells; pain control (Woodhams, Chapman, Finn, Hohmann, & Neugebauer, 2017), feeding behavior (Shrestha et al., 2018), regulation of stress and reward mechanism, sense of general well-being (Volkow, Hampson, & Baler, 2017), thermal homeostatis (Nass et al., 2015).
Immune system	Surface of lymphocytes; immunomodulatory activity, inhibition of inflammatory reaction (Cabral, Rogers, & Lichtman, 2015).

Bone system	Osteoblasts, chondrocytes, nerve terminals; promotion of bone formation and repression of bone resorption, regulation of bone growth during development (Zimmer, 2016).
White fat	Adipocytes; modulation of energy expenditure (Shrestha et al., 2018)

An insight on the structure of the ES will help understand how the ES can perform such diverse functions.

1.1.1 Endocannabinoid receptors

The molecular components of the ES can be broadly sub-classified into three classes of molecules: receptors (CBs), endocannabinoids (ECs) and regulating enzymes.

To date, we know two kinds of endocannabinoid receptors, namely cannabinoid receptor 1 (CB_1), and cannabinoid receptor 2 (CB_2). The identity number of these receptors refers to the timing of their discovery: CB_1 was the first CB to be discovered and characterized from rat brain (W. A. Devane, Dysarz, Johnson, Melvin, & Howlett, 1988; Matsuda, Lolait, Brownstein, Young, & Bonner, 1990), while CB_2 was identified three years later in rat spleen and in a variety of other tissues, but not in the brain (Munro, Thomas, & Abu-Shaar, 1993). Both CB_1 and CB_2 are heteroreceptors which share the typical structure of GPCRs: they both are made up of seven transmembrane domains, connected by three extracellular and three intracellular loops, with a glycosylated N-terminus and an intracellular C-terminus (Hua et al., 2016; Shao et al., 2016). The specific mechanism of action varies among cell types; in most cases, though, once the CBs are activated by interaction with their ligands (Table 1), the $G_{\alpha i}$ subunit coupled to them inhibits adenylyl cyclase, thus lowering the intracellular concentration of adenosine monophosphate (cAMP). cAMP activates cAMP-dependent protein kinases (PKAs), which have many different roles in the cell through many different mechanisms – these vary greatly depending on the cell type (R. G. Pertwee, 2006; R G Pertwee et al., 2010). A review of these mechanisms lies far beyond the aims of this dissertation, but we can (very briefly) summarize the roles of PKAs as having an "activating" role in the cell; the CBs, being indirect inhibitors of their activity, can be therefore roughly considered "dampeners" of the activity of the cell. CBs also raise the cellular levels of mitogen-activated protein kinases (MAPKs), also known as "Extracellular signal-regulated kinases" (ERKs). These kinases, in turn, continue the cascade response, activating an extremely different varied array of responses, including expression of genes and cell differentiation, proliferation and death. Again, a complete review of different MAPK

activation and response should be the subject of a dissertation of its own, but in the context of the ES these processes can be roughly summarized as "stress responses", both at cellular and physiological level (Morena, Patel, Bains, & Hill, 2016; Volkow et al., 2017).

CB_1 can be found mainly across the central nervous system (CNS), where the ES acts as a neuromodulator. Here, the ES activity can have a twofold output in terms of physiological response: in the case of excitatory (e.g. glutamatergic) neurons, its activity results in a decreased rate of neural activity; but should the ES activate at the synapse between two GABAergic (inhibitory) neurons, the result would be an increase in physiological neural transmission. CB1-mediated response may act as an endogenous mechanism of pain control through the elevation of ECs levels in the regions of acute and chronic pain, acting as "endogenous analgesics" (Woodhams et al., 2017). CB_1s can also have an important role in human metabolism and feeding behavior (Shrestha et al., 2018): they are expressed in various tissues including fat, muscle and liver cells, as well as throughout the digestive tract. These receptors can also be found across a variety of glands within the endocrine system, including the pituitary, thyroid and adrenal gland, and within the reproductive system in both sexes (Pagotto, Marsicano, Cota, Lutz, & Pasquali, 2006). The most recent breakthrough in the study of CB_1, though, has been the resolution of its crystal structure (fig.1) (Hua et al., 2016; Shao et al., 2016), opening the perspective of structure-based drug design for this receptor.

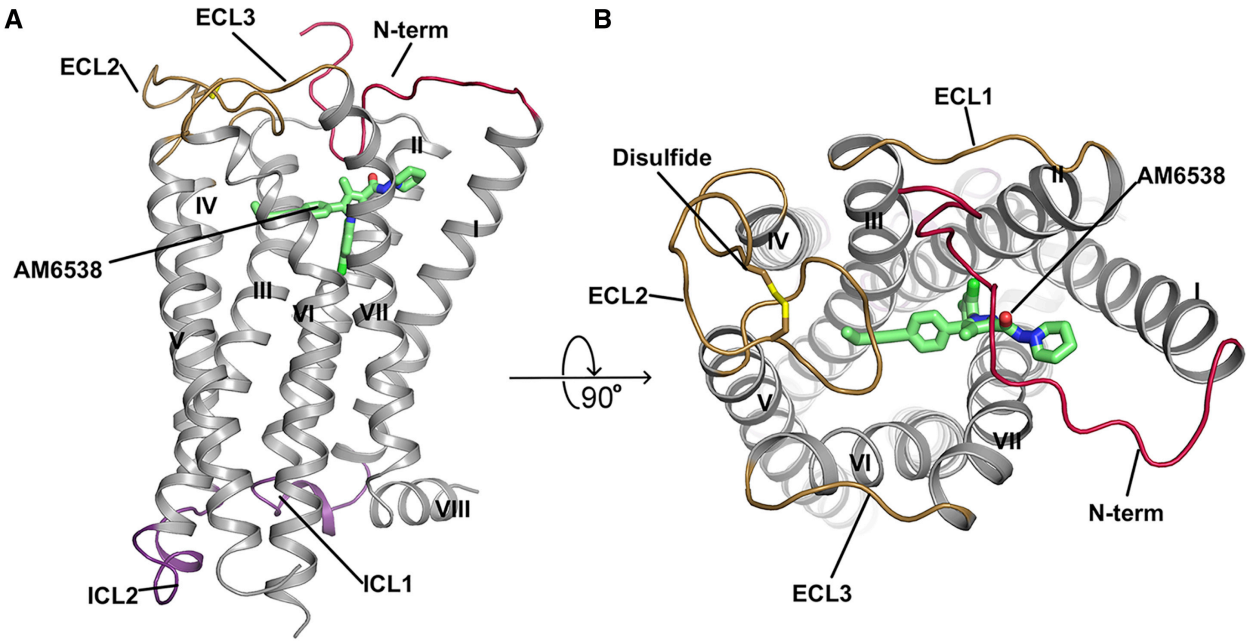

Figure 1. Crystal structure of CB1 receptor in complex with the inhibitor AM6538, transmembrane (A) and top (B) view. The position of AM6538 marks the location of the binding pocket, partially blocked by the N-ter loop (right, in red). Also marked are the extracellular and intracellular loops (ECL and ICL, respectively) and ECL2 disulfide bond. The Roman numerals label the various helix numbers. Image taken from Hua et al., 2016.

The main endogenous agonist for CB_1 is 2-arachidonoylglycerol (2-AG), with a K_i of 58.3

nM (R G Pertwee et al., 2010); the famous phytocannabinoid (−)-*trans*-Δ^9-tetrahydrocannabinol (THC), the main psychoactive constituent of *Cannabis sativa*[1], is a partial agonist of both CB_1 and CB_2 receptors, though its affinity for the receptor is about ten times that of 2-AG. It is activated also by noladin ether, with a K_i of 21.2 ± 0.5 nM (L. Hanuš et al., 2001) – for a complete perspective on CB ligands, refer to Table 1.

A complete crystal structure for CB_2 is not available yet, but various *in-silico* surrogates have been published (Cichero, Menozzi, Guariento, & Fossa, 2015; Tuccinardi et al., 2006). The precise distribution of CB_2 across the human body is still uncertain: earlier studies described CB_2 as a "peripheral" endocannabinoid receptor and excluded its presence in the brain (Munro et al., 1993), but later immunohistochemical studies found it was localised in the mice brain as well (Onaivi et al., 2006). Problem was, the same antibodies shown analogous results when used on CB_2-knockdown mice (Baek, Darlington, Smith, & Ashton, 2013), and it was later demonstrated that these antibodies were sensitive but not specific (Cecyre, Thomas, Ptito, Casanova, & Bouchard, 2014). To add further uncertainty, some studies connect the effect of dopamine on CB_2 receptors to drug addiction behaviour in mice and rats (Xi et al., 2011; Zhang et al., 2014, 2017) which seems to indicate their presence in the brain. CB_2 even mediate antipsychotic effects of drugs acting on muscarinic receptor CHRM4 in mice models (Foster et al., 2016). Today we still don't know with certainty if CB_2 is a purely peripheral receptor, but recently developed tools for its investigation, including antagonists for CB_2 which are extremely specific, and mice which express GFP if CB_2 is expressed as well (Rogers, 2015), will maybe allow us to finally understand its true tissue distribution. What we know for sure, though, is that CB_2s are present within cells of the immune system, where they play an important role in modulating the immune response (Cabral & Griffin-Thomas, 2009). The general view on what the CBs exactly are is not so defined, however. Different receptors are, or have been in time, indicated as a "CB_3" receptor.

The transient receptor potential cation channel subfamily V member 1 (vanilloid receptor 1, capsaicin receptor, TRPV1), strongly implied in nociception and, potentially, pain therapy (Knotkova, Pappagallo, & Szallasi, 2008) is activated by monoacylglycerols including 2-AG and anandamide, to the point that anandamide is suggested to be an endovanilloid as well (Zygmunt et al., 2013) and, paradoxycally, may enhance the pain sensation. On the other side,

[1] It is actually debated if *Cannabis indica* and *C. ruderalis*, all of which biosynthesize THC, are species of their own or instead subspecies of the *C. sativa* species; we will embrace this last view and leave the debate to specialists in plant taxonomy.

N-arachidonoyl dopamine (NADA), the endogenous ligand for TRPV1 (Bisogno et al., 2000), is an agonist of CB1 and CB2 as well, even if with limited potency (Huang et al., 2002). TRPV1 is not considered a constituent of the ES, but all these findings indicate that the ES and the pain mechanism mediated by TRPV1 share more than one mechanism of action.

The Peroxisome-proliferator activated receptor α (PPAR-α), a transcription factor and regulator of lipid metabolism found in the liver, can be activated by anandamide, virodhamine and noladin ether, showing that the importance of ECs in lipid metabolism is multi-faceted, and the levels of these molecules can have an impact in unforeseen ways. AEA can also activate PPAR-γ, another member of the family (O'Sullivan, 2007).

A few G-protein coupled receptors (GPRs) have been in time identified as novel CB receptors: GPR18 has a role in immune regulation, is activated by the AEA metabolyte N-arachidonoylglycine (Kohno et al., 2006), even if not in a canonical way (Lu, Puhl, & Ikeda, 2013). GPR55 is activated by 2-AG, anandamide, and noladin ether as well as THC, so was classified as a novel cannabinoid receptor (Ryberg et al., 2007). However, later studies found that the activity mediated by endogenous N- ethanolamides was moderate at best (Godlewski, Offertáler, Wagner, & Kunos, 2009). GPR55 also binds Lysophospatidylinositol (LPI) (Oka, Nakajima, Yamashita, Kishimoto, & Sugiura, 2007), definitely seems to be its main endogenous ligand (Piñeiro & Falasca, 2012). GPR55 has various analogies with "proper" CBs, since its action is mediated by lipid signaling and has an important role in metabolic disease (Arifin & Falasca, 2016) as well as pain perception (Godlewski et al., 2009). The final candidate, GPR119, acts following oleoylethanolamide binding (Overton et al., 2006) and seems to have a role in the regulation of food intake behaviour (Godlewski et al., 2009).

To date, no "true" CB_3 has yet been definitely identified. There are some clear interactions beetween the ES and other lipid signaling pathways, to the point that it is entirely possible that in the future no "endocannabinoid system" will be considered, but it will rather be included in "a wider lipid-based signaling system" (Di Marzo & De Petrocellis, 2012).

The puzzle has yet to be solved.

1.1.2 Endocannabinoids

The discovery of cannabinoid receptors subsequently led to the research of endogenous ligands: in 1992, a group led by professor Raphael Mechoulam, the same researcher who in 1964 discovered THC (Gaoni & Mechoulam, 1964), isolated and then synthesized an endogenous arachidonic acid derivative from porcine brain, which demonstrated to be able to

bind CB_1: this compound was named Anandamide (Arachidonoyl ethanolamide, AEA), "from the sanskrit word "Ananda" meaning bliss, and from the chemical nature of the compound" (W. Devane et al., 1992). It was later retrieved in human brain, thus confirming its role as an endocannabinoid (Felder et al., 1996).

However, anandamide was present in very low levels among brain tissues (Felder et al., 1996), and it acted only as a partial agonist for both CB_1 and CB_2 (Mackie, Devane, & Hille, 1993). A few years later, another compound binding the cannabinoid receptors originally discovered in canine intestines (Mechoulam et al., 1995) was found in human brain: this compound was 2-arachidonoylglycerol (2-AG), which is present in the human brain in about 170 times the concentration of anandamide (Stella, Schweitzer, & Piomelli, 1997).

The generally accepted mechanism fo AEA biosynthesis starts from membrane phospholipids, to have them into converted AEA through a 2-steps n-acylation of phosphatidilethanolamine (PE). Ca^{2+}-dependent N-acyltransferase (NAT) catalyzes the first step, the acylation of the amino group of PE with an arachidonoyl coming from a glycerophospholipid, leading to the formation of N-arachidonoylphosphatidylethanolamine (NAPE). NAPE is then hydrolized to a phosphatidic acid and AEA by the enzyme N-acylphosphatidylethanolamine-hydrolyzing phospholipase D (NAPE-PLD) (J. Wang & Ueda, 2009). It is interesting to note that the activity of NAPE-PLD is regulated by bile acids, suggesting that this enzyme could play a central role in the orchestration between ES signaling regulation and food intake (Magotti et al., 2015).

2-AG binds CB_1 receptors with more or less the same affinity of AEA, and CB_2 with about twice the affinity (Table 1); more important, 2-AG is a full agonist of both receptors, unlike anandamide, which even attenuates 2-AG activity (Gonsiorek et al., 2000). It is considered the main signaling lipid in the ES.

Table 1. Agonists of the cannabinoid receptors. FA= full agonist; PA=partial agonist

Endogenous ligands					
Compound	**Structure**	**K_i for CB1**	**K_i for CB2**	**Reference**	**Notes**
2-Arachidonoyl glycerol (2-AG)	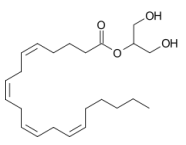	58.3 nM	145 nM	(R G Pertwee et al., 2010)	FA

Anandamide (AEA)	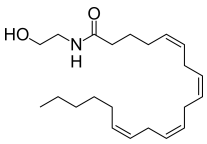	61 nM	279 nM	(R G Pertwee et al., 2010)	PA
N-arachidonoyl dopamine (NADA)	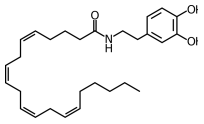	250 nM	12 μM	(Bisogno et al., 2000)	EC_{50} for TRPV1: 40 ± 6 nM (Huang et al., 2002)
2-Arachidonyl glyceryl ether (2-AGE, Noladin ether)	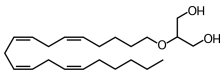	21.2 ± 0.5 nM	480 nM	(Shoemaker, 2005)	FA
Docosatetraenylethanolamide (DEA)	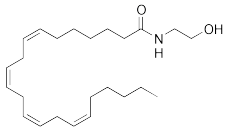	34.4 ± 3.2 nM (on synaptosomal rat membrane)		(Lumir Hanuš, Gopher, Almog, & Mechoulam, 1993)	
Homo-γ-linolenylethanolamide	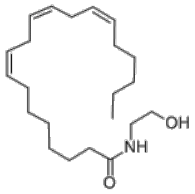	53.4 ± 5.5 nM (on synaptosomal rat membrane)			
Virodhamine	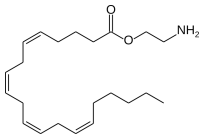	912 ± 99 nM	No available data	(Steffens, Zentner, Honegger, & Feuerstein, 2005)	

Exogenous ligand (phytocannabinoid)

Compound	Structure	K_i for CB1	K_i for CB2	Reference	Notes
(−)-*trans*-Δ^9-tetrahydrocannabinol (THC)	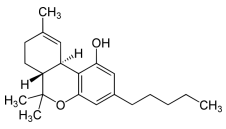	5.05 ± 0.65 nM	3.13 ± 0.34 nM	(Iwamura, Suzuki, Ueda, Kaya, & Inaba, 2001)	PA; this is the most recent of many reported different values - Pertwee, 2008

The biosynthesis of 2-AG starts from inositol phospolipids containing arachidonic acid: a phospholipase–C hydrolyzes phosphatidylinositol-4,5- bisphosphate (PIP_2) to inositol 1,4,5-trisphosphate and diacylglycerol (DAG). The DAG is subsequently hydrolyzed at *sn*-1 position into a free fatty acid and a monoacylglycerol, 2-AG by one of two diacylglycerol lipases (DAGL) – DAGLα and DAGLβ (Murataeva, Straiker, & Mackie, 2014; J. Wang & Ueda, 2009). Two alternate pathways for the biosynthesis of 2-AG are the dephosphorylation

of arachidonoyl-lysophosphatidylinositol and the sequential action of PLA1 and a lysophospholipase C (lyso-PLC) (Murataeva et al., 2014).

Other putative endocannabinoids have then been discovered, from amides like Homo-γ-linolenylethanolamide, Docosatetraenylethanol amide (DEA) (Lumir Hanuš et al., 1993), N-arachidonoyl dopamine (NADA) (Huang et al., 2002) and the ether compounds Noladin ether, which binds to CB_1 but very weakly to CB_2 (L. Hanuš et al., 2001), and Virodhamine, for which we have only data regarding CB_1 (Steffens et al., 2005).

Other ethanolamides classified as "putative endocannabinoids" have been found in tissues, like Palmitoylethanolamide (PEA) and Oleoylethanolamide (OEA); these saturated or monoinsaturated amides do not bind directly the CBs, but rather the PPAR-α, GPR119 and the TRPV-1 receptors (Godlewski et al., 2009; Keppel Hesselink, De Boer, & Witkamp, 2013; Laleh et al., 2018; Petrosino, Iuvone, & Di Marzo, 2010). OEA and PEA have also been found to potentiate anandamide effect (the so-called "entourage effect") in non-vascular tissues in rats, through the activation of TRPV1 (Ho, Barrett, & Randall, 2008; Petrosino et al., 2010), thus further suggesting that AEA/ethanolamides stand at the crossing between different lipid signaling pathways.

Endocannabinoids signaling at the synaptic cleft

Synaptic depolarization or activation of Gq/11-coupled GPCRs (such as glutamate receptors) trigger the activation of the PLC in the postsynaptic neuron. The hydrolysis of membrane PIP_2 yields a DAG which, in turn, is the substrate of DAGL. The newly synthesized 2-AG is hydrophobis enough to cross the cell membrane without transporters of sort, and is released into the synaptic cleft. Here, it reaches the presynaptic neuron through a process which has not been fully identified yet, probably through a transporter of some sort, where it reaches the CB_1 of the presynaptic neuron. Upon ligand binding and receptor activation, CB_1 receptors are primarily coupled to pertussis toxin (PTX)- sensitive Gi/o type G proteins which lead to a rapid decrease in levels of cAMP by inhibiting adenylate cyclase activity. The decrease in cAMP levels, in turn, inhibit Ca^{2+} metabotropic channels; the G protein activity inhibits also voltage-gated Ca^{2+} channels and K^+ channels, avoiding hyperpolarisation. The closing of Ca^{2+} prevents the release of more neutransmitter in the synaptic cleft, completing the general inhibitory action of CB_1, the so-called endocannabinoid-generated short-term depression (Kendall & Yudowski, 2017; Ohno-Shosaku & Kano, 2014). The CB_1 receptor will then enter 2-AG into the cell, where it will be inactivated by monoacylglycerol lipase (fig. 2).

Mechanisms of action for AEA have not been fully elucidated yet; it is thought to participate both in a retrograde signaling pathway, resembling the action of 2-AG, and an intracellular one, acting onto the postsynaptic neuron TRPV1 receptors, thus lowering the Ca^{2+} levels of this cell to induce postsynaptic depression. Since it is degraded inside the cell, at the endoplasmic reticulum, its main role seems that of intracellular signaling (Deutsch, 2016; Ohno-Shosaku & Kano, 2014).

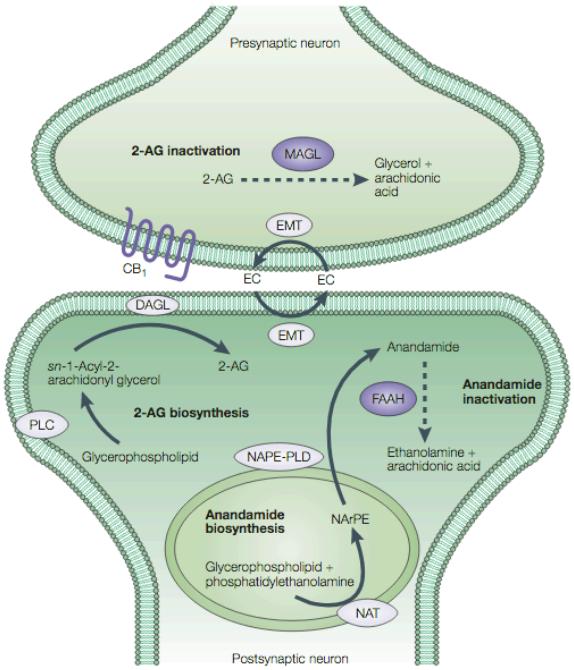

Figure 2. Endocannabinoid system signaling at the synaptic cleft. Image from Di Marzo, Bifulco & De Petrocellis, 2004.

1.1.3 Regulatory enzymes

Once ECs have exerted their function on CBs, their signaling function must be shut down in order to be regulated. This is achieved through their hydrolysis to the corresponding fatty acid and the conjugated alcohol or amine: this function is controlled by the hydrolytic regulatory enzymes of the ES.

These hydrolases are fatty acid amide hydrolase (FAAH), monoacylglycerol lipase (MAGL) and α/β-Hydrolase domain (ABHD)-containing protein 6 and 12 (ABHD6 and ABHD12). All of them are serine hydrolases and integral membrane proteins or, in the case of MAGL, membrane-bound enzymes (Blankman, Simon, & Cravatt, 2007; Labar et al., 2010; Mileni et al., 2010), which seems to fit their role of fine tuning the ECs levels right after their action on CBs (J. R. Savinainen, Saario, & Laitinen, 2012).

FATTY ACID AMIDE HYDROLASE (FAAH)

FAAH was the first regulating enzyme to be discovered (Dale G. Deutsch & Chin, 1993). It is a member of the amidase signature family, which can hydrolyze *in vitro* both amides and esters, as well as other N-acilethanolamines (fig. 3) (Cravatt et al., 2001). At physiological level, however, the pharmacological blockade of FAAH in rats has demonstrated to greatly raise the levels of AEA, but not those of 2-AG (Kathuria et al., 2003) and to contribute to the hydrolysis of ~1% of brain 2-AG (Blankman et al., 2007). Actually, in 2006 it was discovered that two FAAH proteins are encoded in humans and higher mammals, FAAH-1 and FAAH-2: FAAH-2 showed to hydrolyze preferentially OEA, while FAAH-1 has a substrate preference for AEA (Wei, Mikkelsen, McKinney, Lander, & Cravatt, 2006), thus suggesting the crossing between different lipid signaling systems. FAAH has a unique cellular location, at the endoplasmic reticulum: AEA is brought here by a putative transporter, known as Fatty Acid Binding Protein (FABP) (Deutsch, 2016).

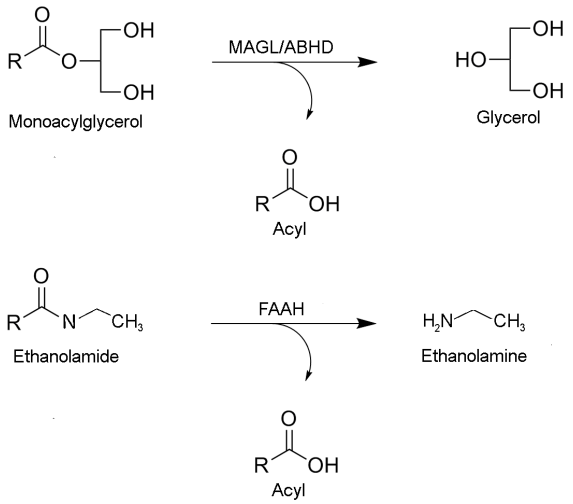

Figure 3. General reaction scheme for hydrolysis catalyzed by MAGL and ABHD esterases (top) and FAAH amidase (bottom).

MONOACYLGLYCEROL LIPASE (MAGL)

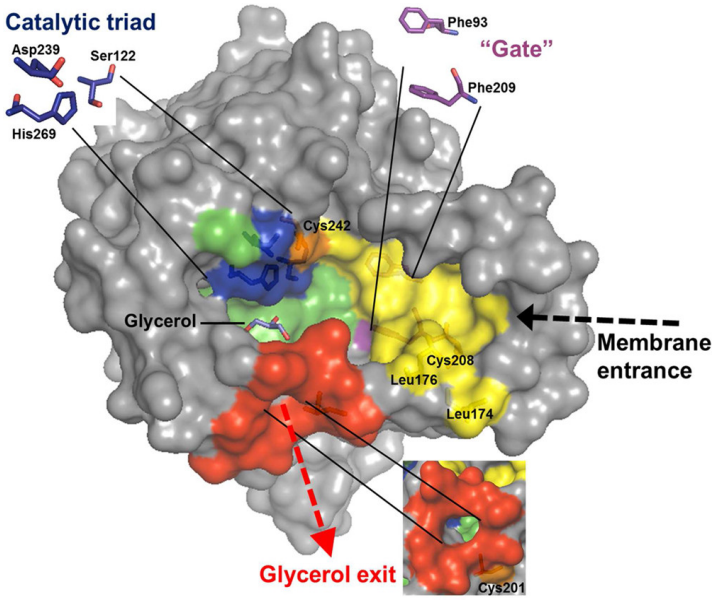

Figure 4. MAGL structure, with the catalytic triad (blue), leaving group exit channel (orange), hydrophobic (yellow) and hydrophilic (green) binding pockets highlighted. The enzyme is depicted here with the A4 membrane binding helix on the right. The "gate" phenylalanine residues 93 and 209 (purple) are a putative "gate" which is thought to control substrate access to the catalytic site during conformational changes. Cys208 and Cys 242 are thought, along with Cys201, to stabilize MAGL conformation and interact with some substrates, such as maleimides. Moreover, these three cysteines have been proposed to control MAGL inhibition through an oxidation-dependent mechanism (Scalvini et al., 2016).
Image from Tuo et al., 2017.

MAGL is the main responsible for the regulation of 2-AG at CB1 neuronal sites (Dinh et al., 2002), accounting for about 85% of its hydrolysis (Saario et al., 2005), although capable of hydrolyzing many different 1-AG molecules (fig. 3) (Navia-Paldanius, Savinainen, & Laitinen, 2012). MAGL structure is summarized in fig. 4: it is a 33 Kda protein, anchored to the membrane through the hydrophobic A4 helix, situated next to the lid domain where the substrate is recruited (Bertrand et al., 2010; Labar et al., 2010). This peculiar structural feature also accounts for the proposed catalytic cycle of MAGL, consisting in the recruitment of the substrate from the membrane, which is then hydrolyzed and released in the cytoplasm folowing a membrane detachment of the enzyme; MAGL then binds the membrane again via the A4 helix, and the cycle can begin anew. The catalytic cycle is made possible by the plasticity of the lid domain, and this substrate recruitment mechanism could account for its substrate specificity in the cell (Riccardi et al., 2017). MAGL structure also has some peculiar features: once the substrate is recruited in its lid domain, it enters the enzyme through a hydrophobic channel which leads to the catalytic site. Here, the substrate is accommodated so that the ester oxygen faces the serine of the catalytic triad, composed by Ser122, His 269 and Asp239 (Karlsson, Contreras, Hellman, Tornqvist, & Holm, 1997). The ester is hydrolyzed via a classic serine hydrolase mechanism, then the glycerol leaving group is thought to exit the protein core through a side exit channel, leading into the cytoplasm (Labar et al., 2010). It is interesting to note that the synaptic localization of these two enzymes is different in rats, with FAAH being found mainly in postsynaptic regions, and MAGL in presynaptic ones: this

seems to follow the main role of 2-AG as a retrograde signaling molecule, and the one of AEA as being primarily an intracellular messenger (Gulyas et al., 2004).

A/B DOMAIN-CONTAINING HYDROLASE 6 AND 12 (ABHD6 AND ABHD12)

In the central nervous system, the remaining 2-AG is hydrolyzed by two other lipases: ABHD6 (~4%) and ABHD12 (~9%) (fig.3), while the remaining ~1% is hydrolyzed by FAAH (Blankman et al., 2007). Both ABHD6 and ABHD12 are predicted to be integral membrane proteins: ABHD6 is a ~36 Kda protein, thought to have its active site facing the interior of the cell, while ABHD12 (a ~45KDa glycoprotein) should face the outward of the cell. In addition to MAGL hanging on the cytosolic side of the membrane, these three enzymes were thought to control the action of 2-AG in neurons (Blankman et al., 2007; Marrs et al., 2010; Navia-Paldanius et al., 2012) and microglia where, in cells which lack the expression of MAGL, ABHD6 grants the control of levels of 2-AG (Marrs et al., 2010; Muccioli et al., 2007). More recently, however, they both have been found to have an *in vitro* substrate preference for 1(3)-acylglycerols of unsaturated fatty acids (Navia-Paldanius et al., 2012); *in vivo*, ABHD12 hydrolyzes lysophosphatidylserine (LPS) in mammalian brain, and has been straightforwardly linked to the neurodegenerative disease which involves polyneuropathy, hearing loss, ataxia, retinitis pigmentosa, and cataract (PHARC), (Blankman, Long, Trauger, Siuzdak, & Cravatt, 2013; Fiskerstrand et al., 2010). While still not much is known about these hydrolases, there indeed are some tools useful for their study: the carbamate inhibitor WWL70 was found to have specificity for ABHD6 (W. Li, Blankman, & Cravatt, 2007). Also, specific inhibitors for ABHD12 in the form of triterpenoids have recently been developed (Parkkari et al., 2014).

1.1.4 Therapeutical interest

The ES has been of therapeutical interest at least since the days of Ancient Egypt, around 1700 B.C. - but more uncertain references could date its medicinal use back to 2350 B.C. (Russo, 2007). The *Papyrus Ramesseum III* reports a preparation of ground celery and hemp, which had to be used to wash the eyes of the patient – a possible reference to glaucoma, one of the most common conditions for which cannabis is still used (Novack, 2016).

Due to the fact that the ES exerts its modulating activity on a variety of systems, its therapeutic potential is vast, and is being investigated since the early days of its discovery. The first approach was that of directly targeting the CBs, with both agonists (THC-like): aside

from and THC and cannabis-derived molecules, the first approved drug in Europe for treatment of obesity through the inhibition of CB1 was Rimonabant, in 2006. Rimonabant is an inverse agonist for the selective blockade of CB1, and gave hopes for an effective treatment of multiple metabolic risk factors, including smoking cessation (Gelfand & Cannon, 2006). While effective, in 2009, however, Rimonabant was retired from the EU market due to its severe psychological side effects: about 11.5% of the patients suffered from depression and anxiety, and a few planned suicide (Moreira & Crippa, 2009; Sam, Salem, & Ghatei, 2011). This taught that drugs targeting the ES have to be tuned very finely, since the vast extent of its activities can bring unpredictable consequences.

The inhibition of regulatory enzymes, thus enhancing the levels of endocannabinoids, has been a promising way for the development of new drugs targeting the ES as well (Toczek & Malinowska, 2018; Tuo et al., 2017). FAAH, the first regulating enzyme to be discovered and the best characterized one, has recently been the target of a clinical trial in the hope that FAAH blockade would have been able to treat pain, anxiety and inflammatory states. The blockade of FAAH was achieved through the irreversible inhibitor BIA 10-2474. After only 5 days from the start of a multiple-ascending dose (MAD) phase which was planned to last for 10 days, four of the five volunteers were hospitalized with severe neurological symptoms, and a fifth died of brain microhaemorrages. The precise cause of death was never determined, but it was confirmed that all of them suffered from an acute and rapidly progressive neurological syndrome (Chaikin, 2017b; Kerbrat et al., 2016). No deaths in any clinical trial were registered since 2006. While the trial followed all clinical good practices, two mistakes of biochemical nature were found: a study conducted with the Activity-Based Protein Profiling (ABPP) technique (W. Li et al., 2007) showed that BIA 10-2474 has relatively poor specificity for FAAH, since it inhibits various other hydrolases including ABHD6. Also, BIA 10-2474 is a FAAH covalent inhibitor *in vitro*, but this factor was not correctly considerated when establishing an IC_{50} for it, so probably the 50 mg dose gave a higher percentage of hydrolase blockade than the estimated 50% (Chaikin, 2017a; Van Esbroeck et al., 2017; van Iersel, 2017). The final report found that the drug "showed non-linear pharmacokinetics at doses between 40–100 mg, suggesting elimination pathways had become saturated, leading to accumulation" (Bégaud et al., 2016). This tragic episode taught that specificity assessment and accurate quantification of the inhibition are key factors to consider before clinical experimentation of a putative drug targeting ES regulating enzymes. The tragic BIA trial, however, was not the only one involving a FAAH inhibitor: another irreversible inhibitor, PF-

04457845, has high potency and selectivity and entered a Phase II trial which went fine. The drug, however, gave no sign to help treating pain coming from knee osteoarthritis, so the trials were discontinued (Huggins, Smart, Langman, Taylor, & Young, 2012; Johnson et al., 2011).

The major regulating enzyme for 2-AG, MAGL, is an attractive target as well, especially for the treatment of pain and of some kinds of cancer, and is promising for anxiety as well. Regarding cancer, signaling from CB receptors can in short arrest breast and prostate cancer cell proliferation and migration, and promote apoptosis in colorectal cancer, glioma, leukemia and pancreatic cancer (Fowler, 2012; Gil-Ordóñez, Martín-Fontecha, Ortega-Gutiérrez, & López-Rodríguez, 2018; Hermanson & Marnett, 2011). Inhibitors derivative of the carbamate compound URB602 have shown to inhibit melanoma cell lines proliferation and induce apoptotic death, with good selectivity for MAGL over FAAH and ABHD6/12 (Lauria et al., 2018). To date, no trials involving drugs targeting MAGL or ABHD6/12 have been published; as said, selectivity is a key requisite for these compounds, since dual blockade of MAGL and FAAH has shown cannabinoid-like behavior in rats, while selective blockade of a single EC-degrading enzyme does not cause such behavior (Fowler, 2012). Also, complete inactivation of MAGL has shown to increase endocannabinoid tone and cause CB_1 desensitization, tolerance to CB_1 agonists, and downregulation of CB_1 receptors (Murataeva et al., 2014): fine tuning of the inhibition and deep understanding of the quantitative aspect of this inhibition are pivotal. An accurate screening of putative inhibitors is fundamental in discriminating the most promising compounds for successive, in-depth studies. This is the aim of high-throughput screening assays.

1.1.5 High-throughput screening for hydrolases

More than an analytical technique, high-throughput screening (HTS) is a philoshophy in approaching analytical problems with the aim of resolving a simple, yet complex, problem: to decide which items in a library, which contains them in the order of tens of thousands, are the most promising for an in-depth characterisation. The practice and methods of HTS assays is well established in the pharma industry since the early ‘90s, and has more recently started to be used in the academia and basic research as well. Originated to screen the most promising compounds to become lead ones, HTS has to deal with libraries of 10.000-100.000 compounds (Mayr & Bojanic, 2009), which need to be screened within a reasonable time frame, and with affordable costs.

All this leads to the need of finding a reasonable compromise between the time needed for an assay, and the quality and costs of the analysis.

Among the many targets for HTS, hydrolases are a well renown one, where HTS can serve both for finding the most fit for the purpose mutation in a library of mutants, and for the identification of the most promising lead inhibitory compounds in a library of hundreds of thousands (Schmidt & Bornscheuer, 2005). Fluorometry is a very suitable technique for lipases HTS: it grants selectivity, short times and needs a relatively cheap equipment. Furthermore, under certain conditions it is insensitive to interferences, and allows the determination of lipase activity in crude cell lysates, and even in turbid solutions. Also, the direct observation of hydrolysis products permits the determination of the enzymatic inhibition according to the change in catalysis rate, rather then relying on single time point quantification of the product. Especially when studying the kinetic behavior of an enzyme, it is extremely important to use continuous assays; while practical and popular, endpoint assays may lead to serious misinterpretations of the enzyme activity profile. This is caused by accidental mistakes in fixing the T=0 point of the reaction time course, which may lead to the assumption of having stopped the reaction while it was still in its linear (or steady state) trait, when actually it was not, and subsequently underestimating the reaction velocity (Bisswanger, 2014; Purich, 2010). Fluorometers also offer another advantage in the availability of plate readers using 96-well or 384-well plates, thus allowing the performing of many different experiments in parallel, with a minimal amount of reagents needed. The main drawback of the technique is that the analyte has to be a fluorescent molecule, which greatly reduces the spectrum of potential analytes. To date, a popular assay for hMAGL uses a fluorogenic probe which mimicks the natural substrate 2-AG through an arachidonic acid residue, and, following the hydrolysis, releases the fluorescent compound 4-methylumbelliferone (Y. Wang, Chanda, Jones, & Kennedy, 2008). Our group has already published an improved method, involving resorufin (Lauria, Casati, & Ciuffreda, 2015): this is where we started to develop diverse HTS assays for the screening of MAGL inhibitors.

Moreover, a HTS assay for ABHD6/ABHD12 has been proposed (Juha R. Savinainen, Navia-Paldanius, & Laitinen, 2016b, 2016a) and will be discussed in-depth in paragraph 5.1. Briefly, it involves a four-step reaction with the use of a reaction mix containing four enzymes; furthermore, one of the enzymatic steps relies on the quantitation on glycerol, a reagent which can easily come from accidental labware contamination.

2. AIMS OF THE STUDY

Our main aim was to provide means to ease the characterisation of the enzymatic hydrolytic system for 2-AG. The modulation of MAGL and ABHDs activity can be an important therapeutic target for a variety of pathologies and conditions, therefore this characterisation is extremely useful.

The project is articulated in three points:

- To develop a fluorescence HTS assay for MAGL which is efficient, fast, cheap and versatile, meaning it can be easily adapted to other hydrolases, exploiting their substrate promiscuity.
- To design and develop a bioluminescence HTS assay for MAGL, to take advantage of the extreme sensitivity and specificity offered by this technique.
- To obtain the bacterial recombinant expression of ABHD6 and ABHD12, so that a simpler assay could be developed (2.3.1), and the availability of the pure, isolated proteins might eventually lead to a better characterization, including the resolution of their crystallographic structures.

3. FLUORESCENCE ASSAY

3.1 Introduction

Fluorometry (or fluorescence spectroscopy, or spectrofluorometry) is a widespread technique for enzyme assays, due to various advantages: it is cheap compared to other methods such as mass spectrometry, it does not require any specific sample preparation and, depending on the quantum yield of the chosen analyte, can quantify compounds in the nanomolar range. The classical photometric approach to the lipases assays is to synthesize an artificial ester substrate from a a *p*-nitrophenol molecule and an organic acid: since lipases usually show good substrate promiscuity, the enzyme will cleave the ester bond, giving a free *p*–nitrophenol molecule which absorbs light at 405 nm (yellow), thus allowing a spectrophotometric quantification of the enzyme activity. A widespread variant consists in the esterification of the p-nitrophenol with phosphoric acid, obtaining a phosphate ester useful for the detection of phosphatase activity. While very popular in the past (Menger & Ladika, 1987), this approach offers two major disavantages: the lower limits of quantification of spectrophotometric assays compared to fluorometric ones, and the intrinsic photophysical properties of *p*-nitrophenol, which make it reliable exclusively at pH values above 7.5, thus making its use impractical to detect the activity of enzymes at the physiological pH of 7.4 or lower (this despite the fact that some producers expressely claim *p*-nitrophenyl phosphate to be a suitable substrate for *acid* phosphatases).

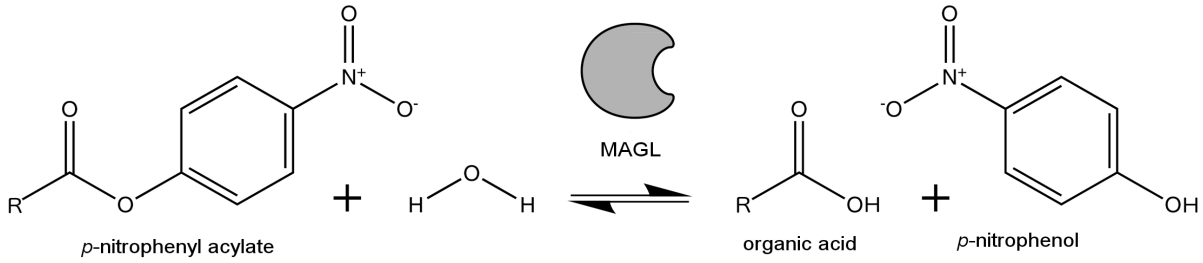

Figure 5. Reaction scheme for p-nitrophenol MAGL assays. The resulting free *p*-nitrophenol is then quantified through spectrophotometric reading.
Image adapted from Pliego et al., 2015.

For our MAGL-dedicated assays, we chose to use resorufin, a phenoxazine-derived compound which shows excellent properties for our purpose. It has a high quantum yield at pH 7.4, is stable in aqueous solutions and is a long-wavelength fluorophore, which emits light in the red region of the visible spectrum, with the emission peak at 588 nm. This is particularly important when long-wavelength fluorophores are employed for assays which involve living cells, since they avoid interferences from cellular autofluorescence (Fritzsche & Mandenius, 2010). In this context, resorufin compounds have a decisive advantage with

respect to coumarins, widely used fluorophores (fig. 6) which emit at a wavelength of about 440-450 nm (blue-violet): the same emission wavelength of NADPH and folic acid, which can be found both in eukaryotic and bacterial cells (Zipfel et al., 2003).

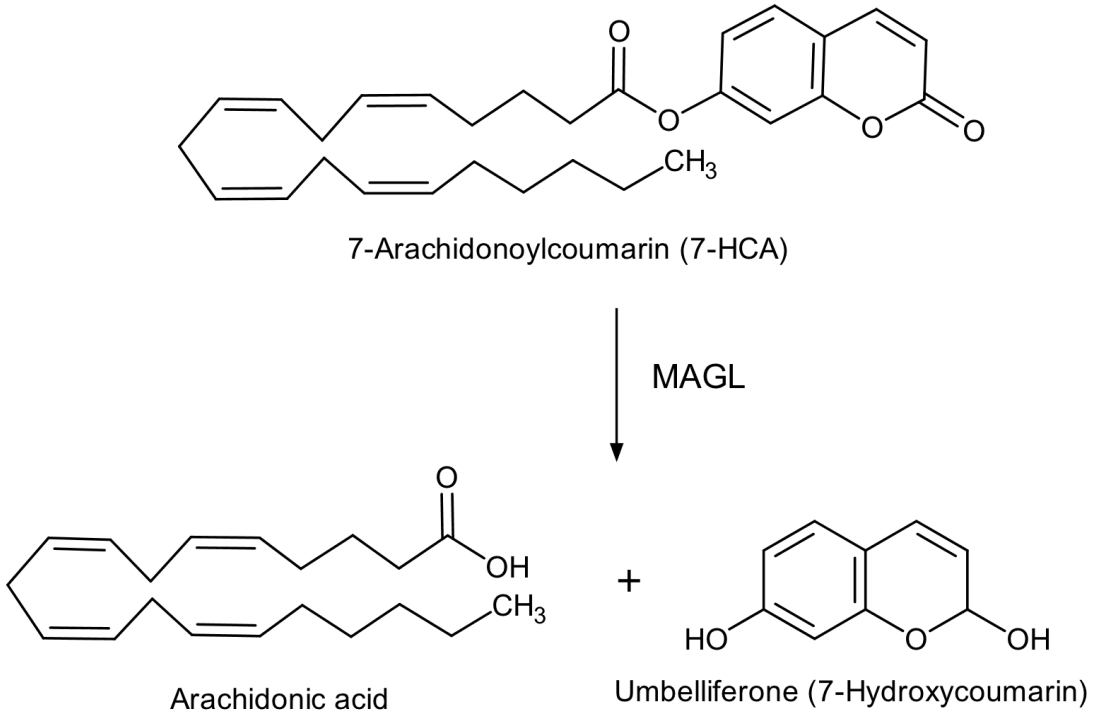

Figure 6. Reaction scheme of the short-wavelength fluorescent assay developed by Y. Wang et al., 2008. The released Umbelliferone is irradiated with light at λ_{ex}=355 nm, and its fluorescnce is recorded at λ_{em}=460 nm.

Resorufin esters as fluorescent substrates for lipases have been studied since the 1960s, and their high quantum yield was found to be accompanied by favorable K_m values. Also, resorufin had proven to be an excellent leaving group with respect to *p*-nitrophenoxide, meaning faster initial "bursts" of catalytic speed. Their main disadvantages were the proximity of the absorption and emission peaks (small bathochromic shift) and the tendency to hydrolyse spontaneously once dissolved in aqueous solution (Guilbault & Kramer, 1965; Kitson & Kitson, 1997; Lam et al., 2012). While the small (about 60 nm) gap between the two peaks is no more a problem due to the spectral resolution of the contemporary instrumentation, spontaneous hydrolysis can be an unsormountable problem in developing an assay. Nonetheless, the length and shape of the size chain was found to have a role in spontaneous hydrolysis of these esters (Guilbault & Kramer, 1965): this was the point from where we started. As previously published (Lauria et al., 2015), our group had already successfully developed an assay using an arachidonic acid residue esterified with resorufin, 7-hydroxyresorufinyl arachidonate (7-HRA), which showed next to none spontaneous

hydrolysis. But, due to the many unsaturations, both arachidonic acid and its esters can incur into autoxidation (peroxidation) (Porter, 2013); also, arachidonic acid is a relatively expensive reagent. So we decided to explore the possibility of having a better fluorescent probe, and subsequently a better assay, to quantify the activity of MAGL in a quick and reliable way. With "better", here we mean more sensitive, quicker, and cheaper: HTS assays need to be performed on a very large scale, so every saving is important when designing them. Also, we wanted to investigate the changes in the kinetic behaviour of MAGL according to variations in the alkylic side chain of its substrates. Finally, we wished to interpret the experimental data analysing the structural aspects of the enzyme-substrate interaction through in silico analysis, with the aim of finding new structural guidelines for the optimisation of MAGL substrates and inhibitors. To pursue these aims, we decided to synthesize ten alkyl esters of fluorogenic resorufin with different types of acyl chains: linear, employing acetate (**1a**), butyrate (**1b**), octanoate (**1c**), dodecanoate (**1d**), icosanoate (**1e**), oleate (**1f**); branched, including 2-methylhexanoate (**1h**), 2-ethylhexanate (**1i**) and 2-butyloctanoate (**1j**); and aromatic, using benzoate (**1k**) (fig.7). The behavior of these esters as fluorescent substrates for the measurement of MAGL activity was to be evaluated, as well as their structural relationships with the enzyme using a docking software.

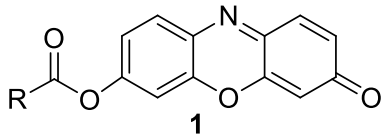

1

a R= CH_3; **b** R= $CH_3CH_2CH_2$; **c** R= $CH_3(CH_2)_5CH_2$; **d** R= $CH_3(CH_2)_9CH_2$; **e** R= $CH_3(CH_2)_{17}CH_2$;

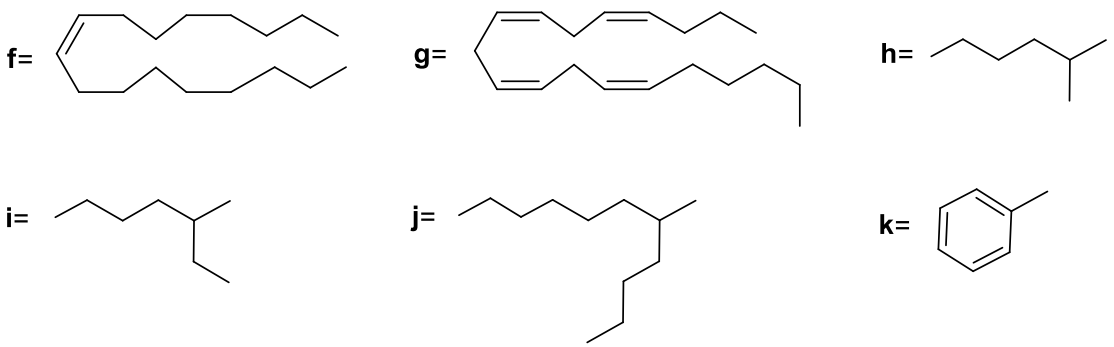

Figure 7. Structures of 7-hydroxyresorufynil-acetate (**1a**), butyrate (**1b**), octanoate (**1c**), dodecanoate (**1d**), icosanoate (**1e**), oleate (**1f**), arachidonate (**1g**), 2-methylhexanoate (**1h**), 2-ethylhexanate (**1i**) and 2-butyloctanoate (**1j**), and benzoate (**1k**).

3.2 Results and discussion

3.2.1 Synthesis of substrates

Syntheses of 7-hydroxyresorufinyl-derivatives **1a-1k** were performed by conversion of opportune carboxylic acid in the corresponding acyl chloride, using oxalyl chloride and DMF in dry CH_2Cl_2 following the classic method for acyl chloride formation in neutral conditions. Treatment of carboxylic acid with 2.0 equiv. of oxalyl chloride in dry CH_2Cl_2 with catalytic amount of DMF resulted in slow gas evolution over a period of 3 hours. Removal of the solvent and exposure of the resulting acyl chloride to free phenol form of resorufin in dry CH_2Cl_2 with triethylamine gave the desired compounds in yields varying from 65 to 92 % (3.4, Table 3).

Resorufin esters **1h**, **1i**, and **1j** instead, could be conveniently prepared by the DMAP-catalyzed DCC method (Steglich esterification (Neises & Steglich, 1978)). The yields are considerably higher than those obtained in the non-catalyzed reaction. With this method, a solution of the acid was prepared in anhydrous CH_2Cl_2, to which resorufin and DMAP were added. Then DCC was added to the reaction mixture at 0 °C at the same final concentration as the acid, and the obtained solution stirred for 3 h at room temperature.

The possibility of synthesizing esters of **1h**, **1i**, and **1j** reaches a limit with more bulky, i. e. sterically hindered carboxylic acids. Thus, in the case of 2-methylhexanoic acid, 2-ethylhexanoic acid and 2-butyloctanoic acid, the symmetrical anhydrides were isolated instead of the esters and the tendency for undesirable *N*-acylureas to be formed was observed. In the Steglich esterification, the addition of 3 mol % DMAP accelerates the DCC-activated esterification of carboxylic acids with alcohols to such an extent that formation of side products is suppressed and even sterically demanding esters are formed in good yields at room temperature.

Unambiguous assignments of protons and carbons were recognized by 1D NMR spectra, as well as 2D NMR homocorrelation (COSY) and heterocorrelation (HMQC and HMBC) spectra were employed for complete structural assignments. The ^{1}H-NMR and ^{13}C-NMR spectra are reported in the Appendix (Table 7). The purity of all compounds measured with NMR was greater than 98%.

3.2.2 Assay development and validation

To obtain proof-of-concept for the compounds newly synthesized (**1a-k**), in MAGL assays, reaction conditions close to that reported by Lauria et al (Lauria et al., 2015) were chosen; in the cited study, the amount of enzyme used in the assay was already optimized to 25 ng to maintain linearity over time and to maintain substrate consumption below 10%, adhering to the assumptions of the Michaelis–Menten equation.

The substrates were readily dissolved in DMSO to make 1.0 mM stock solutions, which were further diluted with DMSO to 50 μM working solutions. The exception to this was substrate **1e**, which could not be dissolved in DMSO and was excluded from further studies. Good reproducibility was obtained by making "assay substrate solutions" from slowly adding the buffer to the DMSO working solution until a final concentration of 5 μM substrate. There was no sign of turbidity or precipitation of substrate under any conditions. For characterization of surrogate substrates **1a-k** we chose the commercially available human recombinant enzyme MAGL (Cayman Chemical) to have a known reference activity independent from the variability of cell extracts. Typical MAGL assays use bovine serum albumin (BSA) since it assists in the solubility of the substrate and might prevent the non-specific binding of the substrate to the walls of the tubes (Y. Wang et al., 2008). We, however, decided not to use BSA because of its reported esterase-like activity (Sakurai et al., 2004). Results of activity assays for all substrates are shown in fig. 8, and indicate enzyme activity and stability of the substrates.

MAGL hydrolyzed a variety of resorufin derivatives with a distinct substrate preference (fig. 8). Of all the compounds newly synthesized, the fastest one was found to be **1c** (Table 2). Of the others, six compounds (namely **1a**, **1b**, **1c**, **1d**, **1f**, **1h**) proved to be "proper" substrates for MAGL, while **1i**, and **1j** showed a very low hydrolytic activity, but were subsequently characterized nonetheless, and **1k** did not show an hydrolytic activity at all (fig. 8). Substrate **1k** was therefore excluded from further investigations.

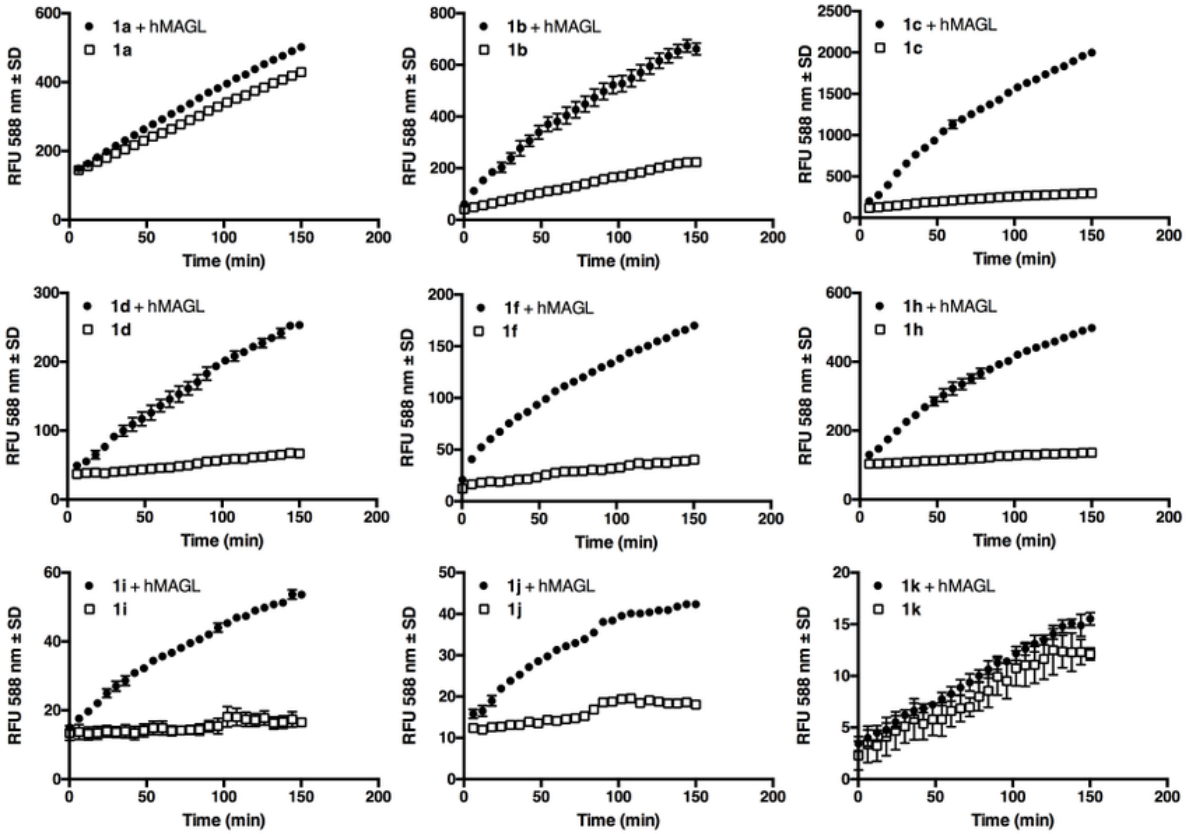

Figure 8. time course of surrogate substrates **1a**, **1b**, **1c**, **1d**, **1f**, **1h**, **1i**, **1j** and **1k** hydrolysis by MAGL. 25ng/well of human recombinant MAGL (circles) or buffer alone (empty squares) were incubated in 96-well black plate, at room temperature, with 5 μM for all compounds in total volume of 100 μL per well, as described in the experimental section (3.4). Fluorescence was measured at indicated time points using a Jasco FP-8300 fluorometer using the kinetic mode (λex=571 nm, λem=588nm, slit = 5.0). Data are mean ± standard error of independent experiments. The data reported represent one data point every two, in order to grant readability of the graphs.

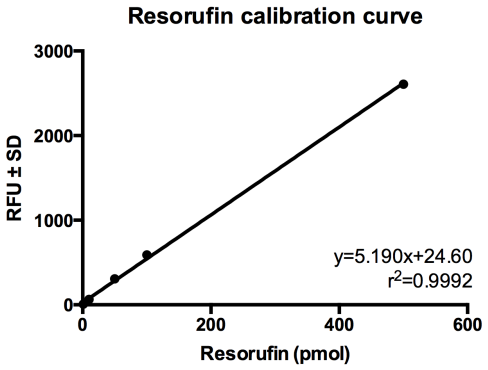

Figure 9. The typical resorufin standard curve. The values represent the average of triplicate values ± SD. Resorufin concentrations were 0, 0.01, 0.1, 0.5, 1, and 5 µM.

Enzyme kinetics were analyzed by measuring initial product formation rates in the presence of varied substrate amounts, the maximal value set according to solubility limits. In order to obtain the fluorescence coming from the enzymatic activity substrate depletion was determined by establishing the amount of free resorufin produced using a resorufin standard curve, and subtracting the amount of free resorufin released at the same time from the spontaneous hydrolysis of the substrate. For this purpose, standard curves showing fluorescence response *vs* substrate/product concentration, were constructed from five concentrations of resorufin (fig. 9).

The initial linear trait of the resulting curve was taken into account, and its slope was

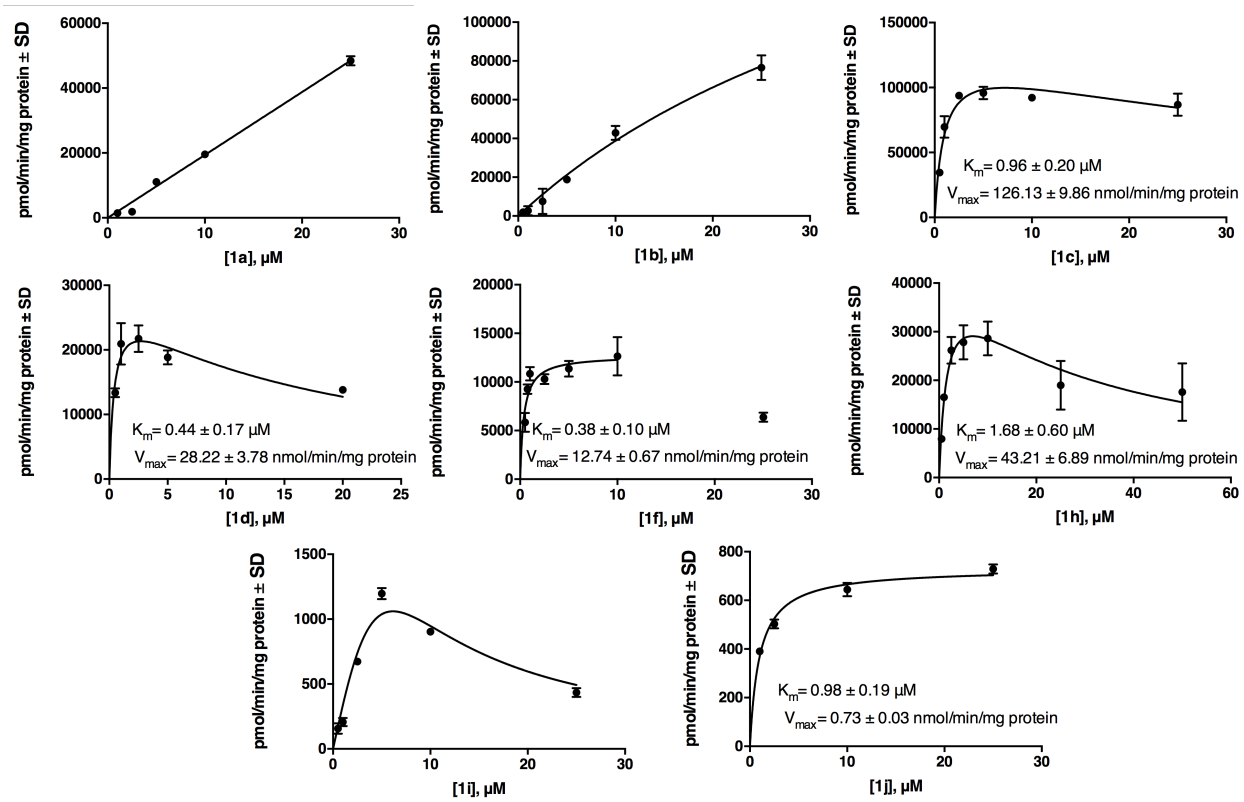

Figure 10. Action of human recombinant MAGL on different concentrations of surrogate substrates **1a**, **1b**, **1c**, **1d**, **1f**, **1h**, **1i**, and **1j**, in the presence of DMSO (10%, v/v). The reactions were conducted in a final volume of 50 mM Tris-HCl buffer (pH 7.4, 1 mM EDTA) with 25 ng/well of MAGL. Values are the means of triplicates ± standard error. The kinetic parameters *K*m and *V*max were determined via computer-assisted nonlinear regression analysis using GraphPad Prism 6.0c.

considered as the measure of enzyme activity (Bisswanger, 2014). Concentrations ranging from 0.5 µM to 25 µM were used.

Table 2. Kinetic values, lipophily, expressed as LogD, and docking scores (3.2.4) of the resorufin moieties in the assay conditions.
a: data from Navia-Paldanius et al., 2012

Compound	LogD at pH 7.4[a]	K_m (μM)	V_{max} (nmol/min/mg protein)	Docking score	MM-GBSA
1a	1.69	n/a	n/a	-6.7	-52.4
1b	2.83	n/a	n/a	-7.7	-60.5
1c	4.61	0.96 ± 0.20	126.13 ± 9.86	-8.2	-72.0
1d	6.39	0.44 ± 0.17	28.22 ± 3.78	-10.5	-81.4
1e	9.94	n/a	n/a	-9.8	-67.8
1f	8.69	0.38 ± 0.10	12.74 ± 0.67	-10.8	-73.2
1g	8.50	0.87 ± 0.13	25.84 ± 0.88	-10.7	-76.0
1h	4.26	1.68 ± 0.60	46.21 ± 6.89	-8.5	-60.3
1i	4.71	n/a	n/a	-8.8	-62.8
1j	6.49	0.98 ± 0.19	0.73 ± 0.03	-8.4	-65.4
1k	3.74	n/a	n/a	-8.9	-63.2
2-AG	4.56	110 ± 15[a]	120 ± 10[a]	-10.4	-53.1

Resorufin calibration curves and negative controls, containing 90 μl of buffer, 10 μl DMSO and no MAGL, were measured at the same time and in the same conditions. Fig. 9 illustrates the action of human recombinant MAGL on different concentrations of all synthetized substrates in the presence of DMSO (10%, v/v).

Compound **1a** and **1b** did not behave in a Michaelis-Menten way under the assay conditions, while the catalytic speed **1f**, had a sharp decrease at concentrations above 10 μM. The Prism software was not able to calculate kinetic constants for **1i** (fig.10). Since MAGL hydrolytic activity on this enzyme was very limited, we did not investigate its kinetic properties further.

All substrates have K_m values ranging from 0.44 to 1.68 μM, which seem in accordance to that of 0.87 μM already calculated for **1g** (Lauria et al., 2015). Maximum velocities are similar as well, ranging from 12.74 to 46.21 nmol/min/mg protein, values which resemble that

of 26 nmol/min/mg protein calculated for 7-HRA. The notable exception to this is compound **1c**, with a V_{max} of 126 nmol/min/mg protein (fig. 10).

In order to validate our method for use in enzyme inhibition assay two known MAGL inhibitors, URB602 and MAFP (King et al., 2007; Saario, Savinainen, Laitinen, Järvinen, & Niemi, 2004), were assessed using the standard assay conditions with 5 μM **1c** as substrate and DMSO as solubilizer to validate the ability to identify inhibitors. The dose–response curves are shown in fig. 11. 25 ng/well of MAGL were incubated at room temperature for 60 minutes at 25 °C with different concentrations of inhibitor dissolved in DMSO; after the rapid addition of **1c** solution, the fluorescence was measured every minute for a period of 1 hour. The activity of MAGL was calculated as described for the kinetic assay.

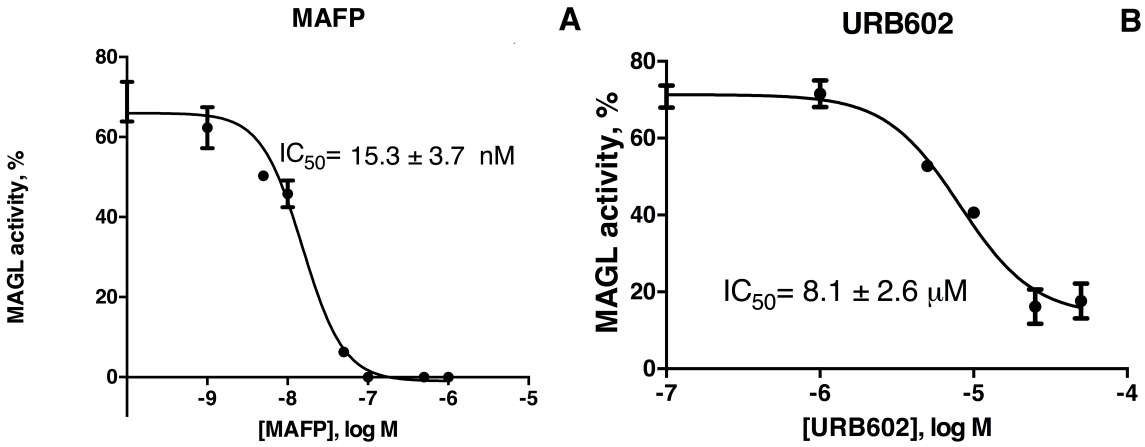

Figure 11. Inhibition of human recombinant MAGL with reference inhibitors: methyl arachidonyl fluorophosphonate (MAFP) (**a**), URB602 (**b**). Data derived from two independent experiments performed in triplicate and calculated as non linear regressions using sigmoid dose-response setting with variable Hill slope by GraphPad Prism 6.0c.

IC_{50} for URB602 was found to be 8.1±2.6 μM, which is in line with literature data (Matuszak, Muccioli, Labar, & Lambert, 2009). As already known, MAFP had the lowest IC_{50} value, 15.3±3.7 nM, which is in the range of values indicated in different works (Lauria et al., 2015; Matuszak et al., 2009). Data derived from two independent experiments performed in triplicate and calculated as non linear regressions using sigmoid dose-response setting with variable Hill slope by GraphPad Prism 6.0c. These data confirm that the assay is able to identify MAGL inhibitors appropriately.

3.2.3 Suitability for cell hydrolase imaging

1c cannot be considered specific for MAGL (Kapoor & Gupta, 2012); however, the use of fluorescent substrates can be useful for the study of unspecific lipase activity within the cell (Kim, Kim, Choi, & Kim, 2015), especially if long-wavelength substrates such as resorufin are used (see 2.1.1). To assess the potential of **1c** to act as a reporter of hydrolase activity in

living cells, B16-F10 melanoma cell lines, a cancer cell line known to express MAGL, were used (Lauria et al., 2018).

The cells were cultured to convergence in 6-well plates, then they were incubated with 5 mM **1c** in DMSO (1µl/1 mL culture medium, final concentration 1‰ DMSO, 5 µM substrate) for 5 minutes. A negative control was set at the same time, using DMSO in the same quantity, but with no substrate dissolved into it. After these 5 minutes, the culture medium was removed from the wells, then 1 mL of fresh medium was pipetted onto that. The procedure was repeated twice, to ensure that any residual substrate was washed away. The wells were then examined at the fluorescence microscope, using a green (530-550 nm) excitation filter.

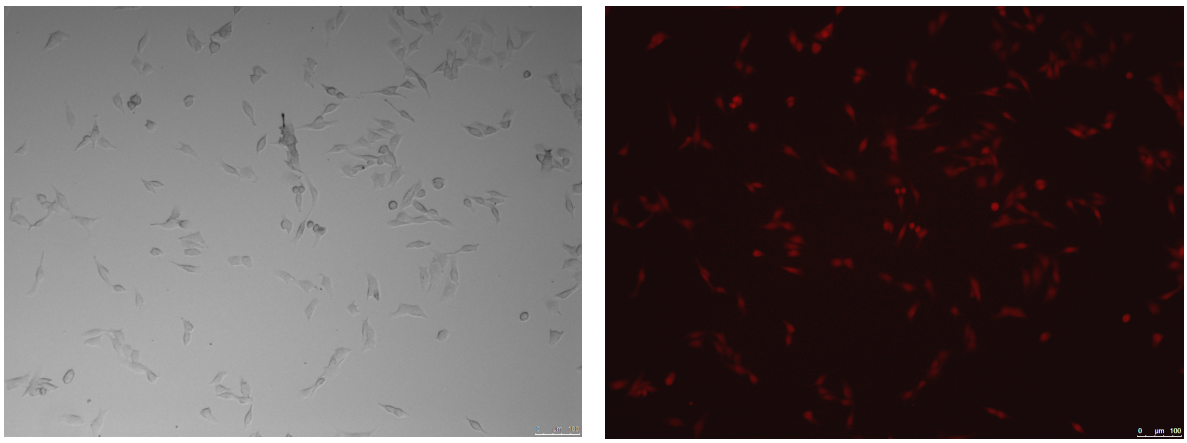

Figure 12. B16-F10 melanoma cell lines after 5 minutes incubation with substrate **1c**, at 10x magnification. The pictures show the same well area, both under phase contrast light (left) and in fluorescence mode (right). Our fluorescent substrate shows its capability to enter the cell and to be hydrolyzed by cell lipases.

3.2.4 In silico molecular docking simulations

The identified binding site corresponds to the catalytic active site identified by Lauria et al (Lauria et al., 2015).

Table 2 (3.2.2) reports the Glide XP docking score and MM-GBSA binding energies for the top scoring pose of each tested compound, showing that all of them are able to bind MAGL in its catalytic site. Docking simulations provided overlapping poses for all the tested compounds and a good superposition of their common resorufin group (fig. 13), confirming the accuracy of this approach. Moreover, the carbonyl group for all the tested compounds, except for **1j**, overlaps the carbonyl group of the natural substrate 2-AG in proximity to Ser122, according to Lauria et al (Lauria et al., 2015).

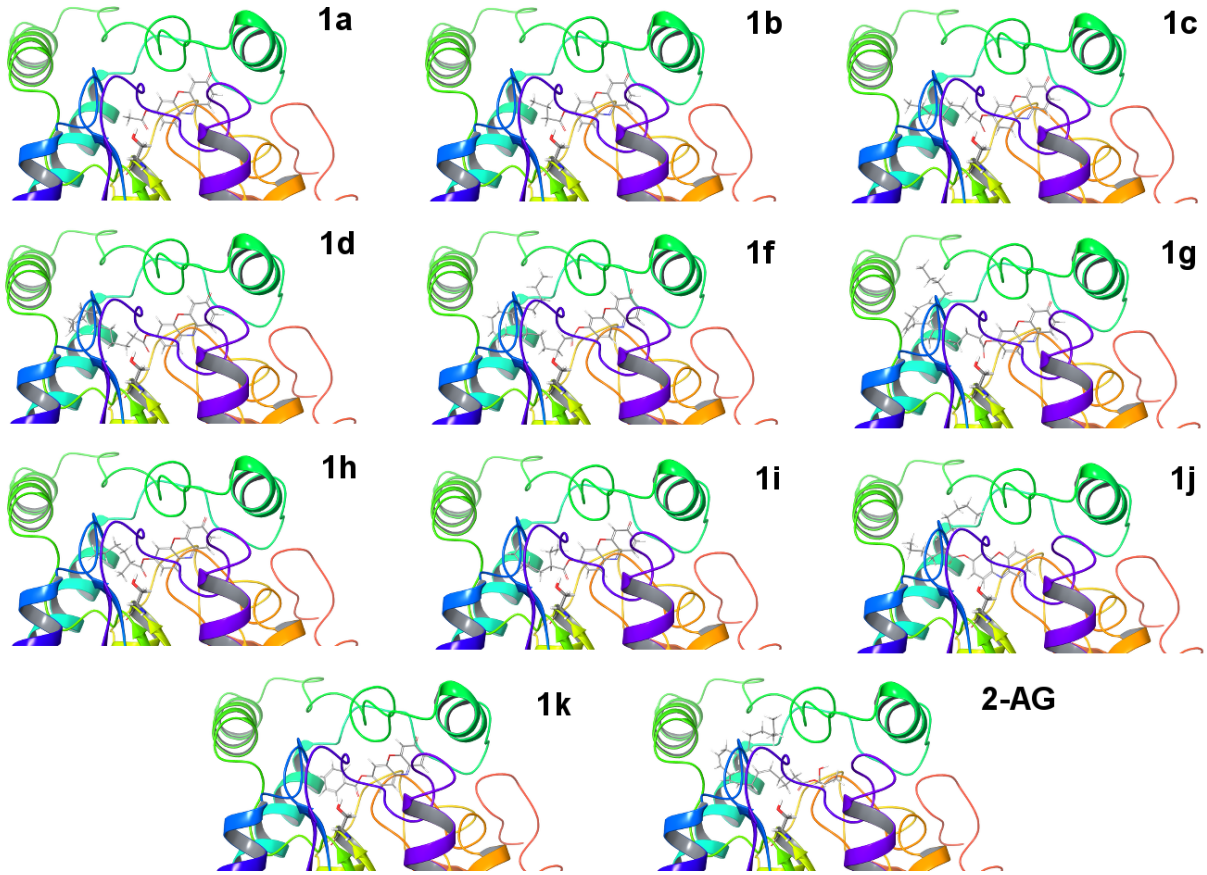

Figure 13. Docking poses of tested compounds, as well as of the native substrate 2-AG, into the MAGL active site. MAGL is shown in ribbon representation; tested compounds and Ser122 are shown as stick representation. All ester oxygen atoms can be seen as headed towards the catalytic Ser residue, except for compound **1j**, in accordance with the experimental results (see text).

Both the Glide XP and MM-GBSA results suggest that 4 compounds (**1c**, **1d**, **1f**, **1g**) can be classified as good MAGL ligands. In particular, compounds **1d**, **1f**, **1g** are associated to a lower Glide XP value than the 2-AG one. Their linear side chains mimic that of a natural MAGL substrate, showing the same orientation into the MAGL hydrophobic pocket. **1c**

mimics 2-AG, but it is shorter than it and it does not present a turn of its side chain in its binding pose (fig. 13). Moreover, these 4 compounds have a MM-GBSA binding energies lower than 70 kcal/mol, outstripping the other ones of approx. 10 kcal/mol (Table 2).

Branched side chains compounds **1h-j**, **1k** and short linear side chain compounds (**1a**, **1b**) can be classified as weak binders, considering both Glide XP and MM-GBSA scores. Among them, **1j** is the unique compound with a carbonyl group which does not overlap the reference 2-AG position due to effect of its branched side chain placement. **1e**, that has a linear side chain composed by 20 carbons, shows intermediate values of both Glide XP and MM-GBSA scores.

Globally, compounds with linear side chains longer than 8 carbons fit the MAGL hydrophobic pocket better than compounds with branched/aromatic side chains, while compounds with linear side chains shorter than 6 carbons are penalized in binding.

3.3 Conclusion

We have readily synthesized long-wavelength putative fluorogenic substrates characterized by different acylic side chains and applied them to the fluorometric determination of MAGL activity. The relationship between the structure of alkyl esters of fluorogenic resorufin and their different behaviors towards MAGL was examined. An in-silico evaluation of how these different side chains interact with the active site of MAGL has been performed as well. **1c**, was found to be a better substrate than their homologs for the fluorimetric assay of MAGL, being the substrate with the higher rate of hydrolysis and the best K_m and V_{max} values. **1c** looks way better than 7-HRA (**1g**) since, containing an eight carbon atoms unbranched chain instead of a twenty carbon one, has higher water solubility, making its use in screening easier, is cheaper and provides a higher sensitivity. The test assay using **1c** was validated using the well-known MAGL inhibitors URB602 and MAFP.

The method described in this section can act as an interesting tool for the HTS screening of MAGL modulators. The octanoyl resorufin substrate proved to be the best candidate in this assay, since, due to the lack of long hydrocarbon fatty acid chains with rather unstable *cis* olefines, it is a very stable compound in aqueous solution, and is easily prepared with a simply scalable technique. Kinetic and modeling data also demostred that, comparated with known fluorescence-based MAGL assay, our method is the quickest and the cheapest one available.

3.4 Experimental section

Reagents and materials

Monoacylglycerol lipase (human recombinant, 50 μg) was purchased from Cayman Chemical (Ann Arbor, MI, USA). Arachidonic acid, resorufin, Tris, ethylendiaminetetraacetic acid (EDTA), Hepes, phosphate buffered saline (PBS) tablets and all other reagents and solvents were purchased from Sigma-Aldrich (St. Louis, MO, USA). Reactions progress was monitored by analytical thin-layer chromatography (TLC) on pre-coated aluminum foils (Silica Gel 60 F254-plate, Sigma-Aldrich) and the products were visualized by UV light. All steps which included resorufin were carried out protecting the compound from light from that step on.

Instruments

Fluorescence signals were recorded by a Jasco FP-8300 fluorometer (Jasco, Tokyo, Japan) using the kinetic mode (λ_{ex}=571 nm, λ_{em}=588nm, slit = 2.5 nm in both cases) with flat bottom 96-well black plate.

^{1}H-NMR spectra were recorded in CDCl3 (isotopic enrichment 99.95%) solutions at 300 K using a Bruker AVANCE 500 instrument (500.13 MHz for ^{1}H, 125.76 MHz for ^{13}C) using 5 mm inverse detection broadband probes and deuterium lock. Chemical shifts (d) are given as parts per million relative to the residual solvent peak (7.26 ppm for 1H) and coupling constants (J) are in Hertz. The experimental error in the measured ^{1}H-^{1}H coupling constants is ± 0.5 Hz. The splitting pattern abbreviations are as follows: s, singlet; d, doublet; t, triplet; q, quartet; m, multiplet, and bs, broad peak. Unambiguous assignments of protons and carbons were recognized by 1D NMR spectra, as well as 2D NMR homocorrelation (COSY) and heterocorrelation (HMQC and HMBC) spectra were employed for complete structural assignments. For two-dimensional experiments, Bruker microprograms using gradient selection (gs) were applied.

Synthesis of 7-hydroxyresorufinyl-derivatives ***1a, 1b, 1c, 1d, 1e, 1f, 1g, 1h***

To a solution of opportune carboxylic acid (0.46 mmol) in dry CH_2Cl_2 (2 mL), oxalyl chloride (58 μl, 0.69 mmol) in dry CH_2Cl_2 (0.5 mL) was added dropwise at 0 °C under stirring. N,N-dimethylformamide (DMF, 1 drop) was added next. The reaction mixture was stirred at room temperature for 3 h and then concentrated under vacuum, giving crude acyl chloride. This residue was dissolved in dry CH_2Cl_2 (1 mL) and added dropwise to an ice-cold suspension of

resorufin (50 mg, 0.23 mmol) and triethylamine (48 µl, 0.35 mmol) in dry CH_2Cl_2 (3 mL) and then stirred overnight at room temperature. After dilution with CH_2Cl_2 the salts residues were removed by filtration obtaining a brick-red solution; that was washed with 0,5 M HCl (2 mL), saturated $NaHCO_3$ (2.5 mL), dried on anhydrous Na_2SO_4 and concentrated to give the crude product. Column chromatography on silica gel by a suitable mobile phase gave the desired compounds in yields varying from 62 to 92 %. The purity of all compounds measured with NMR was greater than 98%. . LogdD data were generated using the Chemicalize ChemAxon software, https://chemicalize.com/.

*Synthesis of resorufin esters **1h, 1i, 1j***

To a stirred solution of opportune carboxylic acid (0.46 mmol) in dry CH_2Cl_2 (3 mL), was added DMAP (2.5 mg. 0.02 mmoli) and resorufin (50 mg, 0.23 mmol). DCC (72 mg, 0.35 mmoli) was added to the reaction mixture at 0 °C. Stirring was continued for 5 min at 0 °C and for 3 h at 20 °C. Precipitated urea is then filtered off and the filtrate evaporated down in vacuo. The residue was taken up in CH_2Cl_2 and, if necessary, filtered free of any further precipitated urea. The CH_2Cl_2 solution was washed twice with 0.5 M HCl (2 mL), saturated $NaHCO_3$ (2.5 mL), dried on anhydrous Na_2SO_4 and concentrated to give the crude product. Products can be obtained in pure form by filtration on column chromatography on silica gel by a suitable mobile phase. The desired compounds were obtained in yields varying from 82 to 92 %. LogdD data were generated using the Chemicalize ChemAxon software, https://chemicalize.com/.

Table 3. Mobile phases used for the separation of synthesis products.

Compound	Yield	Mobile phase	m.p.
1a	65%	CH_2Cl_2/acetone, 98:2	225-226 °C[a]
1b	71%	Petroleum ether/AcOEt gradient, from 7:3 to 5:5.	146-147 °C[a]
1c	68%	Petroleum ether/AcOEt 8:2.	111-112 °C
1d	72%	Petroleum ether/AcOEt gradient, from 8:2 to 7:3.	117-119 °C
1e	75%	CH_2Cl_2/acetone, 98:2	124-125 °C
1f	66%	Petroleum ether/AcOEt 8:2.	82 °C

1g	62%	CH_2Cl_2/acetone, 98:2	Oil[a]
1h	90%	Petroleum ether/AcOEt 75:25.	144-145 °C
1i	82%	CH_2Cl_2/acetone, 98:2	124-125 °C
1j	92%	CH_2Cl_2/acetone, 98:2	94-96 °C
1k	92%	Petroleum ether/ AcOEt 9:1 to remove side products, then CH_2Cl_2/acetone 98:2.	241-242 °C[b]

[a] Guilbault & Kramer, 1965

[b] Lauria et al., 2015

Stability of the substrate

The stability of all substrates was tested in 50mM Tris-HCl buffer (pH 7.4, 1 mM EDTA), according to our previous results (Lauria et al., 2015).

10 µl of the substrates dissolved in DMSO (final concentration 5 µM) were added to 90 µl of the buffer. The fluorescence increase at 588 nm was monitored at intervals of 1 minute across an incubation period of 90 minutes at controlled room temperature of 25 °C, using a Jasco FP-8300 fluorometer in kinetic mode (λ_{ex}=571 nm, λ_{em}=588nm, slit = 5.0 nm in both cases) (Jasco).

Substrates screening

The assays were performed on a 96-well plate. MAGL activity was monitored following the increase of resorufin fluorescence (λ_{ex}=571 nm, λ_{em}=588nm), at intervals of 1 minute. Each reaction well contained 80 µl Tris-HCl 50 mM with EDTA 1 mM, 10 µl of buffer with 25 ng MAGL and the putative substrate dissolved in 10 µl of DMSO (final concentration 5 µM), total volume 100 µl (Lauria et al., 2015). The measurements were carried at a controlled room temperature of 25 °C. Resorufin calibration curves and negative controls, containing 90 µl of buffer and no MAGL, were measured at the same time and in the same conditions. All experiments were performed in triplicate, and each experiment was independently replicated at least once. All resorufin ester solutions were freshly prepared in DMSO from powder, then divided into aliquots and stored at -80 °C, to be used without any further freeze-thaw cycle.

Kinetic assays of MAGL.

For all assays, MAGL was diluted to 250 ng/mL in 50 mM Tris-HCl buffer (pH 7.4), with 1mM EDTA (reaction buffer). For each substrate concentration (0.5 μM, 1 μM, 2.5 μM, 5 μM, 10 μM, 25 μM and 50 μM), a reagent solution was prepared by diluting first at 5 mM dimethyl sulfoxide (DMSO) stock in DMSO to 5 μM, 1 μM, 25 μM, 50 μM, 100 μM, 250 μM and 500 μM solutions, then by diluting these solutions 1:10 in reaction buffer to obtain reagent solutions. The enzyme preparation was added in triplicate (10 μl) to wells in a black, flat-bottomed, 96-well polystyrene microtiter plate (BD Falcon). Each reagent solution (90 μl) was added to the wells to a final concentration of 0.5 μM, 1 μM, 2.5 μM, 5 μM, 10 μM, 25 μM and 50 μM. The final MAGL concentration was 25 ng/100 μl (7.6 nM), and the final DMSO concentration was 10%.

To assess the fluorescent signal coming from the substrate with no enzyme added, negative controls were performed in the same way as above and in triplicate, but 10 μl of reaction buffer were added instead of enzyme preparation. A blank sample containing no enzyme (90 μl of reaction buffer, 10 μl DMSO) was also prepared in triplicate wells. Fluorescence was measured in the same instrumental conditions as per the substrates screening, for 40 cycles with a cycle time of 1 min. All readings were performed in triplicate and averaged. A standard curve was generated by plotting fluorescence of five concentrations of resorufin (0.01 μM, 0.1 μM, 0.5 μM, 1 μM, 5 μM) prepared by diluting DMSO stocks in reaction buffer and adding to microtiter plate wells in triplicate (100 μl, final DMSO concentration 10%). All readings from triplicate wells were averaged.

Data analysis.

Fluorescence was measured and recorded as above. The mean fluorescence value of a blank was subtracted from the value of each sample and control well to normalize data at each time point, then the mean value of control wells was subtracted to the mean value of corresponding enzyme wells. The curve generated from the standards was used to convert raw fluorescence data into nmol/mL/min of resorufin produced. The values of the curve coming from wells with the substrate without the enzyme were subtracted from the enzymatic curve: initial velocities were determined from the linear portion of the resulting curve. Kinetic data were elaborated using GraphPad Prism 6.0c (GraphPad Software, San Diego, CA, USA) and Microsoft Excel graphing software; kinetic parameters Km and Vmax were calculated using GraphPad, employing a nonlinear regression analysis (substrate inhibition or Michaelis-Menten, according to best fit). The quantitative data were calculated as means ± standard

errors. The Z'-factor was calculated using the equation $Z'=1-(3\sigma h+3\sigma l)/|\mu h-\mu l|$, where σh and σl are the standard deviations of the high and low signal controls, respectively, and μh and μl are the mean signal intensities of the high and low signal controls, respectively (Zhang Ji-Hu, Chung Thomas D.Y., 1999).

Continuous assay using known MAGL inhibitor

Methyl arachidonyl fluorophosphonate (MAFP) and URB602 were chosen for the method validation (King et al., 2007; Saario et al., 2004). Diluted MAGL (10 μl) was added to 27 wells in a black, flat-bottomed, 96-well polystyrene microtiter plate. Inhibitor solutions were added to wells at eight different concentrations in triplicate, and well volume was adjusted to 95 μl with reaction buffer. A set of triplicate wells received no inhibitors, and well volume was adjusted to 95 μl with reaction buffer. Final concentrations of MAFP were 1.00 μM, 500 nM, 100 nM, 50.0 nM, 10.0 nM, 5 nM, 0.1 nM, and 0.00 nM; final concentrations of URB602 were 75 μM, 50 μM, 25 μM, 10 μM, 5 μM, 1 μM, and 100 nM. A 100 μM substrate reagent solution was prepared by diluting a 5 mM DMSO stock 1:50 in DMSO. After 60 mins of incubation at 25 °C, 5 μl of the substrate reagent solution was added to each well to give a final substrate concentration of 5 μM. The final concentration of enzyme in all wells was 0.76 pM and the DMSO concentration was 10%. A blank sample containing no enzyme (90 μl of reaction buffer, 10 μl DMSO) was also prepared in triplicate wells. Instrument settings were the same used for the substrates screening. Fluorescence was recorded at room temperature for 30 cycles, with a cycle time of 1 min. All readings were performed in triplicate and averaged. The mean fluorescence value of a blank was subtracted from the value of each sample and control well to normalize data at each time point then the mean value of control wells was subtracted to the mean value of corresponding enzyme wells. IC50 was determined as the concentration of inhibitor that results in an initial velocity 50% that of the sample containing no inhibitor. IC50 was used along with previously calculated K_m to determine K_i.

In-silico molecular docking simulations

All the computational procedures were carried out by the Schrödinger Small-Molecule Drug Discovery Suite 2018-01. The crystallographic structure of the core domain of human MAGL was downloaded from the RCSB PDB (PDB ID: 3PE6, resolution of 1.35 Å) (Schalk-Hihi et al., 2011) Schrödinger Protein Refinement tool was used to mutate Ala36, Ser169 and Ser176 in Lys36, Leu169 and Leu176, respectively. The wild-type MAGL structure was then energy

minimized using the Schrödinger Protein Preparation Wizard in order to fix structural issues in the three-dimensional (3D) structure.

Tested ligands were built through the Schrödinger Maestro Build Toolbar and prepared for docking by the Schrödinger Ligand Preparation, generating the stereoisomers of **1b**, **1i** and **1h**.

The molecular docking procedure was carried out by the Schrödinger Glide Docking in the "extra precision (XP)" mode in order to evaluate the ability of the tested ligand to bind the MAGL catalytic domain, keeping only the twenty top-scoring poses.

The top-scoring solution for each ligand was submitted to the Schrödinger Prime MM-GBSA, which integrates molecular mechanics energies combined with the generalized Born and surface area continuum solvation (Genheden & Ryde, 2015) in order to compute ligand binding and ligand strain energies for a set of ligands and a single receptor.

4. BIOLUMINESCENCE ASSAY

4.1 Introduction

Bioluminescence (BL) is a form of chemiluminescence (CL) (the emission of visible light produced by a chemical reaction) produced by an organism. There are many reasons for which different organisms have evolved BL several times: in the depths of the oceans, an environment where BL is extremely widespread, potential preys did not have many choices but to reach the deepest waters, where the darkness would have hid them from the sight of their predators. Here, light-emitting organs help them to find mates, or to escape predators through a wide array of tactics: producing a flash of BL to blind or distract their stalker (some animals can even detach bioluminescent parts of their body to distract their chaser), discouraging the predator through the menace of sticking bioluminescent tissues to its body (so that other predators will easily localise it), or emitting an ambient-like light from their bellies so that the predator swimming under them will not see their shadow against the dim sunlight above[2]. On the other front, BL can serve to find preys for their bearers, illuminating or attracting them. In other environments, where the landscape provides plenty of hideouts, BL is rarer: in freshwater it is almost absent, while on land it is of domain almost exclusively of insects, and serves mostly for mating. This extreme variety helps to explain why the emission of BL from WT luciferases can cover a lot of different wavelengths: underwater, the blue light is the one which travels furthest, and thus is the most widespread (although examples of specially evolved red light emission are present in the oceans as well among predatory fishes (Herring & Cope, 2005)), while on land the most present is green-yellow light, since leaves reflect it best (Widder & Falls, 2014). The main differences with respect to CL reactions lie in the mechanism and the yield of the reaction. With respect to the mechanism, BL is the result of a biochemical oxido-reduction between an enzyme, a *luciferase*, and a substrate, a *luciferin*. These are very generic names, so different biochemical systems are usually differentiated by the use of a taxon prefix, e.g. "PpyWT" generally stands for "Wild-type luciferase from the *Photinus pyralis* firefly". It is important to bear in mind that bioluminescent systems found in different organisms are based on luciferase-luciferin systems which vary

[2] This strategy, named "counterillumination", is epitomized by a group of cephalopods known as "bobtail squids": the squid *Euprymna scolopes* is symbionts with the bioluminescent bacterium *Aliivibrio fischeri*, which they host inside a specialised organ, providing the bacteria a sugar and aminoacid solution. The organ can also regulate the wavelength, intensity and direction of the light produced by the bacteria, so that the light matches perfectly that of the above sky condition and hour of the day.

widely from one another. Moreover, BL reactions usually have a much higher quantum yield than CL ones: e.g. the PpyWT luciferase has a quantum yield of 0.48 at pH 8.0, a much higher value than that of any CL reaction (Niwa et al., 2010). The first important advantage of BL as an analytical technique directly descends from its mechanism: specificity. The luciferase can emit a luminescent signal exclusively if it reacts with its specific luciferine and cofactors, with no other possible causes other than technical problems (e.g. the detector is exposed to light coming from a different source). The second one is sensitivity: CL reactions in general offer interesting sensitivity, with the capability to detect attomoles of analyte in solution even with quantum yields as low as 0.01 (Roda et al., 2016). Combined with the high quantum yields of BL, this makes the use of luciferases the most sensitive methods of detection available, while keeping the costs for the instrumentation relatively low. The firefly luciferase/luciferin are the most sensitive methods of detection available, with detection capabilities down to 10^{-17} mol (tens of attomoles), to the point that the ATP emission from a single bacterial cell can be detected via BL (Roda et al., 2016; Satoh, Kato, Takiguchi, Ohtake, & Kuroda, 2004). Luciferases catalyse an oxido-reductase reaction, which requires oxygen and, when the reaction occurs within the cellular environment, a cofactor: these include Ca^{2+} in jellyfishes, Mg^{2+} and ATP in fireflies, H^{+} in dinoflagellates, H_2O_2 in earthworms, $FMNH_2$ and NADH in bacteria, cyanide ions in Bermuda fire worms, and ferrous ions in parchment tube worms (Widder & Falls, 2014). The necessity of these cofactors can be conveniently exploited in the detection of these small molecules.

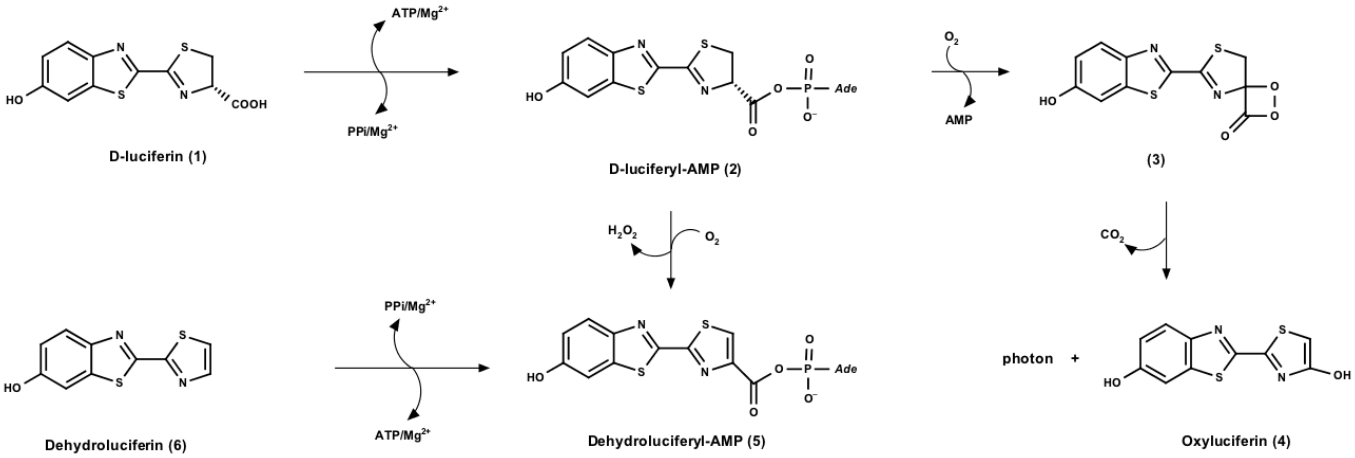

Figure 14. The classic proposed firefly luciferase-luciferin reaction scheme (White, Rapaport, Seliger, & Hopkins, 1971). Through the use of an ATP molecule in the presence of a magnesium atom, the luciferase produces D-luciferyl adenylate (2). The subsequent reaction of LH2-AMP with O_2 brings to the release from luciferase of a dioxethanone product (3), which decarboxylates spontaneously to produce Oxyluciferin in an electronically excited state; the thiazole oxygen atom then relaxes through the release of a photon, yielding Oxyluciferin (4). Dehydroluciferin (6), a product of luciferin degradation, acts a luciferase inhibitor, since its derivative dehydroluciferyl adenylate (5) is unable to react with oxygen, and subsequently to leave the enzyme active site.

In the case of firefly luciferase, it oxidizes firefly luciferin to oxiluciferin through a key dioxietanone intermediate; spectroscopic data show the involvement of a superoxide anion in the formation of this dioxietanone through a single-electron transfer mechanism (Branchini, Behney, et al., 2015). The reaction is strongly stereospecific for D-luciferin: L-luciferin is an inhibitor of the light-emitting reaction, as is the oxyluciferin product. The fact that the reaction is inhibited by its product is thought to cause the "flash" pattern of firefly luciferase light emission, in lieu of the continuous "glow" emission seen in bioluminescent bacteria, which work on a totally different mechanism based on $FMNH_2$ and a long-chain aliphatic aldehyde (Pinto Da Silva & Esteves Da Silva, 2014; Widder & Falls, 2014). A common application which involves the use of BL is probing, in cellular biology and living tissues in general, or biophotonics: in these cases, BL offers the additional advantage of being non-destructive and non-lethal for the tissues and organisms being studied. Luciferases can be used directly to quantify enzymatic reactions through the quantification of reaction products or to detect other small molecules, like ATP or NADPH, cells can be transfected with luciferase genes to analyse gene espression in tissues and organisms, or disease progression in animal models, and bioluminescent bacteria can be employed to map and quantify environmental pollutants (Widder & Falls, 2014). Last but not least, many diverse biosensoristic techniques employ CL and BL as means of detection (Roda et al., 2016), and the possibility to develop luciferase fusion proteins further expands the potential field of application (Smirnova & Ugarova, 2017). The monitoring of bioluminescent tissues in living animals, such as xenographs transfected with luciferase genes, is a well-established practice (Feng et al., 2016; Ke et al., 2016). Cell-based assays on 96- and 384-well plates can be more convenient to the point of being suitable for HTS assays, even if in some cases the actual trasferability to automated practices has yet to be proven (Michelini, Cevenini, Calabretta, Calabria, & Roda, 2014).

Assessment of enzymatic activity *in vitro* through BL is not fully developed yet, but it looks like a promising field of application, with a few examples of ingenious methods studied to exploit the potential of BL, especially for transferases (Ibáñez, McBean, Astudillo, & Luo, 2010; Lin et al., 2018). Regarding hydrolases, the two main strategies for detection remain those of indirect determination of the enzyme activity targeting byproducts of the enzymatic reaction (strategies depend on the reaction), and the "caging" of the luciferin in an artificial substrate, which releases free luciferin after the

hydrolytic reaction occurs (J. Li, Chen, Du, & Li, 2013). Pros and cons of these two strategies remain mostly the same as fluorescence strategies using artificial probes, but with important additions. The added "pros" are those typical of BL in general, which means enhanced selectivity and sensitivity; these are traded for the need of an additional enzyme, which brings additional costs to the analytical setup and the risk of the luciferase being inhibited by the putative hydrolase inhibitors, adding false positives to the screening results. This last point in particular is very delicate: although the differences in catalytic mechanism and structure between luciferases and hydrolases should minimize the number of false positives, we already know that PpyWT is inhibited by 4-10% of the chemicals found in a typical library (Michelini et al., 2014), and there can be no way to completely avoid this phenomen, but testing the chosen luciferase for known hydrolase inhibitors during the assay development is a good idea (Lin et al., 2018).

Aim of this work was to try and develop a screening assay for MAGL inhibitors using BL as detection method. A major issue in this case is that of luciferase stability: preliminary experiments from our group have shown that Lit/PpyWT luciferase does not work in the assay conditions already established for MAGL (Lauria et al., 2015). The main culprit for this is the presence of 10% DMSO (1.43 M!) in the reaction buffer: while MAGL has shown to work in these conditions with no negative effects, it is well-known that DMSO can enchance heavily protein degradation (Tjernberg, Markova, Griffiths, & Hallén, 2006). However, a percentage of DMSO is required, in order to dissolve the largely hydrophobic compounds which are substrates for lipases. This dilemma found a possible solution when prof. Branchini's group published the characterisation of PLG2, a Ppy/Lit chimeric luciferase which showed exceptional resistance to denaturing conditions (Branchini, Southworth, et al., 2015) and has then used for an extremely sensitive ATP assay in cells (Branchini & Southworth, 2017): the work in collaboration with his group then began.

4.2 Results and discussion

4.2.1 Synthesis of the substrate

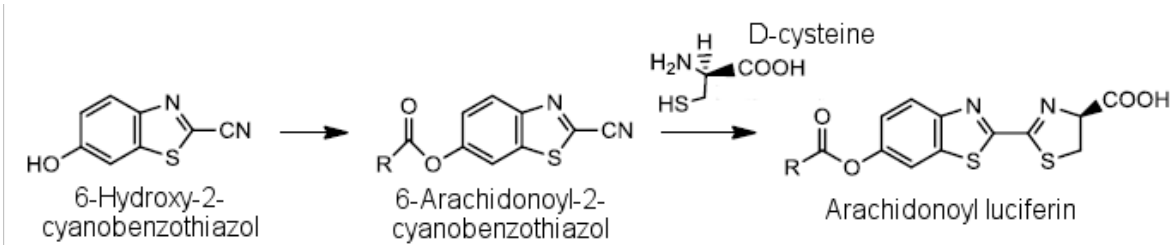

Figure 15. Schematic procedure for the synthesis of ArLuc. R=Arachidonic acid

The substrate arachidonoyl luciferin (ArLuc) was synthesized following an adaptation of the procedure for the synthesis of bioluminescent substrates for the analysis of hydrolytic enzymes by Toya and colleagues (Toya et al., 1992). Since this procedure does not involve luciferin as a reagent, it provides the important advantage of not having to protect and then de-protect the carboxyl free group of luciferin. The modified procedure included the use of DCC and DMAP for the direct coupling of arachidonic acid and the luciferin precursor 6-Hydroxy-2-cyanobenzothiazol. This first reaction produced a nitrile compound, which then readily reacted with D-cysteine hydrochloride, obtaining the desidered D-luciferin ester, with an overall yield of 29.4%.

Unambiguous assignments of protons were recognized by 1D NMR spectra, as well as 2D NMR homocorrelation (COSY), which were employed for complete structural assignments. The purity of the compound measured with NMR was greater than 98%.

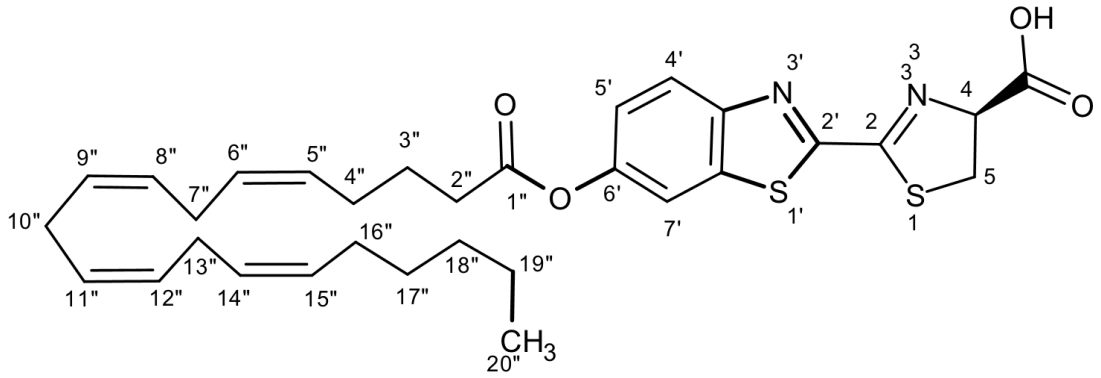

Figure 16. The luminogenic substrate ArLuc, with the carbon atoms mapped.

The ^{1}H-NMR spectra are reported in the Appendix, the assignements are (fig. 16): 0.91 (3H, t, J=7.6, 20¢"-CH3), 1.28-1.40 (6H, m, 17¢”-19¢”-CH2), 1.87 (2H, tt, J=7.0, 7.6, 3¢”-CH2), 2.07 (2H, dt, J=7.6, 7.6, 16¢”-CH2), 2.22 (2H, dt, J=7.0, 7.4, 4¢”-CH2),

2.48 (2H, t, J=7.0, 2¢”-CH2), 2.82-2.88 (6H, m, 7¢”- 10¢”- and 13¢”-CH2), 3.80-3.87 (2H, m, 3-CH2), 5.33-5.46 (9H, m, 5¢”- 6¢”- 8¢”- 9¢”- 11¢”- 12¢”- 14¢”- and 15¢”-CH, 4-CH), 7.29 (1H, dd, J=8.9, 2.3, 5¢’-CH), 7.73 (d, J=2.3, 7¢’-CH), 8.16 (d, J=8.9, 4¢’-CH), 10.16 (1H, bs, COOH).

4.2.2 PLG2 recombinant expression

E. coli cells (JM109) were transformed with the plasmid containing PLG2 cDNA, kindly provided by prof. Branchini’s lab. Transformation was tested using LB agar + ampicillin (LB+Amp) plates. The cells transformed with the vector were plated with no dilution, and at 1:10 and 1:100 dilution (in SOC medium).

Three colonies were picked from the 1:10 plate, and used to inoculate three 5 mL tubes with 5 mL LB+Amp. These tubes were then used to inoculate three flasks with 245 mL LB+Amp liquid medium; these cultures were then left in incubation shaking at 37 °C 300 rpm, while monitoring the OD at 600 nm.

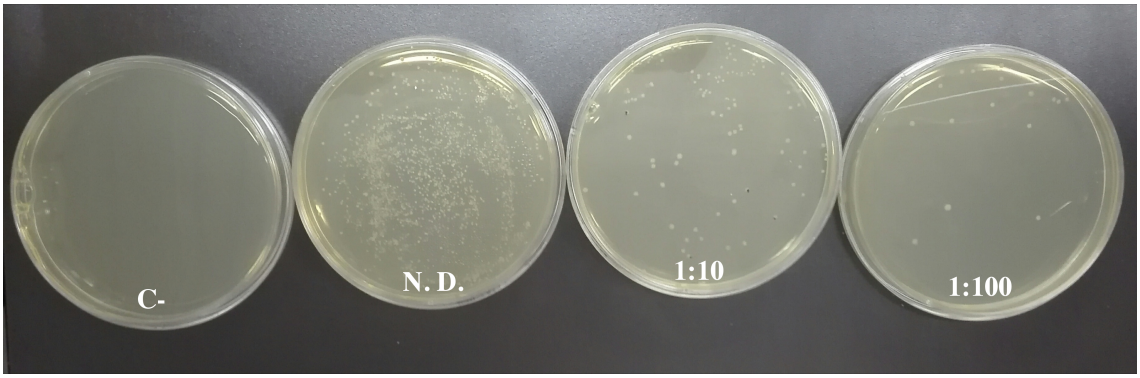

Figure 17. Bacterial plates for PLG2 transformation. JM109 cells were plated on LB-Amp agar after being transformed with the pQE-30 vector, including the PLG2 gene. The cells were plated without being diluted (“N.D.”), or after being diluted ten times (“1:10”) or a hundred times (“1:100”). Non-transformed cells were also plated, as a negative transformation control (C-).

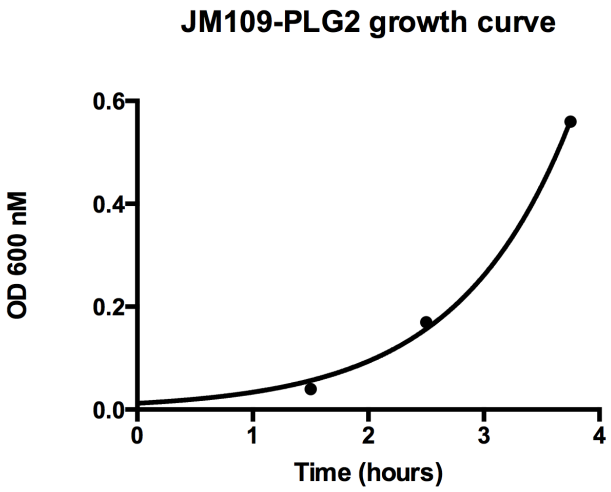

Figure 18. Bacterial growth curve for PLG2 expression.

The 250 mL liquid cultures reached an OD of ~0.56 in less than four hours from incubation, which gave the typical exponential growth curve (fig. 17). At that point the cultures were induced through the addition of IPTG 0.1 mM (final) and transferred at 24 °C, to allow a relatively low-

temperature expression, in order to avoid protein precipitation. The cultures were left to express the protein o/n, shaking at 300 rpm. The following day, the cells were harvested frozen at -80 °C, in order for the protein to be purified later. The cells were then lysed and the protein purified on Ni-NTA agarose resin. A total of five purifications were carried out, their yields are detailed in Table 4.

Table 4. PLG2 yields per purification run.

Culture volume	Total protein yield	Yield per liter
250 mL	8.8 mg	35 mg/l
250 mL	5.5 mg	22 mg/l
375 mL	4.1 mg	11 mg/l
375 mL	10.8 mg	29 mg/l
On average		24.3 mg/l

4.2.3 PLG2 SDS-PAGE analysis

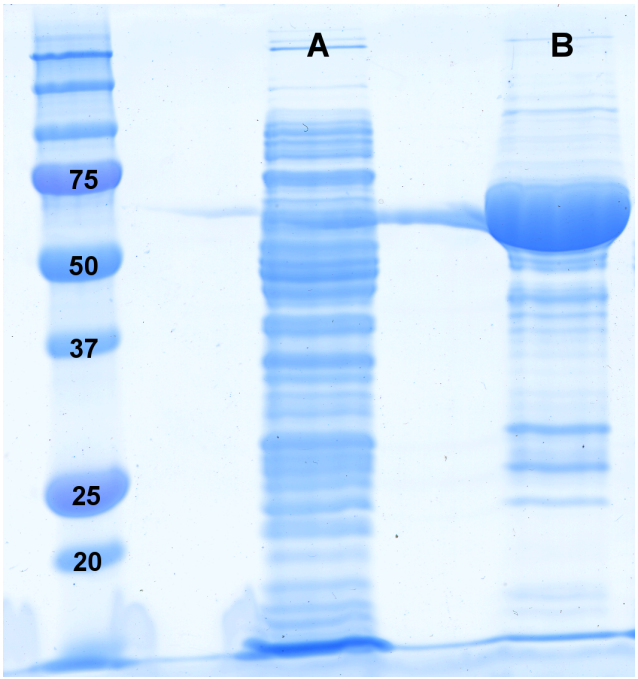

Figure 19. SDS-PAGE gel for PLG2.
On the left lane, the molecular ladder, with some molecular weights indicated in their kDa values.
A: bacterial lysate
B: purified PLG2 concentrate

A SDS-PAGE experiment in denaturing conditions of the bacterial lysate and of the purified protein was set to visually check for the overexpression of the PLG2 luciferase.

The results are shown in fig. 18. The presence of PLG2 (~ 60 kDa) in the lane of the purified protein is evident, however an excess of protein concentrate in this sample (lane B contained 10 µl of concentrated protein, against 2 µl of the lysate in lane A) led to a gel overload. This caused the apparition of some faint bands, belonging to unidentified trace proteins.

4.2.4 PLG2 activity tests with DMSO

The first trial to do was to assess PLG2 emission with different concentrations of DMSO in order to decide the concentration of DMSO in which MAGL substrates could be dissolved into. Five wells of 100 µl of buffer with 50 nM D-luciferin were measured in duplicate with 1%, 2%, 5% and 10% DMSO; five duplicate wells with no DMSO and ten blanks with 100 µl buffer and no luciferine nor DMSO were also measured as well, as positive and negative controls respectively.

The resulting BL was measured each minute for five minutes. The results are reported in figure 20.

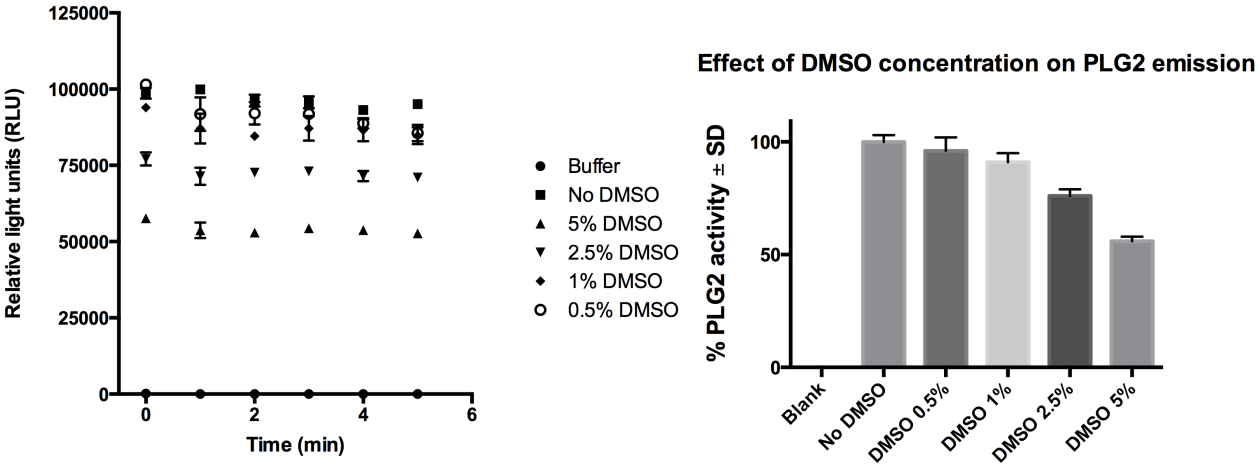

Figure 20. PLG2 luminescence emission in the presence of varying concentrations of DMSO. Each point is the result of a triplicate measurement, and results reported are RLU ± SD.

A final concentration of 2.5% DMSO was chosen for further experiments, since it granted around 75% of the original luciferase activity and allowed a 5% DMSO concentration for dissolving MAGL substrates.

Calibration curves with D-luciferin standards at different concentrations were then built for PLG2, to control the linearity of the response and look for the LOQ of the method. The tested LH_2 concentrations were 0, 5, 12.5, 25, 50, 125, 250, 500, 1000 and 5000 nM; all measurements were performed in triplicate.

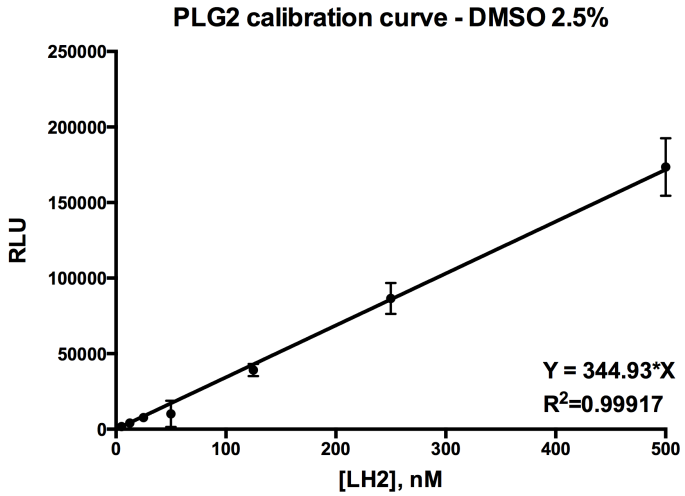

Figure 21. Linearity test for PLG2 on D-luciferin in the presence of 2.5% DMSO. The plotted values are the result of three wells each with the indicated LH_2 concentration, ± SD. The luminescent signal proved to be linear in the 5 – 500 nM range.

The response proved to be linear up to a LH_2 concentration of 500 nM; at 1 mM, the detector was saturated, and higher concentrations could not be determined, therefore a dynamic range of 0-500 nM was established. The LOD and LOQ for the assay were calculated according to these experiments: all blank values from the two independent experiments were averaged (n=6), and the resulting SD was used to calculate LOD and LOQ according to the formulas LOD=3σ/s and LOQ=10σ/s (Shrivastava & Gupta, 2011), where "σ" is the average SD of the blanks and "s" is the slope of the calibration curve. The resulting values were LOD=90 pM and LOQ=300 pM.

4.2.5 Assay development and validation

Since BL had kept its promises of sensitivity, the next step was to test its feasibility for MAGL hydrolysis of ArLuc. All MAGL reactions were performed in-plate, then the PLG2 mix was automatically injected into the plate and the BL intensity measured exactly as reported above.

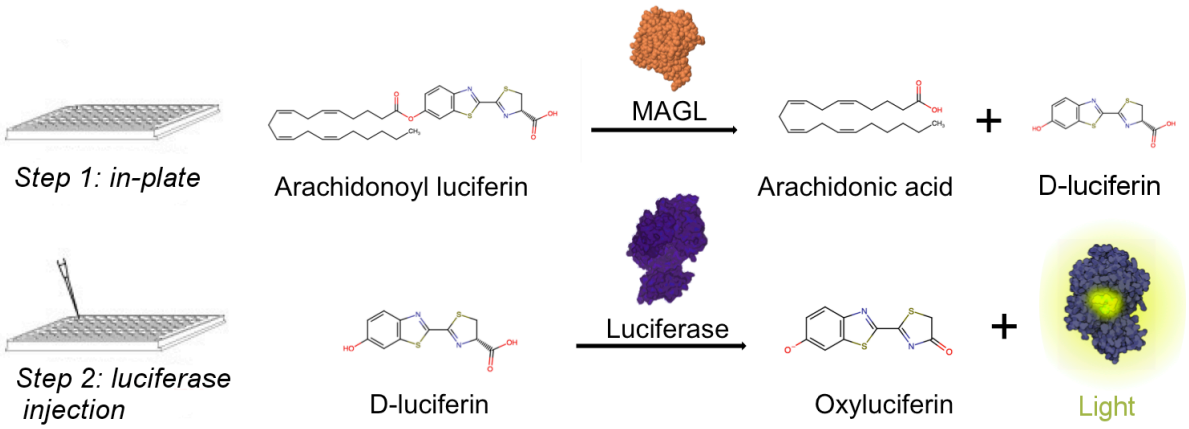

Figure 22. General concept of the assay. MAGL, ArLuc (and the inhibitor, if present) react inside the plate wells. To quantify the LH_2 produced by MAGL hydrolysis, the luminometer injects the PLG2 assay mix, then waits for the non-quantitative flash burst to fade off, and records the luminescence emitted by the PLG2 luciferase.

MAGL experiments were executed as follows. First, 10 µl of MAGL enzyme (25 ng) were pipetted at the bottom of the appropriate well, then 90 µl of the reaction mix, containing the appropriate amout of ArLuc dissolved in 5 µl DMSO (5% final, 2.5% once the PLG2 mix is added), were quickly added to the enzyme, and the plate was read immediately after. The reagent lines and injector were cleaned before and after use with 70% ethanol. For this preliminary test, a solution of ArLuc 10 µM was prepared in DMSO; 45 µl of this solution were pipetted into a test tube and 765 µl of buffer were gradually added, vortexing the tube inbetween the buffer droplets in order to let the DMSO completely dissolve into the aqueous phase. A similar solution was prepared with no MAGL added, to obtain a signal coming exclusively from the spontaneous hydrolysis of ArLuc as well as possible LH_2 impurities. A blank solution was also prepared, mixing 15 µl DMSO with 275 µl buffer.

90 µl of this solution were then quickly added to each well containing MAGL, for a

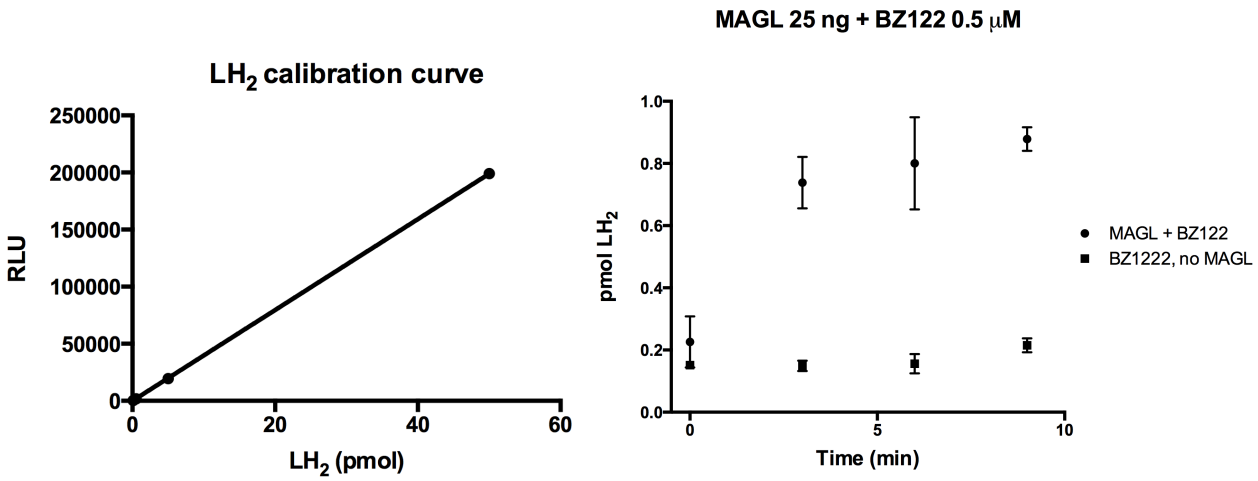

Figure 23. D-luciferin calibration curve for PLG2 (left) (R^2=1.) and tests for MAGL hydrolytic activity on ArLuc (right).

final ArLuc concentration of 25 pmol/well, and the plate was read immediately. Each well was prepared and read in duplicate. The result were four data points from 0 to 9 minutes, each taken 3 minutes after the previous one. A LH_2 calibration curve were also prepared, at final concentrations of 0.1, 0.5, 5 and 50 pmol. The data obtained from the MAGL assay were correlated to pmols of LH_2 according to this curve. MAGL hydrolyzed ArLuc to luciferin and arachidonic acid (fig. 23), yielding 0.66 pmol LH_2 after 9 minutes, about 2.6% of the total ArLuc. Kinetic constants in our conditions were then determined for MAGL with ArLuc as substrate. Experiments were set up in the same fashion as above and, after some preliminary tests to "fish" for a rough K_m value (not shown), we set up an experiment with different ArLuc concentrations to determine the precise K_m and V_{max} values. The concentrations chosen were 0.5, 1, 5, 8, 10 and 20 μM, therefore staying in Michaelis-Menten conditions (Bisswanger, 2014). After the resulting values were converted into LH_2 pmoles in accordance with the calibration curves, the data points were regressed to a linear curve. The slope of each curve was converted into pmoles/min/mg produced by the enzyme, and the values between the various experiments were averaged and fit to a Michaelis-Menten equation, corrected for substrate inhibition (fig. 24).

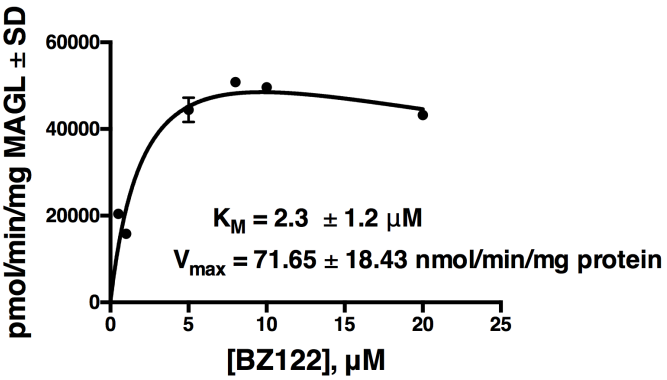

Figure 24. Kinetic profile for MAGL in the assay conditions. Every point is the average of three values ± SD. The curve model is that of the Michaelis-Menten equation corrected for substrate inhibition: Y=Vmax*X/(Km + X*(1+X/Ki))

The final step was validation with a known MAGL inhibitor. In order to avoid false positive results, the behavior of PLG2 was tested in the presence of known MAGL inhibitors: MAFP, URB602 and JZL184.

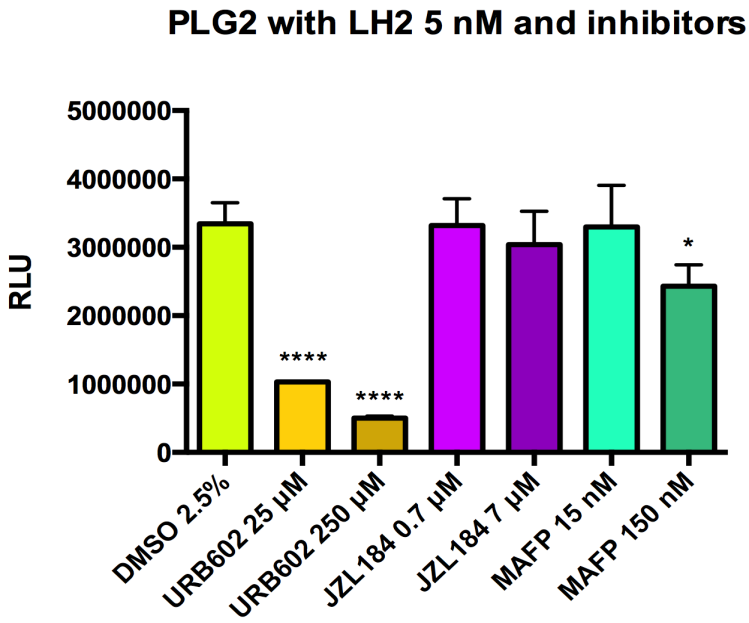

Figure 25. PLG2 luminescence emission in the presence of different concentrations of various known MAGL inhibitors.The values reported are the average of three replicates. The asterisks indicate a significant deviance of the values from the 2.5% DMSO samples with no inhibitor added (yellow bar). ****: adjusted P value < 0.0001; *: adjusted P value = 0.0403.

The assay was carried out in the same conditions as negative controls for MAGL ones: the DMSO was used to dissolve the appropriate inhibitor concentration instead of ArLuc, and the wells contained 5 nM LH_2 (final). Each data point was taken in triplicate. The concentrations used were the IC_{100} (defined as the IC_{50} literature value plus the SD, rounded up afterwards), and ten times this concentration.

The results are shown in fig. 25. According to the results, it looked like relatively high concentrations of MAFP can have an effect on PLG2, while JZL184 has no relevant effect on PLG2. It is very interesting to note, though, that a carbamate inhibitor studied for hydrolases like URB602, inhibits a luciferase in a quantitative fashion.

For our validation, we then chose JZL184, the well-known first specific inhibitor for MAGL with high potency (Long et al., 2009).

The inhibitor was prepared in DMSO stocks forty times more concentrated than the final JZL184 concentration. The procedure followed was the same as for determination of kinetic constants, but this time the stock concentration of ArLuc was 320 µM (dilution factor 40, final concentration 8 µM), and the DMSO volume added to the mix was half as before for both inhibitor and substrate. Each point was assayed in triplicate, then the slopes were calculated as described above, but this time without converting

them to LH_2 picomoles; instead, the slope of the line coming from the assay without inhibitor was taken as the 100% of the activity, while the slopes of the other curves were converted into various activity percentages referred to this curve.

The final JZL184 concentrations used were 0,10 nM, 100 nM, 500 nM, 1 μM, and 100 μM. Results are reported in fig. 26; the found IC_{50} is about half that found in literature, but still stays in the order of magnitude of that reported previously, and at the lower range found in our previous publication (Lauria et al., 2015; Juha R. Savinainen, Yoshino, Minkkilä, Nevalainen, & Laitinen, 2010).

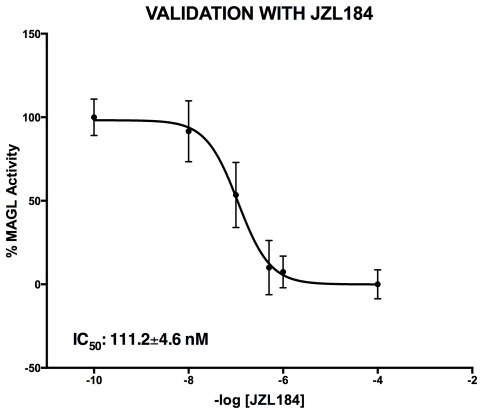

Figure 26. Inhibition profile for JZL184 on MAGL in the assay conditions. Each point is the average of three different wells ± SD.

4.3 Conclusion

We synthesized ArLuc, an arachidonoyl luciferin compound specially designed for MAGL BL assays. MAGL was found to be able to hydrolyze it, producing free D-luciferin which can be detected via BL methods.

We also produced and purified recombinant PLG2 from bacterial cells, with good yields. It is interesting to note that, as reported in Table 4, while the difference in yield between the single purification runs is noteworthy, the average protein yield conforms precisely to the expected yield of ~24 mg/l of culture reported by Branchini's group (Branchini & Southworth, 2017). The luciferase was then proved capable of catalyzing its peculiar reaction even in the presence of significant concentrations of DMSO, which confirms its exceptional stability and resistance to denaturing conditions.

The method itself has, as promised, various pros and cons: it has an astonishing sensitivity, with a LOQ below the nanomolar range – namely, the assay is able to quantify LH_2 from 60 attomoles per well. On the other hand, the very nature of luciferase emission in the fashion of "flashes" makes it necessary to prepare a different experiment for each time point, if continuous production of enzymatic action is to be monitored. Even adopting this way to circumvent this limitation, it won't be as reliable as a continuous assay anyway, since each point actually is an experiment on its own. Also, this makes the assay less practical and cheap than a fluorometric one. A single-

point measurement could solve these issues: while unsuitable to detect the initial rate of the enzyme activity (Bisswanger, 2014; Purich, 2010), the assay could be further tailored to use a sub-V_{max} substrate concentration and to measure the hydrolase activity at its steady state in presence of absence of an inhibitor at a set time point (3-6 minutes seem suitable beginning points for assay design). This should be an easy adaptation assaying methodology, though, and it would solve most of the current disadvantages. BL assays, however, intrinsically offer multiple potential applications due to their selectivity and sensitivity. It was also interesting to find that a carbamate inhibitor such as URB602, which initially seemed extremely selective for MAGL, inhibits our luciferase. If nothing else, this reminds us of the unpredictability of unwanted interactions when developing a new drug, which should be investigated as carefully and early as possible. Regardless of assay developments, a luciferase which works in the presence of high quantities of DMSO is a precious addition to the enzymatic assay toolbox.

4.4 Experimental section

Reagents and materials

All reagents and solvents were bought from Sigma-Aldrich, unless specified. IPTG and ampicillin were bought as powders and dissolved into ddH_2O to a 0.84 M (200 mg/mL) and a 100 mg/mL stock solution, respectively. The solutions were then filtered on a 0.2 μm membrane, divided into 200 μl aliquots and stored at -20 °C. SOC medium for transformation was bought from Thermo Fisher (Waltham, MA, USA). All other buffers were made in-house according to the following recipes; these buffers should be stored at 4 °C and are viable for one week, unless specified. All plasticware used to work with bacteria was sterile, the culture mediums were sterilized using the autoclave, while the buffers were filtered on a 0.2 μm membrane.

LB (LB-Lennox) culture medium: 10 g/l tryptone, 5 g/l yeast extract, 5 g/l NaCl. Bring to desired volume with ddH_2O. When needed, ampicillin 100 μg/mL was added right before use, to minimize degradation.

LB agar: 15 g/l agar, 10 g/l tryptone, 5 g/l yeast extract, 5 g/l NaCl. Bring to desired volume with ddH_2O. When needed, ampicillin 100 μg/mL was added right before preparing the plates, to minimize thermal degradation.

PCB buffer: 50 mM Tris, 150 mM NaCl, 1 mM DTT, 1 mM EDTA. Adjust to pH 7 with HCl.

PBS buffer: the buffer is commonly prepared as a 10x solution with 400 mM NaCl, 27 mM KCl, 100 mM Na_2HPO_4, 1.8 mM KH_2PO_4 in ddH2O (pH 7.3), then filtrated on 0.2 μm membranes and stored at RT. The solution is viable for a long time (about 6 months). When PBS buffer is needed, the above 10x solution is diluted 1:10 with ddH_2O; the PBS buffer is then normally stored at 4 °C and viable for 1 week.

Four 10 mL elution solutions were prepared prior to the purification step dissolving imidazole in PBS at the final concentrations of 50 mM, 100 mM, 250 mM and 500 mM. These solutions were then kept in cold room at 4 °C.

TE buffer: 10 mM Tris, 1 mM EDTA. Bring to pH 8 with HCl.

Tris-HCL buffer: 50 mM Tris, 1 mM EDTA. Bring to pH 8 with HCl.

PLG2 assay mix for LH2 determination: 0.8 mM ATP, 10 mM MgSO4 in 50 mM Tris-HCl buffer.

Lysozyme (from egg white) solution is prepared by dissolving 10 mg/mL lysozyme in PBS and stored at 4 °C until use. RnaseA (from bovine pancreas) solution was prepared dissolving 10 mg/mL RNaseA in 10 mM Tris buffer, pH 7.5, containing 15 mM NaCl. DNaseI solution is 5 mg/mL DNaseI (from bovine pancreas) in 10 mM Tris buffer, pH 7.5 containing glycerol (1:1, v/v), 50 mM NaCl, 10 mM MgCl2, and 1 mM DTT.

Synthesis of the bioluminescent substrate

To a stirred solution of arachidonic acid (0.18 mmol) in anhydrous CH_2Cl_2 (3 mL), under an argon athmosphere and cooled in an ice bath, was added DMAP (2 mg, 0.01 mmol) and 6-Hydroxy-2-cyanobenzothiazol (30 mg, 0.18 mmol). DCC (72 mg, 0.35 mmoli) was added to the reaction mixture at 0 °C, dropwise. Stirring was continued o/n at room temperature. Product formation was confirmed by TLC (silica gel, mobile phase 95% petroleum ether, 5% ethyl acetate). The CH_2Cl_2 solution was washed twice with saturated $NaHCO_3$ (2.5 mL), dried on anhydrous Na_2SO_4 and concentrated to give the crude product. The resulting brown oil was filtrated on column chromatography on silica gel by the same mobile phase as TLC, 95% petroleum ether, 5% ethyl acetate. The column chromatography was followed *via* TLC in the same conditions, and gave a yield of 80 mg (0.17) of the nitrile product, a colorless oil.

The nitrile and D-cysteine hydrochloride monohydrate (0.19 mmol) were dissolved in a mixed solvent of 1.5 mL MeOH and 400 µl CH_2Cl_2, in an argon atmosphere. 500 µl ddH_2O and K_2CO_3 (0.19 mmol) were added, and the solution was kept stirring at RT for 1 hour. Another TLC was performed, in the same conditions as above, to control the product formation. HCl 1M was added until the solution reached a 2-3 pH value. A few mL of the organic reagents were evaporated under vacuum using a rotary evaporator, then the precipitate was collected and washed with water, to give ArLuc as a white solid. The filtration gave 30 mg of ArLuc (MW=566.77 U), which structure and purity were confirmed by NMR analysis.

Bacterial transformation

The vector used for PLG2 recombinant expression was pQE-30 plasmid, containing the PLG2 cDNA sequence and His-tag. The vector samples were kindly provided by prof. Branchini's lab. The vector was carried to Italy adsorbed on filter paper, and was desorbed as follows: the paper was cut 1-2 mm around the area where the plasmid had originally been spotted (and circled with a pencil), then the paper circle was put into a

1.5 mL Eppendorf tube with clean tweezers. 100 µl TE buffer were pipetted into the tube, then the tube was vortexed briefly and incubated at RT for 5 minutes. The tube was then vortexed briefly again and centrifuged at 500 x g for a few seconds. 1 µl of the DNA was used to quantify the cDNA plasmid at a NanoDrop™ 2000 Microvolume Spectrophotometer (Thermo Fisher Scientific, Waltham, MA, USA), using the DNA preset protocol (quantitation based on λ=260 nm, λ=280 nm, and A_{260}/A_{280} nm ratio).

The *E. coli* cells used for the transformation and expression were Single-Use Promega JM109 Competent Cells (Promega, Fitchburg, WI, USA). All steps involving the cells were performed wearing sterile gloves, and in proximity to a Bunsen burner with blue flame, to avoid bacterial or mold contamination. Two aliquots (50 µl each) of cells were taken out of the deep freezer (-80 °C), and left to thaw on ice. After thawing, 10 µl of the TE plasmid solution (final plasmid concentration 0.22 ng/µl) was added to one aliquot. The other aliquot was used as a negative control of the transformation, adding 10 µl of ddH_2O instead of the TE+vector solution. Both tubes were then left on ice for 10 minutes. A heat shock procedure was now carried out: the cells were put into a water bath at 42 °C for 45 seconds, then quickly put on ice again for 2 minutes, being careful not to shake the tubes in order to avoid mechanical stress to the cells. 900 µl of SOC culture medium was added to each tube, which were then put at 37 °C, shaking at 300 rpm, for 1 hour. Transformation was tested plating the cells on LB agar + ampicillin 100 µg/mL (LB+Amp) plates: the cells were first diluted 1:10 and 1:100 in fresh SOC medium, then 100 µl from each dilution was plated on an LB+Amp agar plate and put into an incubator set at 37 °C, o/n.

PLG2 expression in liquid bacterial cultures

The typical culture setup was of three 500 mL sterile flasks, with 245 mL LB culture medium each, which was poured under a laminar flow hood. During all the subsequent steps, the flasks were open in the proximity of a Bunsen burner lit on blue flame, to avoid external contamination.

Three 5 mL “snap-cap” tubes with 5 mL LB+Amp were inoculated with three colonies picked from the 1:10 plate, using a sterile microbiology inoculation loop. The tubes were left at 37°C, shaking at 300 rpm o/n, along with an uninoculated tube with 5 mL LB+Amp as a control for contaminations.

After 16h of growth, the three inoculated tubes were poured into one of the three 500 mL flasks each (final volume 250 mL); these cultures were then left on incubation shaking at 37 °C 300 rpm, while monitoring the bacterial growth through the measurement of the cultures OD. 1 mL of culture into a disposable plastic cuvette. Meanwhile, the IPTG stock solution was diluted to a 0.1 mM working solution with sterile ddH_2O water.

At that point the cultures were added with 250 µl IPTG 100 mM, for a final concentration of 0.1 mM and transferred outside the incubator at controlled temperature of 24 °C, still shaking at 300 rpm, o/n. The following day, the cultures were evenly poured into two centrifuge bottles, dividing them into two ~325 mL aliquots, and the cells were harvested through 10 min ultracentrifugation at 5000 x g, with the rotor bucket at 4 °C. The supernatant was discarded and the two aliquots of cells deep-frozen at -80 °C, in order for the protein to be purified at a later time.

PLG2 protein purification

During purification, all solutions were kept on ice and all centrifugation steps were performed with the rotor bucket set at a temperature of 4 °C. Resuspension buffer was prepared immediately prior to the purification, adding imidazole 5 mM and 38 µl of a PMSF solution (2.5 mg of PMSF dissolved into 100 µl ethanol 95%, prepared right before use) to 38 mL PBS buffer. Each bacterial pellet was thawed on ice and resuspended in the 38 mL of resuspension buffer (10% volume of culture) using a pipette, being careful to avoid foaming or bubbling. 3.8 mL of a lysozyme 10 mg/mL solution were added, then the cells were left on ice for 20 minutes. The cell lysis was then completed with sonication, carefully keeping the cells on ice and applying 3 bursts of 10 seconds each. The sonicator used was a SONOPULS HD2070 (BANDELIN, Berlin, Germany), at ~50% power (~35W). 38 µl of the DNase and RNase solutions were added to the lysate, and it was left on ice for 5 minutes. After a last addition of 1% (v/v) Triton X-100, the lysate was left on ice for 5 more minutes. The lysate was now centrifuged at 20.000 x g, for 45 minutes, then kept on ice.

For affinity chromatography purification of the protein, 0.5 mL of Ni-NTA agarose slurry (Thermo Fisher) were used. The slurry was pipetted into a 50 mL tube, centrifuged at 500 x g for 5 minutes, and the supernatant was removed with the aid of a micropipette. The Ni-NTA agarose was washed with 20 mL of PBS, then it was centrifuged at 500 x g for 5 minutes, and the buffer discarded. This was repeated for

four more times in order to completely remove the storing ethanol from it. The lysate was now added to the slurry and incubated for 120 minutes in a cold room at 4 °C, shaking gently in order to allow PLG2 binding to the resin.

After the binding, the resin was centrifuged at 500 x g, for five minutes and the supernatant removed and stored at 4 °C, in case of poor binding. The resin was washed with 5 mL ice cold PBS + 20 mM imidazole for four times, each time centrifuging it at 500 x g for 2 minutes, then discarding the buffer.

The resin was poured into a 10 mL Pierce™ Disposable Column (Thermo Fisher). The protein was eluted with PBS with increasing concentrations of imidazole. The imidazole concentrations used were 50 mM, 100 mM, 250 mM and 500 mM. For each elution step 1 mL of elution solution was pipetted onto the resin and collected in an Eppendorf tube, except for the last one (500 mM) where 2 mL were used. The whole elution process was carried out in cold room at 4 °C.

The fractions were then put on ice and quantified using the Bradford Protein Assay (Bio-Rad, Hercules, CA, USA), with BSA as a standard. The fractions with at least 1 mg/mL were pooled. In order to remove the imidazole bound to PLG2, the protein concentrate was trasferred with a 10 mL disposable syringe into a 3-12 mL Slide-A-Lyzer™ (Thermo Fisher) dialysis cassette with a 10.000 Da cutoff, and put into 1 L PCB buffer. The cassette was left to dialyze at 4°C for 24 hours with slow stirring. The buffer was changed every 3-4 hours (or o/n) for 5 times.

The protein was then recovered from the cassette with a new 10 mL disposable syringe and quantified a second time with the Bradford assay. The protein concentrate was fractioned into 100-200 µl aliquots (the typical concentration of the protein concentrate was ~2 mg/mL), using 250 µl PCR tubes. The tubes were flash-frozen putting them into liquid nitrogen, and stored at -80 °C.

PLG2 SDS-PAGE

SDS-PAGE experiments were performed using Mini-PROTEAN® II handcast systems (Bio-Rad, Hercules, CA, USA) kits for both equipment and reagents, unless specified. All SDS-PAGE gels were handcast into 50 mL Falcon tubes. Table 5 reports the quantities used for each gel casting.

Table 5. Recipes for SDS mini gels. The table reports the quantities needed to cast two complete gels.

	Resolving gel	**Stacking gel**
dH2O	3.3	1.7
30% Acrilamide/BIS	4.0	2.0
1.5M Tris HCl ph 8.8	2.5	1.25
10% SDS	100 µl	50
10% APS	100 µl	50
Temed	5 µl	2.5
Totale volume	**10 mL**	**5 mL**

Glass plates for the glass cassette sandwich were checked for the absence of chips or dents and carefully cleaned with 95% ethanol and lint-free cloths prior to assembling the glass cassette sandwich. The stacking and resolving gel were prepared in two separate 50 mL Falcon tubes, mixing carefully all reagents except for Tetramethylethylenediamine (TEMED). Then the TEMED was added to the resolving gel solution, the tube was closed, the solution gently mixed by inverting the tube, and the gel was immediately poured into the glass chamber for casting. Ethanol was poured on top of the separating gel solution during the polymerization process.

After about one hour, once the resolving gel polymerized completely, the overlay ethanol was poured off, the resulting empty space was rinsed with ddH_2O, and then carefully dried with lint-free tissue paper. TEMED was added to the stacking gel solution, then the solution was mixed as per above and the stacking gel solution was poured on top of the separating gel. The plastic comb was placed on top of the glass cassette, and the solution was left to polymerize for about another hour. The comb was then removed, and the gel was ready for use. More than one gel could be cast at the same time to be used within 24 hours: in this case, the comb was not removed, the whole glass cassette was enveloped with plastic paraffin film (Parafilm M – Bemis NA, Neenah, WI, USA) and stored at 4°C until use.

The lysate samples were prepared adding 5 µl of the bacterial lysate to 1 µl 500 mM DTT, 2.5 µl Laemmli buffer 4x and 1.5 µl H_2O. Purified protein samples were prepared adding 10 µl of the concentrated protein to 2 µl 500 mM DTT, and 4 µl Laemmli buffer. The tubes with the samples were put for 5 minutes into a Thermoblock set at 95°C, then

the gel was put into the electrophoretic cassette, the cassette was filled with running buffer, and the sample was carefully pipetted into the wells of the gel. The first and last well of the gel were loaded with 5 µl Precision Plus Protein Standards™ – All Blue. The gel was run at 200V for 40 minutes.

The gel was coloured with Coomassie Blue through a microwave-assisted, water-based method: first, it was immersed in 100 mL dH_2O, microwaved for 1 minute at 800W, then left on mild agitation for 2 minutes. The whole procedure was repeated two additional times. The staining was achieved immersing the gel in 100 mL SimplyBlue™ SafeStain (Thermo Fisher, Waltham, MA, USA), microwaving the gel at 800W for 30 seconds, then leaving it on mild agitation for 15 minutes. The excess staining was removed by repeated washing steps with dH_2O and leaving the gel in dH_2O on mild agitation o/n.

PLG2 DMSO trials

For all experiments, the buffer used was Tris-HCl 50 mM pH 8.0, EDTA 1 mM.

Before each experiment, the PLG2 fractions were unthawed at 37°C until only a small fraction of the solution (the size of about a small grain of rice) was still frozen, then left to unthaw at 4 °C. These unthawed fractions were used to prepare PLG2 assay mixes as needed.

A PLG2 assay mix was prepared with Tris-HCl 50 mM pH 8.0 EDTA 1mM, NaATP 0.8 mM, $MgSO_4$ 10 mM, PLG2 0.2 mg/mL. NaATP was prepared by dissolving a small amount (typically the amount picked by the tip of a small spatula) of powder in 1 mL Tris-HCl buffer, then 20 µl of the solution were added to 980 µl uf buffer, and the concentration of the solution was spectrophotometrically determined at λ=260 nm, applying Lambert-Beer's law as $C = \frac{A}{15400} \times 200 \times 1000$, where "A" is the recorded absorbance. Any leftover mix could be stored at 4 °C and used within 48 hours with no loss in performance.

A concentrated solution of LH_2 was prepared in a similar fashion to the NaATP one: the reading wavelength was λ=266 nm, and the formula applied $C = \frac{A}{7600} \times 200 \times 1000$, in accordance to LH2 different ε (Branchini & Southworth, 2017).

The luminometer used was a GloMax®-Multi+ Microplate Multimode Reader (Promega, Fitchburg, WI, USA). All measurements were performed as follows: 100 µl

of solution containing the amount of LH2 to be detected were pipetted into the wells of a white 96-well plate. The injection system of the instrument would then automatically inject 100 µl of PLG2 assay mix into the fisrt well to be analysed. After the injection, the luminometer had a lag time of 1 second, then integrated the luminescence signal for 1 second. The luminometer would then pass to the following well to be analysed.

Five wells of 100 µl buffer with 50 nM D-luciferin were measured in duplicate with 1%, 2%, 5% and 10% DMSO; five duplicate wells with no DMSO and ten blanks with 100 µl buffer and no luciferine nor DMSO were also measured as well, as positive and negative controls respectively. Each triplicate was prepared in a tube to ensure reproducibility. First, 12, 24, 60 or 120 µl DMSO, respectively, were pipetted into the tube; then the concentrated solution of LH2 was diluted to a 0.5 µM working solution, 120 µl of this working solution were added to the DMSO – a blank was prepared, skipping this step. The appropriate amount of Tris-HCl buffer was then pipetted to bring the volume to 1.2 mL. 100 µl of this solution was pipetted into each of the ten plate wells.

Linearity tests

Calibration curves with D-luciferin standards at different concentrations were built, pipetting 20 µl DMSO in a test tube, then adding the appropriate amount of a LH_2 working solution (prepared as above, to a final concentration of 50 µM). The tested LH_2 concentrations (in-well) were 0, 5, 12.5, 25, 50, 125, 250, 500, 1000 and 5000 nM; all measurements were performed in triplicate.

MAGL bioluminescent assays and kinetic tests

Reagent solutions for MAGL experiments were prepared as follows. The quantities are intended for the typical assay, where 4 time points, each in triplicate, were read.

The ArLuc substrate was dissolved in DMSO to a 1 mM stock solution; this stock solution was diluted with DMSO to a working solution 20x the final desired concentration in the assay (e.g. 100 µM for a 5 µM assay). A reagent solution was prepared using this working solution: first, 70 µl of the ArLuc working solution were pipetted into an Eppendorf tube (5% final, 2.5% once the PLG2 mix was added), then 1190 µl of Tris-HCl buffer were added dropwise to the DMSO, vortexing the tube two or three times during the addition to avoid substrate precipitation. Reagent solutions for the negative controls were prepared as well, in the same fashion as above, but adding

1330 µl of Tris-HCl buffer instead. A blank solution and a LH_2 calibration curve were also prepared: the blank solution was obtained mixing 15 µl DMSO with 275 µl buffer, while the calibration curve was obtained pipetting appropriate amounts of the 500 nM LH_2 working solution into test tubes with 20 µl DMSO, then adding Tris-HCl ph8 buffer with 1 mM EDTA to a final volume of 400 µl. The final LH_2 concentrations were 2, 5, 10, and 100 nM, DMSO 5%. The data obtained from the MAGL assay were correlated to pmols of LH_2 according to this curve: in order to avoid confusion due to the MAGL reaction volume (100 µl) and the final volume with PLG2 assay mix added (200 µl), all LH_2 quantities were expressed in terms of pmol/well, rather than molar ones.

MAGL assays were set up as follows. The GloMax reagent lines and injector were cleaned before and after use with 70% ethanol, then abundantly rinsed with ddH_2O water. 100 µl of the negative control reaction mix were pipetted in each appropriate well. hMAGL (Cayman Chemical, Ann Harbor, MI) was diluted to 250 ng/mL in 50 mM Tris-HCl buffer pH 8, 1mM EDTA. 10 µl of the diluted MAGL enzyme (25 ng) were pipetted at the bottom of the appropriate well, then 90 µl of the reaction mix were quickly added to the enzyme, and the plate was read immediately after as per above.

The result were four data points from 0 to 9 minutes, each taken 3 minutes after the previous one.

The kinetic values were determined for MAGL with ArLuc as substrate. Experiments were set up in the same fashion as the ones above. This time, six reagent solutions were prepared, for ArLuc in-well final concentrations of 0.5, 1, 5, 8, 10 and 20 µM. The experiment was performed independently for two times, each time in duplicate or triplicate. The signal coming from negative control solutions was subtracted to that of the corresponding concentration and time point, in order to consider only the signal due to enzymatic hydrolysis. After the resulting values were converted into LH_2 pmoles in accordance with the calibration curves, the data points were regressed to a linear curve. The slope of each curve was converted into pmoles/min/mg produced by the enzyme according to the formula $\frac{\frac{pmol}{min}}{mg} = \frac{LH2\ curve\ slope}{mg\ MAGL}$. The values between the various experiments were averaged and fit to a Michaelis-Menten equation, corrected for substrate inhibition, in accordance to the highest r^2 value (best-fit). All calculations were performed with the Prism 6 software (GraphPad Software, La Jolla, CA, USA).

PLG2 inhibition

Prior to the validation, the potential PLG2 inhibition by known MAGL inhibitors was determined.

First, stock solutions were prepared for JZL184, URB602 and MAFP (Sigma-Aldrich): MAFP ethanol solution was diluted in DMSO to a 600 µM inhibitor solution, while JZL184 and URB602 powders were dissolved in DMSO to 280 µM and 10mM inhibitor solutions, respectively. Each inhibitor solution was then further diluted 1:10.

Six reagent solutions were prepared, two for each inhibitor solution (diluted or not). 10 µl DMSO and 10 µl inhibitor solution were slowly added with a 4 µM LH_2 working solution, so that the final concentration would be 100 nM (50 nM after PLG2 addition). Tris-HCl pH8 50 mM, 1 mM EDTA was added dropwise to a final volume of 400 µl, vortexing every 3 drops added to avoid substrate or inhibitor precipitation. 100 µl of each solution were added to the micro plate wells, and the luminescence analysis was performed as described above.

MAGL assay validation

Five JZL184 working solutions were prepared.

Table 6. Concentration of JZL184 working solutions and corresponding concentration on MAGL.

JZL184 working solution concentration	**JZL184 concentration in-well**
4 mM	100 µM
40 µM	1 µM
20 µM	500 nM
4 µM	100 nM
400 nM	10 nM
0	0 (100% MAGL activity)

Validation solutions were prepared pipetting 35 µl JZL working solution into an Eppendorf tube (JZL184 concentrations are reported in Table 6). 1190 µl Tris-HCl pH 8, 50 mM, 1 mM EDTA buffer were carefully added dropwise, vortexing after every 3 drops to avoid inhibitor precipitation. 140 µl diluted MAGL solution (25 ng/well) were added, and the tubes were left to incubate at RT for 30 minutes. A blank solution,

consisting of 20 µl 380 Tris-Hcl buffer, was also prepared, as well as a negative control without MAGL (35 µl DMSO, 1330 µl buffer).

10 µl DMSO with ArLuc 320 µM (in-well concentration 8 µM) were pipetted, and 90 µl of the validation and negative control solutions were pipetted onto it, then the luminescent analysis quickly began. The outptu consisted of a blank value in triplicate and four time points for every other solution, all taken at 3 minutes of distance (0, 3, 6 and 9 minutes) in triplicate.

The blank and negative control values were subtracted from all other RLU values. The resulting points were averaged and regressed to a linear curve ($r^2 \geq 0.8348$ for every curve). The slopes were normalized, then that of the curve coming from the 0 µM JZL184 wells was taken as the 100% value, and the others were related to this one. The IC50 was calculated with Prism 6 (GraphPad software) using a log (inhibitor) vs. response – Variable slope (four parameters) function.

5. BACTERIAL RECOMBINANT EXPRESSION OF ABHD6 AND ABHD12

5.1 Introduction

Most of the knowledge we have on the two hydrolases ABHD6 and ABHD12 comes from studies conducted on animal models or transiently transfected cell lines (Blankman et al., 2013, 2007; Fiskerstrand et al., 2010; Marrs et al., 2010; Muccioli et al., 2007; Parkkari et al., 2014; J. R. Savinainen et al., 2012). In particular, the ABHD6 and ABHD12 recombinant expression was obtained through transient trasfection in HEK-293 and COS-7 cells (Blankman et al., 2007; Navia-Paldanius et al., 2012); while the use of these cell lines in research is well-established since the '70s and '80s respectively, and the techniques developed for these characterizations are indeed ingenious and trustworthy, they do not allow an intrinsic protein characterization nor, more importantly, provide enough pure protein for crystallographic studies with relative ease.

Moreover, when working with whole cells or cell lysates, even the best experimental setup cannot attribute the observed activity exclusively to the overexpressed enzyme, due to the very nature of cell assays.

The assays reported by the Cravatt group (Blankman et al., 2007) are based on an LC-MS technique: the only screening assay published for these two hydrolases involves a sequence of four enzymatic reactions (Juha R. Savinainen et al., 2016a). After the hydrolysis of the substrate (a 1-AG) by the ABHD, the resulting glycerol is phosphorylated using ATP by a glycerol kinase, giving glycerol-1-phosphate which, in the presence of oxygen, is oxidated by a glucose phosphate oxydase to dihydroxyacetone phosphate, while the oxygen is reduced to hydrogen peroxide. Horseradish peroxidase catalyzes the last step, using H_2O_2 to convert the proprietary reagent Ampliflu™ Red into resorufin, which is finally fluorometrically detected.

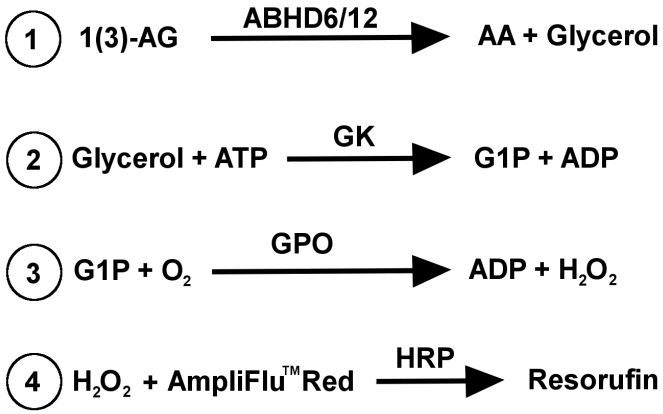

Figure 27. Reaction scheme of the assay for ABHD6 and ABHD12 proposed by Juha Savinainen and colleagues (Savinainen et al., 2016).
The scheme gives a good impression of how the misquantification occurring during a single step may compromise the outcome of the whole assay.
Image made on the footprint of the authors' one.

This assay is tailored to work on

96-well plates and can screen up to 40 inhibitors for each plate: this makes it undoubtedly suitable for HTS. However, it still raises some perplexities. The need for four coupled enzymatic reaction steps means that the chances of an incorrect output due to an undetected activity loss of a stored enzyme aliquot are four times more likely than those of a single-step enzyme assay. A big plus of the assay is that it involves native substrates as the 1-AGs (although for ABHD12 the "native" characteristic of 1-AGs is debatable, see 1.1.3): nonetheless, this necessarily involves glycerol as a substrate which, as the same authors point out, puts the assay at risk of contaminations from residues of glycerol-containing detergents, if these are used for laboratory glassware and plastic reservoirs. Last but not least, the assay remains dependent on hABHD6-HEK cell lysates, carrying over the uncertainty described above.

A more convenient way to explore the properties of ABHD6 and ABHD12 could be the recombinant expression in bacterial hosts, namely the widespread *E.coli* BL21 strains: bacterial recombinant expression is generally viewed as the easiest, fastest, most convenient and economically efficient way to produce active proteins for a variety of purposes, including structural biology applications and enzymes for biochemical assays. The problem is posed by membrane proteins, which are difficult to produce for *E.coli* since the organism doesn't have a dedicated machinery for the membrane insertion of the newly produced protein (Bernaudat et al., 2011; Chen, 2012). However, there are many reported cases of successful recombinant membrane protein expression in *E.coli*, to the point that the bacterium was found to be better than other, more promising, bacterial hosts such as *Lactococcus lactis* for the production of integral membrane proteins (Surade et al., 2006).

As a first step for the development of *in vitro* assays for the determination of ABHD6 and ABHD12 properties and inhibitor screening, we attempted the production of these two human membrane proteins in a *E. coli* BL21 strain. It should be noted that ABHD12 is a glycosylated protein, and this glycosylation cannot be achieved by unmodified *E. coli* cells.

The main problem that can turn up during heterologous protein expression in *E.coli* (be them membrane proteins or not) is the storing of the recombinant protein in inclusion bodies (IBs) by the host organism. IBs are functional, non-toxic amyloids occurring in bacteria during the production of heterologous proteins, usually found in the 50-800 nm size scale (Rinas et al., 2017); they are the result of the overexpression of an insoluble

protein (Jonasson, Liljeqvist, Nygren, Stahl, & Ståhl, 2002), and can be considered a bacterial stress response to the forced overproduction of proteins (Rinas et al., 2017). IBs have traditionally been regarded as an inevitable drawback of bacterial recombinant production, because the protein they contain is mostly inactive due to incorrect or partial folding; while this view is recently being put into discussion by the consideration that they actually can be a valuable source of protein which can be recovered and correctly folded, we still wanted to avoid their formation as much as possible during these initial steps (García-Fruitós et al., 2012; Ramón, Señorale-Pose, & Marín, 2014; Rinas et al., 2017).

A simple, classical way to prevent the accumulation of misfolded, insoluble protein within IBs is the avoidance of excessive protein production following the induction (Jonasson et al., 2002): our attempt was to use mild expression conditions, achieved using a medium culture such as lysogeny broth (LB), running the expression at sub-optimal temperature and using a moderate concentration of inducer instead of the recommended one. These adjustments were meant to avoid excessive stress to the bacteria, which is increased when producing non-bacterial transmembrane proteins with respect to bacterial ones and can lead to stopped growth (Xu & Link, 2009), and an "overcrowded" intracellular milieu, which is more likely to produce amyloid aggregates (Magno, Caflisch, & Pellarin, 2010).

5.2 Results and discussion

5.2.1 ABHD6 and ABHD12 recombinant expression

We decided to use a bacterial plasmid with an His-tag (6 His residues) at the protein N-terminus, pPB-N-His; this was chosen both for future affinity chromatography purification and for antibody recognition.

pPB-N-His plasmids including inserts for human ABHD6 and ABHD12 cDNAs were purchased ready from abm (Applied Biological Materials, Vancouver, Canada). Promega BL21(DE3)pLysS cells were transformed through a heat shock procedure, then transformation was checked using LB agar + kanamicin (LB+Kan) plates: the cells transformed with the vector were plated undiluted, at 1:10 and 1:100 dilution, in SOC medium as well. The plates were then left to grow o/n at 37 °C: plates where cells were plated after dilution showed no sign of growth, indicating a low transformation efficiency, but undiluted plates were spotted with colonies (fig. 28).

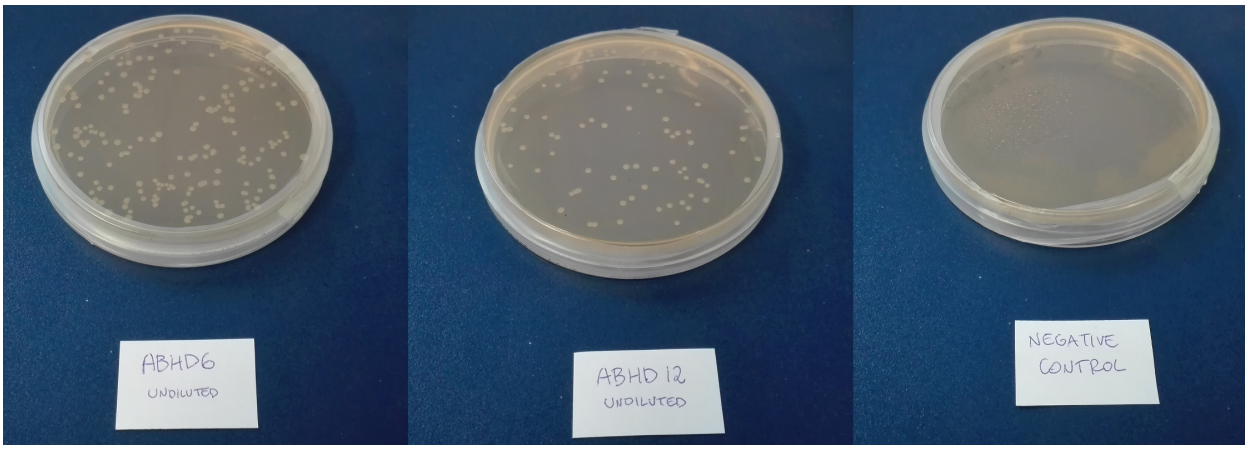

Figure 28. Plates with BL21(DE3)pLysS cells after transformation with ABHD6 (left) and ABHD12 (center) plasmids on LB-Kan agar. The negative control plate (right) was streaked with cells which were not transformed with the plasmid, but with ddH_2O instead.

The first trials were aimed at finding the optimal time after induction to harvest the protein. Five time points were chosen: 2, 4, 6, 16 and 24 expression hours. These were obtained in two runs, where six small cultures were prepared for each protein: the first experiment trialled the 2, 4 and 6 hours time points, while the second one tested the 6, 16, and 24 hours ones. The 6-hours cultures were used as reference between the two experiments for the activity tests. Only three of the cultures were induced; each time an induced culture was harvested, an uninduced one was collected as well. Hydrolytic activity from these cells would serve as a baseline control for fluorometric activity assays (5.2.4).

Colonies from both plates were picked, and used to inoculate three "snap-cap" tubes with 10 mL LB+Kan each, along with a third, uninoculated tube, which served as a contamination control. After 16h of growth, the inoculated tubes showed distinct turbidness, while the uninoculated one was clear. The three tubes were then used to inoculate six flasks, each with 45 mL LB+Kan liquid medium; these cultures were then left in incubation shaking at 37°C 300 rpm, while monitoring the OD at 600 nm. The 50 mL liquid cultures reached an OD of ~0.8 in around four hours from inoculation. At that point, the cultures were induced with IPTG 0.1 mM (final) and transferred at 24 °C, still shaking at 300 rpm, and left expressing the protein o/n. The following day, the cells were harvested through 10 min centrifugation at 5000 x g. The supernatant was discarded and the two aliquots of cells frozen at -80 °C, in order for the hydrolase activity test to be performed at a convenient time.

The membranes were then resuspended in 600 µl ABHD buffer, then the fluorescence analysis immediately began (5.2.4). The remaining membranes were put at 4 °C, to be used in SDS-PAGE (5.2.2) and immunoblotting (5.2.3) experiments.

5.2.2 Protein SDS-PAGE

A SDS-PAGE experiment in denaturing conditions of the bacterial lysates was set to visually check for the overexpression (or an expression at all) of ABHD proteins.

The results are reported in fig. 29, and do not show overexpression of any protein.

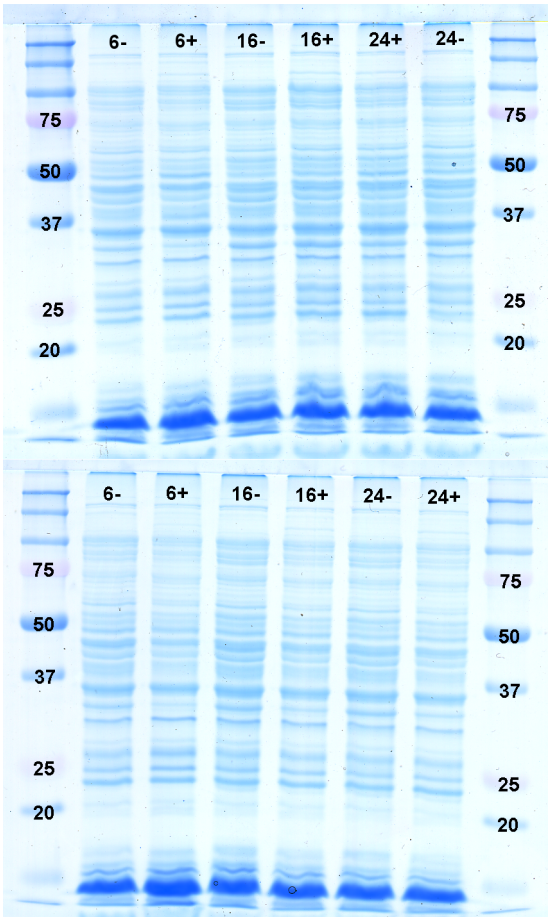

Figure 29. SDS-PAGE results for ABHD6 (top) and ABHD12 (bottom)**.** The first and last column are loaded with the Precision Plus Protein™ Standards Dual Color: the numerals indicate the molecular weight, expressed in kilodaltons, of the corresponding molecular standard.
The other lanes were loaded with lysate samples harvested after different amounts of hours past the induction with IPTG. The numerals on top of the lanes indicate the amount of hours; a "plus" symbol means that the culture was actually induced, while a "minus" that the cells were not induced, but harvested at the same time (negative control).
None of the samples shows a clear overexpression of the proteins. This could be due to the conditions of the expression, which were not geared towards a heavy protein overexpression, both in terms of culture medium and temperature.

5.2.3 ABHD6 and ABHD12 immunoanalysis

In order to assess the presence of the two recombinant proteins, a western blot analysis using anti-His tag antibodies was performed. The blotting results are reported in fig. 30, and confirm the presence of two His-tagged proteins at the expected molecular weights.

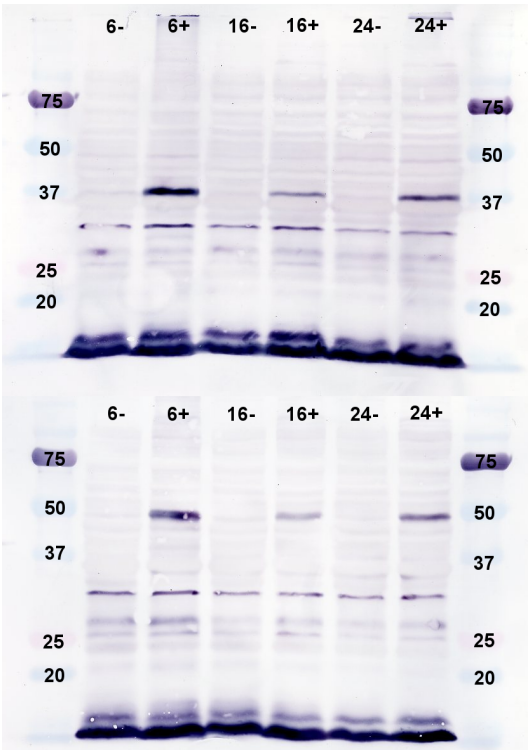

Figure 30. Western blot results for ABHD6 (top) and ABHD12 (bottom)**.** The first and last column are loaded with the Precision Plus Protein™ Standards Dual Color: the numerals indicate the molecular weight, expressed in kilodaltons, of the corresponding molecular standard.
The other lanes were loaded with lysate samples harvested after different amounts of hours past the induction with IPTG. The numerals on top of the lanes indicate the amount of hours; a "plus" symbol means that the culture was actually induced, while a "minus" that the cells were not induced, but harvested at the same time (negative control).
The immunoblotting shows evident bands at the expected molecular weight for both proteins, which are 37 kDa for ABHD6 and 45 kDa for ABHD12. At this resolution, the lack of ABHD12 glycosylation is not appreciable.

5.2.4 ABHD6 and ABHD12 membrane activity assay

For the activity assay, we chose to use a simple variation of our fluorometry assay (Section 3), employing 7-Hydroxyresorufinyl laurate (**1d**) as the substrate. The decision was taken because it seemed a good compromise choice for the substrate preferences of the two enzymes (Navia-Paldanius et al., 2012), and also because we expected high base activity from other bacterial hydrolases, and did not want to saturate the RFU counter of the instrument. The results of the assay are reported in fig. 31.

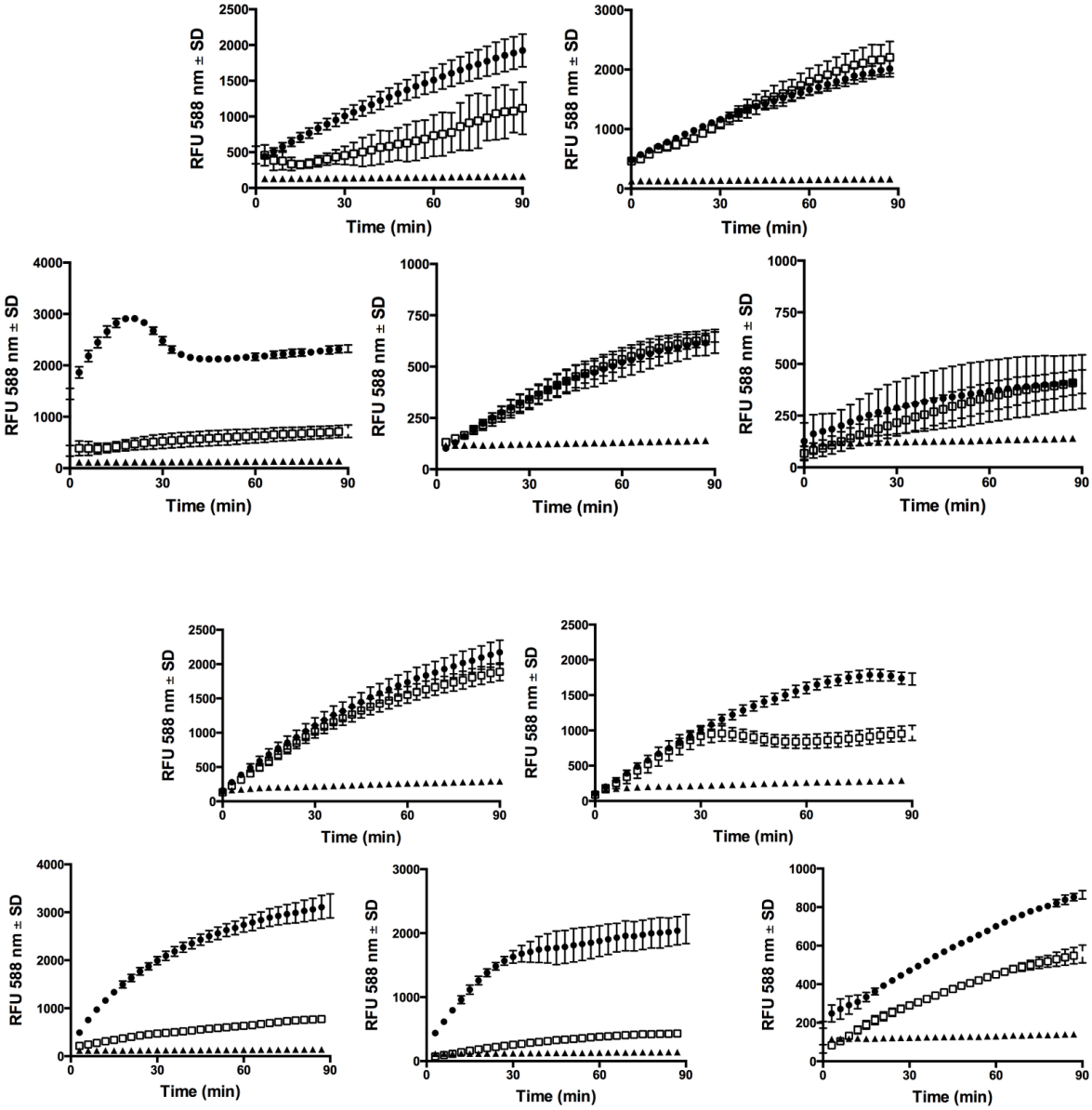

Figure 31. Fluorescence time course for ABHD6 (top) and ABHD12 (bottom). The time courses reported refer to the hydrolytic activity of membrane suspension on 7-hydroxyresorufinyl laurate (compound **1d**, 2.1.3), leading to lauric acid and 7-hydroxyresorufin. The membrane suspensions come from lysates harvested after 2, 4, 6, 16 and 24 hours, from left to right and top to bottom.

The signals reported come from 7-hydroxylaurylresorufin with no membranes added (triangles), membranes of non-induced cells (empty squares) and membranes of induced cells (circles).

5.3 Conclusion

The preliminary results for the heterologous expression of ABHD6 and ABHD12 in engineered *E. coli* BL21 strains are extremely promising. Despite the intrinsic

difficulties of the expression of mammalian integral membrane proteins in bacterial hosts, both the immunoblotting tests and the activity assays in fluorometry suggest that the expression was successfully carried out, and at least a portion of the expressed protein is active.

The experimental protocol has provided important indications on the optimal expression time: the cultures harvested six hours after the expression have provided the highest levels of enzymatic hydrolysis of the substrate for both ABHD6 and ABHD12 – actually, at the current point this seems the *only* viable time point for ABHD6. These are, of course, only preliminary data, providing plenty of fascinating future possibilities: the experimental protocol has shown the potential to express these two hydrolases in bacterial hosts, but at the moment this expression looks relatively limited in quantity, so the protocol itself should be tuned for higher yields. Before this, a purification procedure should be established: it is imperative that the process is designed with the precise aim of maintaining the proteins in their active conformations, therefore mild detergents which use is specially established for this purpose is highly recommended. The His-tag at the N-ter of the two proteins should help in the purification process using the IMAC technique, providing this would not lower the yield in terms of active proteins, due to phenomena of denaturation.

The activity assays show that a simple one-step analysis using a single fluorogenic probe can quantitate the activity of the ES ABHD hydrolases, as well as giving important clues that the proteins expressed are, at least in some percentages, active. Should the purification be achieved, the development of such a simple assay, taking advantage of the availability of isolated recombinant protein, should subsequentially achieved with relative ease.

5.4 Experimental section

For general principles of working with bacteria, preparation of solutions, and buffer and culture medium recipes, refer to 4.4.

Reagents and solutions

Kanamicin was bought as a powder from Sigma, and dissolved into ddH_2O to a 50 mg/mL stock solution. The solution was then filtered on a 0.2 µm membrane, divided into 200 µl aliquots and stored at -20 °C. When needed, kanamicin 50 µg/mL was added to the culture mediums right before use (inoculation of the liquid culture or plate casting liquid), to minimize degradation.

TGS buffer pH 8.3 was prepared as a 10x stock solution, dissolving 30.3g Tris base, 144.0g glycine and 10.0g SDS in 1L dH_2O. It was then filtered on a 0.2 µm membrane and stored at RT. Prior to use, it was diluted ten times to a working solution with dH_2O, and stored (and used) at 4 °C.

Towbin transfer buffer was prepared as a 10x stock solution, dissolving 30.3g Tris-Base 144.15 g Glycine, 100mL. It was then filtered on a 0.2 µm membrane and stored at RT. Prior to use, it was diluted ten times to a working solution with dH_2O.

TBS buffer was prepared as a 20 mM Tris pH 7.6, 137 mM NaCl, solution in ddH_2O, filtered as above and stored at RT in the dark.

ABHD buffer was prepared according to the twin methods from Savinainen and colleagues (Juha R. Savinainen et al., 2016b): 100 mM Tris-HCl pH 7.4, 2 mM EDTA, 10 mM $MgCl_2$, and 200 mM NaCl, stored at 4 °C and brought to RT before use.

Bacterial transformation

pPB-N-His plasmids including inserts of human ABHD6 and ABHD12 cDNAs were purchased ready from abm (Applied Biological Materials, Vancouver, Canada). The cells used for the transformation and expression were BL21(DE3)pLysS cells (Promega). All steps involving the cells were performed wearing sterile gloves, and in proximity to a Bunsen burner with blue flame, to avoid bacterial or mold contamination. Three aliquots (50 µl each) of cells were taken out of the deep freezer (-80 °C), and left to thaw on ice. 0.5 µl (25 ng) of plasmid were pipetted onto each of them; one aliquot received the plasmid containing ABHD6, another one the plasmid containing ABHD12 and the last one was pipetted with 0.5 µl of ddH_2O, as a negative control. After a 10-

minute incubation on ice, the cells were put into a water bath at 42 °C for 45 seconds and then quickly put back on ice for 2 minutes. During this step, particular attention was paid not to shake the tubes in order to avoid mechanical stress to the cells. Then, 900 µl of SOC culture medium (Invitrogen) at room temperature were added to each tube. The tubes were then put at 37°C, shaking at 300 rpm, for 1 hour. Transformation was checked using LB agar + kanamicin 50 µg/mL (LB+Kan) plates: the cells transformed with the vector were plated undiluted, at 1:10 and 1:100 dilution, in SOC medium as well. The plates were then left to grow o/n at 37 °C.

Bacterial liquid cultures

Three colonies were picked from each plate, and used to inoculate three "snap-cap" tubes, filled with 15 mL LB + Kan each. The tubes were put in an incubator at 37°C, shaking at 300 rpm o/n, together with an uninoculated tube with 5 mL LB+Kan as a control for the likelihood of contaminations from unwanted microorganisms. After 16h of growth, the inoculated tubes showed distinct turbidness, while the uninoculated one was clear. The two inoculated tubes were then used to inoculate six flasks (one tube inoculated three flasks, 5 mL per flask,), each with 45 mL LB+Kan liquid medium (final volume 50 mL); these cultures were then put into the incubator, shaking at 37°C 300 rpm, while monitoring the OD at 600 nm. Meanwhile, the IPTG stock solution was diluted to a 0.1 mM working solution with sterile ddH_2O water. When the cultures reached an OD of ~0.8, they were induced with 50 µl IPTG 100 mM, for a final concentration of 0.1 mM, and transferred outside the incubator at controlled temperature of 24 °C, still shaking at 300 rpm, o/n. The following day, the cells were harvested through 10 min centrifugation at 5000 x g, with the rotor bucket at 4 °C. The supernatant was discarded and the two aliquots of cells deep-frozen at -80 °C, in order for the membranes to be tested at a later time.

Bacterial membrane isolation

During this step, all solutions were kept on ice and all centrifugation steps were performed with the rotor bucket set at a temperature of 4 °C. Each bacterial pellet was thawed on ice and resuspended in 5 mL of PBS buffer (10% volume of culture) using a pipette, being careful to avoid foaming or bubbling. 0.5 mL of a lysozyme 10 mg/mL solution were added, then the cells were left on ice for 20 minutes. The cell lysis was completed with sonication, carefully keeping the cells on ice and applying 3 bursts of 10 seconds each. The sonicator used was a SONOPULS HD2070 (BANDELIN, Berlin,

Germany), at ~50% power (~35W). 5 µl of the DNase and RNase solutions were added to the lysate, and it was left on ice for 5 minutes. The lysate was now centrifuged at 20.000 x g, for 45 minutes, then the supernatant was removed, the membranes briefly resuspended in ice-cold PBS and centrifuged again in the same conditions for 5 minutes. The PBS was discarded. The membranes were then resuspended in 600 µl ABHD buffer, then the fluorescence analysis immediately began. The residual membranes (~60 µl) were put at 4°C, to be used in SDS-PAGE and immunoblotting experiments.

ABHD6 and ABHD12 SDS-PAGE

SDS-PAGE experiments procedures and gel recipes can be found at paragraph 4.4.

The lysate samples were prepared adding 5 µl of the bacterial lysate to 1 µl 500 mM DTT, 2.5 µl Laemmli buffer 4x and 1.5 µl H_2O, and the molecular ladder used was 5 µl Precision Plus Protein Standards™ – Dual Color (Bio-Rad).

ABHD6 and ABHD12 immunoblotting

10 µl of resuspended membranes from each culture were added with 3.5 µl 4x Laemmli Sample Buffer and 1.5 µl of 500 mM dithiothreitol as a reducing agent. The samples were denatured for 5 minutes into a Thermoblock at 95°C, then they were removed and immediately put on ice. The samples were briefly centrifuged at 500 x g in order to collect the whole sample at the bottom of the tube, then they were pipetted into the wells of an SDS-PAGE gel immersed in running buffer. The gel was ran for 35 minutes, 200V.

The gel was equilibrated in Towbin transfer buffer at RT for 10 minutes on mild agitation, along with 6 sheet of 0.8 mm filter paper. Meanwhile, the blotting membrane was cut from an Immobilon-P PVDF sheet (-Merck), and activated by immersing it in methanol for 30 seconds. The membrane was then washed (2-minutes immersion in dH_2O) and equilibrated through immersion in Towbin buffer for 10 minutes, on mild agitation.

After both the gel and the membrane were equilibrated, the proteins were transferred to the membrane through a "transfer sandwich", stacking three sheets of filter paper, the gel, the PVDF membrane, and then three more sheets of filter paper on the transfer cassette. The components were stacked on top of the anode, and the cathode was put at

the top of the sandwich. The transferral system was Bio-Rad Trans-Blot Turbo, and the "Standard SD" protocol (30 minutes at 25V, 1.0 A) was used.

Once the transfer was completed, the membrane was "blocked" from aspecific membrane binding of the antibody through immersion in a TBS 3% BSA solution and kept o/n at 4°C on mild agitation.

The antibody (abcam Anti-6X His tag® antibody [HIS-1] (Alkaline Phosphatase)) was diluted 1:1000 (10 µl antibody in 10 mL TBS added with 1% BSA). The membrane was immersed in the antibody solution for 1 hour at room temperature, on mild shaking; the membrane was then removed from the antibody solution, and washed three times with TBS with 1% Tween 20 added, for 5 minutes each time.

A Sigma SIGMA *FAST*™ BCIP/NBT tablet was dissolved in 10 mL dH_2O to obtain the phosphatase substrate solution. The final step of the immunoblotting consisted in immersing the membrane for 10 minutes in this solution, then rinsing it with dH_2O, and leaving the membrane to dry in the dark.

ABHD6 and ABHD12 activity assay

7-Hydroxyresorufinyl laurate powder (**1d**, 3.2.1) was dissolved in DMSO in a 1 mM stock solution, then the stock solution was diluted with DMSO to a 50 µM working solution.

20 µl of this working solution were pipetted at the bottom of the wells of 96-well plate, then 180 µl of resuspendend membranes were quickly pipetted on top of each substrate-containing DMSO drop, and the fluorescence analysis immediately began.

The plates were read (λ_{ex}=571 nm, λ_{em}=588 nm) every 3 minutes, for 90 minutes using a Jasco FP-8300 fluorometer (3.4).

6. GENERAL CONCLUSION

In the present work, we illustrate two photochemical approaches to HTS screening of compounds dedicated to the inhibition of the hydrolases which regulate the ES, and the first attempts at the development of a third one.

The fine regulation of the EC signaling is a promising topic for the treatment of various kinds of diseases and pathological conditions, as well as the maintaining of a well-being state. The fluorometric technique is a well-established one, and our assay is a fast and efficient one for the discrimination of promising lead compounds. The bioluminescent assay can be considered a more complex but finer instrument, which can act as a building block in the development of more advanced ones, but that nonetheless demonstrates that this interesting technique can be applied to the study of lipases involving lipophylic substrates. The ES ABHDs are a novel topic which surely needs more addressing, and our studies move forward towards that direction, with the promise of simplifying the characterization of these proteins without interferences from other cellular lipases.

The ES on its own is a system which still holds many discoveries to be done for the near future, and our efforts aim at providing tools which make this investigation more accessible and efficient.

BIBLIOGRAPHY

Arifin, S. A., & Falasca, M. (2016). Lysophosphatidylinositol signalling and metabolic diseases. *Metabolites*, *6*(1), 1–11. https://doi.org/10.3390/metabo6010006

Baek, J. H., Darlington, C. L., Smith, P. F., & Ashton, J. C. (2013). Antibody testing for brain immunohistochemistry: Brain immunolabeling for the cannabinoid CB2 receptor. *Journal of Neuroscience Methods*. https://doi.org/10.1016/j.jneumeth.2013.03.021

Bégaud, B., Bousser, M. G., Cohen, P., Diquet, B., Duprat, P., Janssens, W., … Laurent, V. (2016). Report by the Temporary Specialist Scientific Committee (TSSC), "FAAH (Fatty Acid Amide Hydrolase)", on the causes of the accident during a Phase 1 clinical trial, (May), 1–28.

Bernaudat, F., Frelet-Barrand, A., Pochon, N., Dementin, S., Hivin, P., Boutigny, S., … Rolland, N. (2011). Heterologous expression of membrane proteins: Choosing the appropriate host. *PLoS ONE*, *6*(12). https://doi.org/10.1371/journal.pone.0029191

Bertani, G. (2004). Lysogeny at Mid-Twentieth Century : P1 , P2 , and Other Experimental Systems Lysogeny at Mid-Twentieth Century : P1 , P2 , and Other Experimental Systems. *Journal of Bacteriology*, *186*(3), 595–600. https://doi.org/10.1128/JB.186.3.595

Bertrand, T., Augé, F., Houtmann, J., Rak, A., Vallée, F., Mikol, V., … Mathieu, M. (2010). Structural Basis for Human Monoglyceride Lipase Inhibition. *Journal of Molecular Biology*, *396*(3), 663–673. https://doi.org/10.1016/j.jmb.2009.11.060

Bisogno, T., Melck, D., Bobrov, M. Y., Gretskaya, N. M., Bezuglov, V. V., De Petrocellis, L., & Di Marzo, V. (2000). N-acyl-dopamines: novel synthetic CB1 cannabinoid-receptor ligands and inhibitors of anandamide inactivation with cannabimimetic activity in vitro and in vivo. *Biochemical Journal*, *351*(3), 817. https://doi.org/10.1042/0264-6021:3510817

Bisswanger, H. (2014). Enzyme assays. *Perspectives in Science*, *1*(1–6), 41–55. https://doi.org/10.1016/j.pisc.2014.02.005

Blankman, J. L., Long, J. Z., Trauger, S. A., Siuzdak, G., & Cravatt, B. F. (2013). ABHD12 controls brain lysophosphatidylserine pathways that are deregulated in a murine model of the neurodegenerative disease PHARC. *Proceedings of the National Academy of Sciences*, *110*(4), 1500–1505. https://doi.org/10.1073/pnas.1217121110

Blankman, J. L., Simon, G. M., & Cravatt, B. F. (2007). A Comprehensive Profile of Brain Enzymes that Hydrolyze the Endocannabinoid 2-Arachidonoylglycerol. *Chemistry and Biology*, *14*(12), 1347–1356. https://doi.org/10.1016/j.chembiol.2007.11.006

Branchini, B. R., Behney, C. E., Southworth, T. L., Fontaine, D. M., Gulick, A. M., Vinyard, D. J., & Brudvig, G. W. (2015). Experimental Support for a Single Electron-Transfer Oxidation Mechanism in Firefly Bioluminescence. *Journal of the American Chemical Society*, *137*(24), 7592–7595. https://doi.org/10.1021/jacs.5b03820

Branchini, B. R., & Southworth, T. L. (2017). *A Highly Sensitive Biosensor for ATP Using a Chimeric Firefly Luciferase*. *Methods in Enzymology* (1st ed., Vol. 589). Elsevier Inc. https://doi.org/10.1016/bs.mie.2017.01.004

Branchini, B. R., Southworth, T. L., Fontaine, D. M., Kohrt, D., Talukder, M., Michelini, E., … Grossel, M. J. (2015). An enhanced chimeric firefly luciferase-inspired enzyme for ATP detection and bioluminescence reporter and imaging applications. *Analytical Biochemistry*, *484*, 148–153. https://doi.org/10.1016/j.ab.2015.05.020

Cabral, G. A., & Griffin-Thomas, L. (2009). Emerging role of the cannabinoid receptor CB 2 in immune regulation: Therapeutic prospects for neuroinflammation. *Expert Reviews in Molecular Medicine*, *11*(January 2009), 1–25. https://doi.org/10.1017/S1462399409000957

Cabral, G. A., Rogers, T. J., & Lichtman, A. H. (2015). Turning Over a New Leaf: Cannabinoid and Endocannabinoid Modulation of Immune Function. *Journal of Neuroimmune Pharmacology*, *10*(2), 193–203. https://doi.org/10.1007/s11481-015-9615-z

Cecyre, B., Thomas, S., Ptito, M., Casanova, C., & Bouchard, J. F. (2014). Evaluation of the specificity of antibodies raised against cannabinoid receptor type 2 in the mouse retina. *Naunyn-Schmiedebergs Archives of Pharmacology*, *387*(2), 175–184. https://doi.org/10.1007/s00210-013-0930-8

Chaikin, P. (2017a). Reply to Letter: The Use of IC50 for Potency and MTD as Objective in Study BIA 10-2474, by Mattheus van Iersel, MD. *Journal of Clinical Pharmacology*, *57*(10), 1359–1361. https://doi.org/10.1002/jcph.1000

Chaikin, P. (2017b). The Bial 10-2474 Phase 1 Study—A Drug Development Perspective and Recommendations for Future First-in-Human Trials. *Journal of Clinical Pharmacology*, *57*(6), 690–703. https://doi.org/10.1002/jcph.889

Chen, R. (2012). Bacterial expression systems for recombinant protein production: E. coli and beyond. *Biotechnology Advances*, *30*(5), 1102–1107. https://doi.org/10.1016/j.biotechadv.2011.09.013

Cichero, E., Menozzi, G., Guariento, S., & Fossa, P. (2015). Ligand-based homology modelling of the human CB2 receptor SR144528 antagonist binding site: a computational approach to explore the 1,5-diaryl pyrazole scaffold. *Med. Chem. Commun.*, *6*(11), 1978–1986. https://doi.org/10.1039/C5MD00333D

Cravatt, B. F., Demarest, K., Patricelli, M. P., Bracey, M. H., Giang, D. K., Martin, B. R., & Lichtman, A. H. (2001). Supersensitivity to anandamide and enhanced endogenous cannabinoid signaling in mice lacking fatty acid amide hydrolase. *Proceedings of the National Academy of Sciences*, *98*(16), 9371–9376. https://doi.org/10.1073/pnas.161191698

Deutsch, D. G. (2016). A personal retrospective: Elevating anandamide (AEA) by targeting fatty acid amide hydrolase (FAAH) and the fatty acid binding proteins (FABPs). *Frontiers in Pharmacology*, *7*(OCT), 1–7. https://doi.org/10.3389/fphar.2016.00370

Deutsch, D. G., & Chin, S. A. (1993). Enzymatic synthesis and degradation of anandamide, a

cannabinoid receptor agonist. *Biochemical Pharmacology*, *46*(5), 791–6. https://doi.org/10.1016/0006-2952(93)90486-G

Devane, W. A., Dysarz, F. A., Johnson, R. M., Melvin, L., & Howlett, A. C. (1988). Determination and Characterization of a Cannabinoid Receptor in Rat Brain. *Molecular Pharmacology*, *34*(5), 605–613.

Devane, W., Hanuš, L., Breuer, A., Pertwee, R., Stevenson, L., Griffin, G., … Mechoulam, R. (1992). Isolation and structure of a brain constituent that binds to the cannabinoid receptor. *Science*, *258*(5090), 1946–1949. https://doi.org/10.1126/science.1470919

Di Marzo, V., & De Petrocellis, L. (2012). Why do cannabinoid receptors have more than one endogenous ligand? *Philosophical Transactions of the Royal Society B: Biological Sciences*, *367*(1607), 3216–3228. https://doi.org/10.1098/rstb.2011.0382

Dinh, T. P., Carpenter, D., Leslie, F. M., Freund, T. F., Katona, I., Sensi, S. L., … Piomelli, D. (2002). Brain monoglyceride lipase participating in endocannabinoid inactivation. *Proceedings of the National Academy of Sciences*, *99*(16), 10819–10824. https://doi.org/10.1073/pnas.152334899

Felder, C. C. C., Nielsen, A., Briley, E. M. E. M., Palkovits, M., Priller, J., Axelrod, J., … others. (1996). Isolation and Measurement of the Endogenous Cannabinoid Receptor Agonist, Anandamide, in Brain and Peripheral Tissues of Human and Rat. *FEBS Letters*, *393*(2–3), 231–235. Retrieved from http://linkinghub.elsevier.com/retrieve/pii/0014579396008915

Feng, P., Zhang, H., Deng, Q., Liu, W., Yang, L., Li, G., … Li, M. (2016). Real-Time Bioluminescence Imaging of Nitroreductase in Mouse Model. *Analytical Chemistry*, *88*(11), 5610–5614. https://doi.org/10.1021/acs.analchem.6b01160

Fiskerstrand, T., H'Mida-Ben Brahim, D., Johansson, S., M'Zahem, A., Haukanes, B. I., Drouot, N., … Knappskog, P. M. (2010). Mutations in ABHD12 cause the neurodegenerative disease PHARC: An inborn error of endocannabinoid metabolism. *American Journal of Human Genetics*, *87*(3), 410–417. https://doi.org/10.1016/j.ajhg.2010.08.002

Foster, D. J., Wilson, J. M., Remke, D. H., Mahmood, M. S., Uddin, M. J., Wess, J., … Conn, P. J. (2016). Antipsychotic-like Effects of M4Positive Allosteric Modulators Are Mediated by CB2Receptor-Dependent Inhibition of Dopamine Release. *Neuron*, *91*(6), 1244–1252. https://doi.org/10.1016/j.neuron.2016.08.017

Fowler, C. J. (2012). Monoacylglycerol lipase – a target for drug development? https://doi.org/10.1111/j.1476-5381.2012.01950.x

Fritzsche, M., & Mandenius, C.-F. (2010). Fluorescent cell-based sensing approaches for toxicity testing. *Analytical and Bioanalytical Chemistry*, *398*(1), 181–191.

Gaoni, Y., & Mechoulam, R. (1964). Isolation, Structure, and Partial Synthesis of an Active Constituent of Hashish. *Journal of the American Chemical Society*, *86*(8), 1646–1647. https://doi.org/10.1021/ja01062a046

García-Fruitós, E., Vázquez, E., Díez-Gil, C., Corchero, J. L., Seras-Franzoso, J., Ratera, I., … Villaverde, A. (2012). Bacterial inclusion bodies: Making gold from waste. *Trends in Biotechnology*, *30*(2), 65–70. https://doi.org/10.1016/j.tibtech.2011.09.003

Gelfand, E. V., & Cannon, C. P. (2006). Rimonabant: A Cannabinoid Receptor Type 1 Blocker for Management of Multiple Cardiometabolic Risk Factors. *Journal of the American College of Cardiology*, *47*(10), 1919–1926. https://doi.org/10.1016/j.jacc.2005.12.067

Genheden, S., & Ryde, U. (2015). The MM/PBSA and MM/GBSA methods to estimate ligand-binding affinities. *Expert Opinion on Drug Discovery*, *10*(5), 449–461. https://doi.org/10.1517/17460441.2015.1032936

Gil-Ordóñez, A., Martín-Fontecha, M., Ortega-Gutiérrez, S., & López-Rodríguez, M. L. (2018). Monoacylglycerol lipase (MAGL) as a promising therapeutic target. *Biochemical Pharmacology*, (July), 0–1. https://doi.org/10.1016/j.bcp.2018.07.036

Godlewski, G., Offertáler, L., Wagner, J. A., & Kunos, G. (2009). Receptors for acylethanolamides-GPR55 and GPR119. *Prostaglandins and Other Lipid Mediators*, *89*(3–4), 105–111. https://doi.org/10.1016/j.prostaglandins.2009.07.001

Gonsiorek, W., Lunn, C., Fan, X., Narula, S., Lundell, D., & Hipkin, R. W. (2000). Endocannabinoid 2-arachidonyl glycerol is a full agonist through human type 2 cannabinoid receptor: antagonism by anandamide. *Mol Pharmacol*, *57*(5), 1045–1050. Retrieved from http://www.ncbi.nlm.nih.gov/pubmed/10779390%5Cnhttp://molpharm.aspetjournals.org/content/57/5/1045.full.pdf

Guilbault, G. G., & Kramer, D. N. (1965). Resorufin Butyrate and Indoxyl Acetate as Fluorogenic Substrates for Cholinesterase. *Analytical Chemistry*, *37*(1), 120–123. https://doi.org/10.1021/ac60220a031

Gulyas, A. I., Cravatt, B. F., Bracey, M. H., Dinh, T. P., Piomelli, D., Boscia, F., & Freund, T. F. (2004). Segregation of two endocannabinoid-hydrolyzing enzymes into pre- and postsynaptic compartments in the rat hippocampus, cerebellum and amygdala. *European Journal of Neuroscience*, *20*(2), 441–458. https://doi.org/10.1111/j.1460-9568.2004.03428.x

Hanuš, L., Abu-Lafi, S., Fride, E., Breuer, A., Vogel, Z., Shalev, D. E., … Mechoulam, R. (2001). 2-Arachidonyl glyceryl ether, an endogenous agonist of the cannabinoid CB1 receptor. *Proceedings of the National Academy of Sciences*, *98*(7), 3662–3665. https://doi.org/10.1073/pnas.061029898

Hanuš, L., Gopher, A., Almog, S., & Mechoulam, R. (1993). Two New Unsaturated Fatty Acid Ethanolamides in Brain That Bind to the Cannabinoid Receptor. *Journal of Medicinal Chemistry*, *36*(20), 3032–3034. https://doi.org/10.1021/jm00072a026

Hermanson, D. J., & Marnett, L. J. (2011). Cannabinoids , endocannabinoids , and cancer, (October), 599–612. https://doi.org/10.1007/s10555-011-9318-8

Herring, P. J., & Cope, C. (2005). Red bioluminescence in fishes: On the suborbital photophores of Malacosteus, Pachystomias and Aristostomias. *Marine Biology*, *148*(2), 383–394.

https://doi.org/10.1007/s00227-005-0085-3

Ho, W. S. V., Barrett, D. A., & Randall, M. D. (2008). "Entourage" effects of N-palmitoylethanolamide and N-oleoylethanolamide on vasorelaxation to anandamide occur through TRPV1 receptors. *British Journal of Pharmacology*, *155*(6), 837–846. https://doi.org/10.1038/bjp.2008.324

Hua, T., Vemuri, K., Pu, M., Qu, L., Han, G. W., Wu, Y., … Liu, Z. J. (2016). Crystal Structure of the Human Cannabinoid Receptor CB1. *Cell*, *167*(3), 750–762.e14. https://doi.org/10.1016/j.cell.2016.10.004

Huang, S. M., Bisogno, T., Trevisani, M., Al-Hayani, A., De Petrocellis, L., Fezza, F., … Di Marzo, V. (2002). An endogenous capsaicin-like substance with high potency at recombinant and native vanilloid VR1 receptors. *Proceedings of the National Academy of Sciences of the United States of America*, *99*(12), 8400–5. https://doi.org/10.1073/pnas.122196999

Huggins, J. P., Smart, T. S., Langman, S., Taylor, L., & Young, T. (2012). An efficient randomised, placebo-controlled clinical trial with the irreversible fatty acid amide hydrolase-1 inhibitor PF-04457845, which modulates endocannabinoids but fails to induce effective analgesia in patients with pain due to osteoarthritis of th. *Pain*, *153*(9), 1837–1846. https://doi.org/10.1016/j.pain.2012.04.020

Ibáñez, G., McBean, J. L., Astudillo, Y. M., & Luo, M. (2010). An enzyme-coupled ultrasensitive luminescence assay for protein methyltransferases. *Analytical Biochemistry*, *401*(2), 203–210. https://doi.org/10.1016/j.ab.2010.03.010

Iwamura, H., Suzuki, H., Ueda, Y., Kaya, T., & Inaba, T. (2001). In Vitro and in Vivo Pharmacological Characterization of JTE- 907, a Novel Selective Ligand for Cannabinoid CB 2 Receptor. *The Journal of Pharmacology and Experimental Therapeutics*, *296*(2), 420–425.

Johnson, D. S., Stiff, C., Lazerwith, S. E., Kesten, S. R., Fay, L. K., Morris, M., … Ahn, K. (2011). Discovery of PF-04457845: A highly potent, orally bioavailable, and selective urea FAAH inhibitor. *ACS Medicinal Chemistry Letters*, *2*(2), 91–96. https://doi.org/10.1021/ml100190t

Jonasson, P., Liljeqvist, S., Nygren, P.-A. A., Stahl, S., & Ståhl, S. (2002). Genetic design for facilitated production and recovery of recombinant proteins in Escherichia coli. *Biotechnol Appl Biochem*, *35*(Pt 2), 91–105. https://doi.org/10.1042/BA20010099

Kapoor, M., & Gupta, M. N. (2012). Lipase promiscuity and its biochemical applications. *Process Biochemistry*, *47*(4), 555–569. https://doi.org/10.1016/j.procbio.2012.01.011

Karlsson, M., Contreras, J. A., Hellman, U., Tornqvist, H., & Holm, C. (1997). cDNA cloning, tissue distribution, and identification of the catalytic triad of monoglyceride lipase. *Journal of Biological Chemistry*, *272*(43), 27218–27223. https://doi.org/10.1074/jbc.272.43.27218

Kathuria, S., Gaetani, S., Fegley, D., Valiño, F., Duranti, A., Tontini, A., … Piomelli, D. (2003). Modulation of anxiety through blockade of anandamide hydrolysis. *Nature Medicine*, *9*(1), 76–81. https://doi.org/10.1038/nm803

Ke, B., Wu, W., Liu, W., Liang, H., Gong, D., Hu, X., & Li, M. (2016). Bioluminescence Probe for Detecting Hydrogen Sulfide in Vivo. *Analytical Chemistry*, *88*(1), 592–595. https://doi.org/10.1021/acs.analchem.5b03636

Kendall, D. A., & Yudowski, G. A. (2017). Cannabinoid Receptors in the Central Nervous System: Their Signaling and Roles in Disease. *Frontiers in Cellular Neuroscience*, *10*(January), 1–10. https://doi.org/10.3389/fncel.2016.00294

Keppel Hesselink, J. M., De Boer, T., & Witkamp, R. F. (2013). Palmitoylethanolamide: A natural body-own anti-inflammatory agent, effective and safe against influenza and common cold. *International Journal of Inflammation*, *2013*. https://doi.org/10.1155/2013/151028

Kerbrat, A., Ferré, J.-C., Fillatre, P., Ronzière, T., Vannier, S., Carsin-Nicol, B., … Edan, G. (2016). Acute Neurologic Disorder from an Inhibitor of Fatty Acid Amide Hydrolase. *New England Journal of Medicine*, *375*(18), 1717–1725. https://doi.org/10.1056/NEJMoa1604221

Kim, S., Kim, H., Choi, Y., & Kim, Y. (2015). A New Strategy for Fluorogenic Esterase Probes Displaying Low Levels of Non-specific Hydrolysis. *Chemistry (Weinheim an Der Bergstrasse, Germany)*, *21*(27), 9645–9. https://doi.org/10.1002/chem.201501127

King, A. R., Duranti, A., Tontini, A., Rivara, S., Rosengarth, A., Clapper, J. R., … Piomelli, D. (2007). URB602 Inhibits Monoacylglycerol Lipase and Selectively Blocks 2-Arachidonoylglycerol Degradation in Intact Brain Slices. *Chemistry and Biology*, *14*(12), 1357–1365. https://doi.org/10.1016/j.chembiol.2007.10.017

Kitson, T. M., & Kitson, K. E. (1997). Studies of the esterase activity of cytosolic aldehyde dehydrogenase with resorufin acetate as substrate. *The Biochemical Journal*, *322 (Pt 3*, 701–708. https://doi.org/10.1042/bj3220701

Knotkova, H., Pappagallo, M., & Szallasi, A. (2008). Capsaicin (TRPV1 agonist) therapy for pain relief: Farewell or revival? *Clinical Journal of Pain*, *24*(2), 142–154. https://doi.org/10.1097/AJP.0b013e318158ed9e

Kohno, M., Hasegawa, H., Inoue, A., Muraoka, M., Miyazaki, T., Oka, K., & Yasukawa, M. (2006). Identification of N-arachidonylglycine as the endogenous ligand for orphan G-protein-coupled receptor GPR18. *Biochemical and Biophysical Research Communications*, *347*(3), 827–832. https://doi.org/10.1016/j.bbrc.2006.06.175

Labar, G., Bauvois, C., Borel, F., Ferrer, J. L., Wouters, J., & Lambert, D. M. (2010). Crystal structure of the human monoacylglycerol lipase, a key actor in endocannabinoid signaling. *ChemBioChem*, *11*(2), 218–227. https://doi.org/10.1002/cbic.200900621

Laleh, P., Yaser, K., Abolfazl, B., Shahriar, A., Mohammad, A. J., Nazila, F., & Alireza, O. (2018). Oleoylethanolamide increases the expression of PPAR-A and reduces appetite and body weight in obese people: A clinical trial. *Appetite*, *128*(May), 44–49. https://doi.org/10.1016/j.appet.2018.05.129

Lam, V., Henault, M., Khougaz, K., Fortin, L. J., Ouellet, M., Melnyk, R., & Partridge, A. (2012).

Resorufin butyrate as a soluble and monomeric high-throughput substrate for a triglyceride lipase. *Journal of Biomolecular Screening*, *17*(2), 245–251. https://doi.org/10.1177/1087057111422944

Lauria, S., Casati, S., & Ciuffreda, P. (2015). Synthesis and characterization of a new fluorogenic substrate for monoacylglycerol lipase and application to inhibition studies. *Analytical and Bioanalytical Chemistry*, *407*(26), 8163–8167. https://doi.org/10.1007/s00216-015-8991-9

Lauria, S., Perrotta, C., Casati, S., Di Renzo, I., Ottria, R., Eberini, I., … Ciuffreda, P. (2018). Design, synthesis, molecular modelling and in vitro cytotoxicity analysis of novel carbamate derivatives as inhibitors of Monoacylglycerol lipase. *Bioorganic and Medicinal Chemistry*, *26*(9), 2561–2572. https://doi.org/10.1016/j.bmc.2018.04.024

Li, J., Chen, L., Du, L., & Li, M. (2013). Cage the firefly luciferin! – a strategy for developing bioluminescent probes. *Chem. Soc. Rev.*, *42*(2), 662–676. https://doi.org/10.1039/C2CS35249D

Li, W., Blankman, J. L., & Cravatt, B. F. (2007). A functional proteomic strategy to discover inhibitors for uncharacterized hydrolases. *Journal of the American Chemical Society*, *129*(31), 9594–9595. https://doi.org/10.1021/ja073650c

Lin, Y., Gao, Y., Ma, Z., Jiang, T., Zhou, X., Li, Z., … Li, M. (2018). Bioluminescence probe for γ-glutamyl transpeptidase detection in vivo. *Bioorganic & Medicinal Chemistry*, *26*(1), 134–140. https://doi.org/10.1016/j.bmc.2017.11.025

Long, J. Z., Li, W., Booker, L., Burston, J. J., Kinsey, S. G., Schlosburg, J. E., … Cravatt, B. F. (2009). Selective blockade of 2-arachidonoylglycerol hydrolysis produces cannabinoid behavioral effects. *Nature Chemical Biology*, *5*(1), 37–44. https://doi.org/10.1038/nchembio.129.

Lu, V. B., Puhl, H. L., & Ikeda, S. R. (2013). N-Arachidonyl glycine does not activate G protein-coupled receptor 18 signaling via canonical pathways. *Mol Pharmacol.*, *83*(1), 267–82. https://doi.org/10.1124/mol.112.081182

Mackie, K., Devane, W. A., & Hille, B. (1993). Anandamide, an endogenous cannabinoid, inhibits calcium currents as a partial agonist in N18 neuroblastoma cells. *Molecular Pharmacology*, *44*(3), 498–503.

Magno, A., Caflisch, A., & Pellarin, R. (2010). Crowding effects on amyloid aggregation kinetics. *Journal of Physical Chemistry Letters*, *1*(20), 3027–3032. https://doi.org/10.1021/jz100967z

Magotti, P., Bauer, I., Igarashi, M., Babagoli, M., Marotta, R., Piomelli, D., & Garau, G. (2015). Structure of human n-acylphosphatidylethanolamine-hydrolyzing phospholipase D: Regulation of fatty acid ethanolamide biosynthesis by bile acids. *Structure*, *23*(3), 598–604. https://doi.org/10.1016/j.str.2014.12.018

Marrs, W. R., Blankman, J. L., Horne, E. A., Thomazeau, A., Lin, Y. H., Coy, J., … Stella, N. (2010). The serine hydrolase ABHD6 controls the accumulation and efficacy of 2-AG at cannabinoid receptors. *Nature Neuroscience*, *13*(8), 951–957. https://doi.org/10.1038/nn.2601

Matsuda, L. a, Lolait, S. J., Brownstein, M. J., Young, a C., & Bonner, T. I. (1990). Structure of a

cannabinoid receptor and functional expression of the cloned cDNA. *Nature*, *346*(6284), 561–564. https://doi.org/10.1038/346561a0

Matuszak, N., Muccioli, G. G., Labar, G., & Lambert, D. M. (2009). Synthesis and in vitro evaluation of N-substituted maleimide derivatives as selective monoglyceride lipase inhibitors. *Journal of Medicinal Chemistry*, *52*(23), 7410–7420. https://doi.org/10.1021/jm900461w

Mayr, L. M., & Bojanic, D. (2009). Novel trends in high-throughput screening. *Current Opinion in Pharmacology*, *9*(5), 580–588. https://doi.org/10.1016/j.coph.2009.08.004

Mechoulam, R., Ben-Shabat, S., Hanus, L., Ligumsky, M., Kaminski, N. E., Schatz, A. R., … Vogel, Z. (1995). Identification of an endogenous 2-monoglyceride, present in canine gut, that binds to cannabinoid receptors. *Biochemical Pharmacology*, *50*(1), 83–90. https://doi.org/10.1016/0006-2952(95)00109-D

Menger, F. M., & Ladika, M. (1987). Origin of Rate Accelerations in an Enzyme Model: The p-Nitrophenyl Ester Syndrome. *Journal of the American Chemical Society*, *109*(10), 3145–3146. https://doi.org/10.1021/ja00244a047

Michelini, E., Cevenini, L., Calabretta, M. M. addalen., Calabria, D., & Roda, A. (2014). Exploiting in vitro and in vivo bioluminescence for the implementation of the three Rs principle (replacement, reduction, and refinement) in drug discovery. *Analytical and Bioanalytical Chemistry*, *406*(23), 5531–5539. https://doi.org/10.1007/s00216-014-7925-2

Mileni, M., Kamtekar, S., Wood, D. C., Benson, T. E., Cravatt, B. F., & Stevens, R. C. (2010). Crystal structure of fatty acid amide hydrolase bound to the carbamate inhibitor URB597: Discovery of a deacylating water molecule and insight into enzyme inactivation. *Journal of Molecular Biology*, *400*(4), 743–754. https://doi.org/10.1016/j.jmb.2010.05.034

Moreira, F. A., & Crippa, J. A. S. (2009). The psychiatric side-effects of rimonabant. *Revista Brasileira de Psiquiatria*, *31*(2), 145–153. https://doi.org/10.1590/S1516-44462009000200012

Morena, M., Patel, S., Bains, J. S., & Hill, M. N. (2016). Neurobiological Interactions Between Stress and the Endocannabinoid System. *Neuropsychopharmacology*, *41*(1), 80–102. https://doi.org/10.1038/npp.2015.166

Muccioli, G. G., Xu, C., Odah, E., Cudaback, E., Cisneros, J. A., Lambert, D. M., … Stella, N. (2007). Identification of a novel endocannabinoid-hydrolyzing enzyme expressed by microglial cells. *Journal of Neuroscience*, *27*(11), 2883–2889. https://doi.org/27/11/2883 [pii]\r10.1523/JNEUROSCI.4830-06.2007

Munro, S., Thomas, K. L., & Abu-Shaar, M. (1993). Molecular characterization of a peripheral receptor for cannabinoids. *Nature*, *365*(6441), 61–65. https://doi.org/10.1038/365061a0

Murataeva, N., Straiker, A., & Mackie, K. (2014). Parsing the players: 2-arachidonoylglycerol synthesis and degradation in the CNS. *British Journal of Pharmacology*, *171*(6), 1379–1391. https://doi.org/10.1111/bph.12411

Nass, S. R., Long, J. Z., Schlosburg, J. E., Cravatt, B. F., Lichtman, A. H., & Kinsey, S. G. (2015). Endocannabinoid Catabolic Enzymes Play Differential Roles in Thermal Homeostasis in Response to Environmental or Immune Challenge. *Journal of Neuroimmune Pharmacology*, *10*(2), 364–370. https://doi.org/10.1007/s11481-015-9593-1

Navia-Paldanius, D., Savinainen, J. R., & Laitinen, J. T. (2012). Biochemical and pharmacological characterization of human α/β-hydrolase domain containing 6 (ABHD6) and 12 (ABHD12). *Journal of Lipid Research*, *53*(11), 2413–2424. https://doi.org/10.1194/jlr.M030411

Neises, B., & Steglich, W. (1978). Simple Method for the Esterification of Carboxylic Acids. *Angewandte Chemie*, *17*(7), 522–524.

Niwa, K., Ichino, Y., Kumata, S., Nakajima, Y., Hiraishi, Y., Kato, D. I., … Ohmiya, Y. (2010). Quantum yields and kinetics of the firefly bioluminescence reaction of beetle luciferases. *Photochemistry and Photobiology*, *86*(5), 1046–1049. https://doi.org/10.1111/j.1751-1097.2010.00777.x

Novack, G. D. (2016). Cannabinoids for treatment of glaucoma. *Current Opinion in Ophthalmology*, *27*(2), 146–150. https://doi.org/10.1097/ICU.0000000000000242

O'Sullivan, S. E. (2007). Cannabinoids go nuclear: Evidence for activation of peroxisome proliferator-activated receptors. *British Journal of Pharmacology*, *152*(5), 576–582. https://doi.org/10.1038/sj.bjp.0707423

Ohno-Shosaku, T., & Kano, M. (2014). Endocannabinoid-mediated retrograde modulation of synaptic transmission. *Current Opinion in Neurobiology*, *29*, 1–898. https://doi.org/10.1016/j.conb.2014.03.017

Oka, S., Nakajima, K., Yamashita, A., Kishimoto, S., & Sugiura, T. (2007). Identification of GPR55 as a lysophosphatidylinositol receptor. *Biochemical and Biophysical Research Communications*, *362*(4), 928–934. https://doi.org/10.1016/j.bbrc.2007.08.078

Onaivi, E. S., Ishiguro, H., Gong, J. P., Patel, S., Perchuk, A., Meozzi, P. A., … Uhl, G. R. (2006). Discovery of the presence and functional expression of cannabinoid CB2 receptors in brain. *Annals of the New York Academy of Sciences*, *1074*, 514–536. https://doi.org/10.1196/annals.1369.052

Overton, H. A., Babbs, A. J., Doel, S. M., Fyfe, M. C. T., Gardner, L. S., Griffin, G., … Reynet, C. (2006). Deorphanization of a G protein-coupled receptor for oleoylethanolamide and its use in the discovery of small-molecule hypophagic agents. *Cell Metabolism*, *3*(3), 167–175. https://doi.org/10.1016/j.cmet.2006.02.004

Pagotto, U., Marsicano, G., Cota, D., Lutz, B., & Pasquali, R. (2006). The emerging role of the endocannabinoid system in endocrine regulation and energy balance. *Endocrine Reviews*, *27*(1), 73–100. https://doi.org/10.1210/er.2005-0009

Parkkari, T., Haavikko, R., Laitinen, T., Navia-Paldanius, D., Rytilahti, R., Vaara, M., … Laitinen, J. T. (2014). Discovery of triterpenoids as reversible inhibitors of α/β- hydrolase domain containing 12 (ABHD12). *PLoS ONE*, *9*(5). https://doi.org/10.1371/journal.pone.0098286

Pertwee, R. G. (2006). The pharmacology of cannabinoid receptors and their ligands : an overview. *International Journal of Obesity*, 13–18. https://doi.org/10.1038/sj.ijo.0803272

Pertwee, R. G. (2008). The diverse CB1 and CB2 receptor pharmacology of three plant cannabinoids: D9-tetrahydrocannabinol, cannabidiol and D9-tetrahydrocannabivarin. *British Journal of Pharmacology*, *153*, 199–215.

Pertwee, R. G., Howlett, a C., Abood, M. E., Alexander, S. P. H., Marzo, V. Di, Elphick, M. R., … Kunos, G. (2010). International Union of Basic and Clinical Pharmacology . LXXIX . Cannabinoid Receptors and Their Ligands : Beyond CB 1 and CB 2. *Pharmacological Reviews*, *62*(4), 588–631. https://doi.org/10.1124/pr.110.003004.588

Petrosino, S., Iuvone, T., & Di Marzo, V. (2010). N-palmitoyl-ethanolamine: Biochemistry and new therapeutic opportunities. *Biochimie*, *92*(6), 724–727. https://doi.org/10.1016/j.biochi.2010.01.006

Piñeiro, R., & Falasca, M. (2012). Lysophosphatidylinositol signalling: New wine from an old bottle. *Biochimica et Biophysica Acta - Molecular and Cell Biology of Lipids*, *1821*(4), 694–705. https://doi.org/10.1016/j.bbalip.2012.01.009

Pinto Da Silva, L., & Esteves Da Silva, J. C. G. (2014). Study of firefly luciferin oxidation and isomerism as possible inhibition pathways for firefly bioluminescence. *Chemical Physics Letters*, *592*, 188–191. https://doi.org/10.1016/j.cplett.2013.12.047

Pliego, J., Mateos, J. C., Rodriguez, J., Valero, F., Baeza, M., Femat, R., … Herrera-López, E. J. (2015). Monitoring lipase/esterase activity by stopped flow in a sequential injection analysis system using p-nitrophenyl butyrate. *Sensors (Switzerland)*, *15*(2), 2798–2811. https://doi.org/10.3390/s150202798

Porter, N. A. (2013). A perspective on free radical autoxidation: The physical organic chemistry of polyunsaturated fatty acid and sterol peroxidation. *Journal of Organic Chemistry*, *78*(8), 3511–3524. https://doi.org/10.1021/jo4001433

Purich, D. (2010). *Enzyme Kinetics: Catalysis and Control*. Elsevier.

Ramón, A., Señorale-Pose, M., & Marín, M. (2014). Inclusion bodies: Not that bad... *Frontiers in Microbiology*, *5*(FEB), 2010–2015. https://doi.org/10.3389/fmicb.2014.00056

Riccardi, L., Arencibia, J. M., Bono, L., Armirotti, A., Girotto, S., & De Vivo, M. (2017). Lid domain plasticity and lipid flexibility modulate enzyme specificity in human monoacylglycerol lipase. *Biochimica et Biophysica Acta - Molecular and Cell Biology of Lipids*, *1862*(5), 441–451. https://doi.org/10.1016/j.bbalip.2017.01.002

Rinas, U., Garcia-Fruitós, E., Corchero, J. L., Vázquez, E., Seras-Franzoso, J., & Villaverde, A. (2017). Bacterial Inclusion Bodies: Discovering Their Better Half. *Trends in Biochemical Sciences*, *42*(9), 726–737. https://doi.org/10.1016/j.tibs.2017.01.005

Roda, A., Mirasoli, M., Michelini, E., Di Fusco, M., Zangheri, M., Cevenini, L., … Simoni, P. (2016). Progress in chemical luminescence-based biosensors: A critical review. *Biosensors and*

Bioelectronics, *76*, 164–179. https://doi.org/10.1016/j.bios.2015.06.017

Rogers, N. (2015). Cannabinoid receptor with an "identity crisis" gets a second look. *Nature Medicine*, *21*(9), 966–967. https://doi.org/10.1038/nm0915-966

Russo, E. B. (2007). History of cannabis and its preparations in saga, science, and sobriquet. *Chemistry and Biodiversity*, *4*(8), 1614–1648. https://doi.org/10.1002/cbdv.200790144

Ryberg, E., Larsson, N., Sjögren, S., Hjorth, S., Hermansson, N. O., Leonova, J., … Greasley, P. J. (2007). The orphan receptor GPR55 is a novel cannabinoid receptor. *British Journal of Pharmacology*, *152*(7), 1092–1101. https://doi.org/10.1038/sj.bjp.0707460

Saario, S. M., Salo, O. M. H., Nevalainen, T., Poso, A., Laitinen, J. T., Järvinen, T., & Niemi, R. (2005). Characterization of the sulfhydryl-sensitive site in the enzyme responsible for hydrolysis of 2-arachidonoyl-glycerol in rat cerebellar membranes. *Chemistry and Biology*, *12*(6), 649–656. https://doi.org/10.1016/j.chembiol.2005.04.013

Saario, S. M., Savinainen, J. R., Laitinen, J. T., Järvinen, T., & Niemi, R. (2004). Monoglyceride lipase-like enzymatic activity is responsible for hydrolysis of 2-arachidonoylglycerol in rat cerebellar membranes. *Biochemical Pharmacology*, *67*(7), 1381–1387. https://doi.org/10.1016/j.bcp.2003.12.003

Sakurai, Y., Ma, S. F., Watanabe, H., Yamaotsu, N., Hirono, S., Kurono, Y., … Otagiri, M. (2004). Esterase-Like Activity of Serum Albumin: Characterization of Its Structural Chemistry Using p-Nitrophenyl Esters as Substrates. *Pharmaceutical Research*, *21*(2), 285–292. https://doi.org/10.1023/B:PHAM.0000016241.84630.06

Sam, A. H., Salem, V., & Ghatei, M. A. (2011). Rimonabant: From RIO to Ban. *Journal of Obesity*, *2011*. https://doi.org/10.1155/2011/432607

Satoh, T., Kato, J., Takiguchi, N., Ohtake, H., & Kuroda, A. (2004). ATP amplification for ultrasensitive bioluminescence assay: detection of a single bacterial cell. *Bioscience, Biotechnology, and Biochemistry*, *68*(6), 1216–20. https://doi.org/10.1271/bbb.68.1216

Savinainen, J. R., Navia-Paldanius, D., & Laitinen, J. T. (2016a). A Sensitive and Versatile Fluorescent Activity Assay for ABHD12. In M. Maccarrone (Ed.), *Endocannabinoid Signaling: Methods and Protocols* (pp. 169–178). New York: Media, Springer Science+Business. https://doi.org/10.1007/978-1-4939-3539-0_18

Savinainen, J. R., Navia-Paldanius, D., & Laitinen, J. T. (2016b). A Sensitive and Versatile Fluorescent Activity Assay for ABHD6. In M. Maccarrone (Ed.), *Endocannabinoid Signaling: Methods and Protocols* (pp. 169–178). New York: Springer Science+Business Media. https://doi.org/10.1007/978-1-4939-3539-0_18

Savinainen, J. R., Saario, S. M., & Laitinen, J. T. (2012). The serine hydrolases MAGL, ABHD6 and ABHD12 as guardians of 2-arachidonoylglycerol signalling through cannabinoid receptors. *Acta Physiologica*, *204*(2), 267–276. https://doi.org/10.1111/j.1748-1716.2011.02280.x

Savinainen, J. R., Yoshino, M., Minkkilä, A., Nevalainen, T., & Laitinen, J. T. (2010). Characterization of binding properties of monoglyceride lipase inhibitors by a versatile fluorescence-based technique - Supplementary Data. *Analytical Biochemistry*, *1*(1), XLV. https://doi.org/10.1016/j.ab.2009.12.009

Scalvini, L., Vacondio, F., Bassi, M., Pala, D., Lodola, A., Rivara, S., … Mor, M. (2016). Free-energy studies reveal a possible mechanism for oxidation- dependent inhibition of MGL. *Nature Publishing Group*, (April), 1–12. https://doi.org/10.1038/srep31046

Schalk-Hihi, C., Schubert, C., Alexander, R., Bayoumy, S., Clemente, J. C., Deckman, I., … Kuo, L. C. (2011). Crystal structure of a soluble form of human monoglyceride lipase in complex with an inhibitor at 1.35 A ° resolution. *Protein Science*, *20*(4), 670–683. https://doi.org/10.1002/pro.596

Schmidt, M., & Bornscheuer, U. T. (2005). High-throughput assays for lipases and esterases. *Biomolecular Engineering*, *22*(1–3), 51–56. https://doi.org/10.1016/j.bioeng.2004.09.004

Shao, Z., Yin, J., Chapman, K., Grzemska, M., Clark, L., Wang, J., & Rosenbaum, D. M. (2016). High-resolution crystal structure of the human CB1 cannabinoid receptor. *Nature*, *540*(7634), 602–606. https://doi.org/10.1038/nature20613

Shoemaker, J. L. (2005). The Endocannabinoid Noladin Ether Acts as a Full Agonist at Human CB2 Cannabinoid Receptors. *Journal of Pharmacology and Experimental Therapeutics*, *314*(2), 868–875. https://doi.org/10.1124/jpet.105.085282

Shrestha, N., Cuffe, J. S. M., Hutchinson, D. S., Headrick, J. P., Perkins, A. V., McAinch, A. J., & Hryciw, D. H. (2018). Peripheral modulation of the endocannabinoid system in metabolic disease. *Drug Discovery Today*, *00*(00), 1–13. https://doi.org/10.1016/j.drudis.2018.01.029

Shrivastava, A., & Gupta, V. (2011). Methods for the determination of limit of detection and limit of quantitation of the analytical methods. *Chronicles of Young Scientists*, *2*(1), 21. https://doi.org/10.4103/2229-5186.79345

Smirnova, D. V., & Ugarova, N. N. (2017). Firefly Luciferase-based Fusion Proteins and their Applications in Bioanalysis. *Photochemistry and Photobiology*, *93*(2), 436–447. https://doi.org/10.1111/php.12656

Steffens, M., Zentner, J., Honegger, J., & Feuerstein, T. J. (2005). Binding affinity and agonist activity of putative endogenous cannabinoids at the human neocortical CB1 receptor. *Biochemical Pharmacology*, *69*(1), 169–178. https://doi.org/10.1016/j.bcp.2004.08.033

Stella, N., Schweitzer, P., & Piomelli, D. (1997). A second endogenous' cannabinoid that modulates long-term potentiation. *Nature*, *388*(6644), 773–778. https://doi.org/10.1038/42015

Surade, S., Klein, M., Stolt-Bergner, P. C., Muenke, C., Roy, A., & Michel, H. (2006). Comparative analysis and "expression space" coverage of the production of prokaryotic membrane proteins for structural genomics. *Protein Science : A Publication of the Protein Society*, *15*(9), 2178–2189. https://doi.org/10.1110/ps.062312706

Tjernberg, A., Markova, N., Griffiths, W. J., & Hallén, D. (2006). DMSO-related effects in protein characterization. *Journal of Biomolecular Screening*, *11*(2), 131–137. https://doi.org/10.1177/1087057105284218

Toczek, M., & Malinowska, B. (2018). Enhanced endocannabinoid tone as a potential target of pharmacotherapy. *Life Sciences*, *204*(January), 20–45. https://doi.org/10.1016/j.lfs.2018.04.054

Toya, Y., Takagi, M., Kondo, T., Nakata, H., Isobe, M., & Goto, T. (1992). Improved synthetic methods of firefly luciferin derivatives for use in bioluminescent analysis of hydrolytic enzymes; carboxylic esterase and alkaline phosphatase. *Bulletin of the Chemical Society of Japan*, *65*(10), 2604–2610. https://doi.org/10.1246/bcsj.65.2604

Tuccinardi, T., Ferrarini, P. L., Manera, C., Ortore, G., Saccomanni, G., & Martinelli, A. (2006). Cannabinoid CB2/CB1 selectivity. Receptor modeling and automated docking analysis. *Journal of Medicinal Chemistry*, *49*(3), 984–994. https://doi.org/10.1021/jm050875u

Tuo, W., Leleu-Chavain, N., Spencer, J., Sansook, S., Millet, R., & Chavatte, P. (2017). Therapeutic Potential of Fatty Acid Amide Hydrolase, Monoacylglycerol Lipase, and N-Acylethanolamine Acid Amidase Inhibitors. *Journal of Medicinal Chemistry*, *60*(1), 4–46. https://doi.org/10.1021/acs.jmedchem.6b00538

Van Esbroeck, A. C. M., Janssen, A. P. A., Cognetta, A. B., Ogasawara, D., Shpak, G., Van Der Kroeg, M., … Van Der Stelt, M. (2017). Activity-based protein profiling reveals off-target proteins of the FAAH inhibitor BIA 10-2474. *Science*, *356*(6342), 1084–1087. https://doi.org/10.1126/science.aaf7497

van Iersel, M. T. (2017). The Use of IC50for Potency and MTD as Objective in Study BIA 10–2474. *Journal of Clinical Pharmacology*, *57*(10), 1357–1358. https://doi.org/10.1002/jcph.995

Vettor, R., Pagotto, U., Pagano, C., & Pasquali, R. (2008). Here, there and everywhere: the endocannabinoid system. *Journal of Neuroendocrinology*, *20 Suppl 1*, iv–vi. https://doi.org/10.1111/j.1365-2826.2008.01691.x

Volkow, N. D., Hampson, A. J., & Baler, R. D. (2017). Don't Worry, Be Happy: Endocannabinoids and Cannabis at the Intersection of Stress and Reward. *Annual Review of Pharmacology and Toxicology*, *57*(1), 285–308. https://doi.org/10.1146/annurev-pharmtox-010716-104615

Wang, J., & Ueda, N. (2009). Biology of endocannabinoid synthesis system. *Prostaglandins and Other Lipid Mediators*, *89*(3–4), 112–119. https://doi.org/10.1016/j.prostaglandins.2008.12.002

Wang, Y., Chanda, P., Jones, P. G., & Kennedy, J. D. (2008). A fluorescence-based assay for Monoacylglycerol Lipase Compatible with Inhibitor Screening. *Assay And Drug Development Technologies*, *6*(3), 387–393.

Wei, B. Q., Mikkelsen, T. S., McKinney, M. K., Lander, E. S., & Cravatt, B. F. (2006). A second fatty acid amide hydrolase with variable distribution among placental mammals. *Journal of Biological Chemistry*, *281*(48), 36569–36578. https://doi.org/10.1074/jbc.M606646200

White, E. H., Rapaport, E., Seliger, H. H., & Hopkins, T. A. (1971). The chemi- and bioluminescence of firefly luciferin: An efficient chemical production of electronically excited states. *Bioorganic Chemistry*, *1*(1–2), 92–122. https://doi.org/10.1016/0045-2068(71)90009-5

Widder, E. A., & Falls, B. (2014). Review of bioluminescence for engineers and scientists in biophotonics. *IEEE Journal on Selected Topics in Quantum Electronics*, *20*(2). https://doi.org/10.1109/JSTQE.2013.2284434

Woodhams, S. G., Chapman, V., Finn, D. P., Hohmann, A. G., & Neugebauer, V. (2017). The cannabinoid system and pain. *Neuropharmacology*, *124*, 105–120. https://doi.org/10.1016/j.neuropharm.2017.06.015

Xi, Z. X., Peng, X. Q., Li, X., Song, R., Zhang, H. Y., Liu, Q. R., … Gardner, E. L. (2011). Brain cannabinoid CB2receptors modulate cocaine's actions in mice. *Nature Neuroscience*, *14*(9), 1160–1168. https://doi.org/10.1038/nn.2874

Xu, L. Y., & Link, A. J. (2009). Stress responses to heterologous membrane protein expression in Escherichia coli. *Biotechnology Letters*, *31*(11), 1775–1782. https://doi.org/10.1007/s10529-009-0075-5

Zhang, H.-Y., Gao, M., Liu, Q.-R., Bi, G.-H., Li, X., Yang, H.-J., … Xi, Z.-X. (2014). Cannabinoid CB_2 receptors modulate midbrain dopamine neuronal activity and dopamine-related behavior in mice. *Proceedings of the National Academy of Sciences*, *111*(46), E5007–E5015. https://doi.org/10.1073/pnas.1413210111

Zhang, H.-Y., Gao, M., Shen, H., Bi, G.-H., Yang, H.-J., Liu, Q.-R., … Xi, Z.-X. (2017). Expression of functional cannabinoid CB_2 receptor in VTA dopamine neurons in rats. *Addiction Biology*, *22*(3), 752–765. https://doi.org/10.1111/adb.12367

Zhang Ji-Hu, Chung Thomas D.Y., O. K. R. (1999). A Simple Statistical Parameter for Use in Evaluation and Validation of High Throughput Screening Assays. *Journal of Biomolecular Screening*, *4*(2), 67–73. https://doi.org/10.1177/07399863870092005

Zimmer, A. (2016). A collaboration investigating endocannabinoid signalling in brain and bone, *27*(3), 229–235. https://doi.org/10.1515/jbcpp-2015-0125

Zipfel, W. R., Williams, R. M., Christie, R., Nikitin, A. Y., Hyman, B. T., & Webb, W. W. (2003). Live tissue intrinsic emission microscopy using multiphoton-excited native fluorescence and second harmonic generation, *100*(12), 7075–7080.

Zygmunt, P. M., Ermund, A., Movahed, P., Andersson, D. A., Simonsen, C., Jönsson, B. A. G., … Högestätt, E. D. (2013). Monoacylglycerols activate TRPV1 - A link between phospholipase C and TRPV1. *PLoS ONE*, *8*(12). https://doi.org/10.1371/journal.pone.0081618

APPENDIX: NMR SPECTRAL DATA

Table 7. NMR assignments for resorufin compounds (3.2.1).

	1a		***1b***		***1c***		***1d***		***1e***		***1f***	
	δ (H)	*δ* (C)	*δ* (H)	*δ* (C)	*δ* (H)	*δ* (C)	*δ* (H)	*δ* (C)	*δ* (H)	*δ* (C)	*δ* (H)	*δ* (C)
CH(1)	7.46 (d) *9.8*	134.8	7.46 *9.9*	134.8	7.47 *9.8*	134.8	7.47 *9.8*	134.8	7.46 *9.8*	134.8	7.46 *9.8*	134.8
CH(2)	6.89 (dd) *9.8, 2.0*	135.2	6.89 *9.9, 2.1*	135.1	6.90 *9.8, 2.0*	135.1	6.90 *9.8, 2.0*	135.1	6.89 *9.8, 2.0*	135.1	6.90 *9.8, 2.0*	135.1
C(3)		186.3		186.3		186.4		186.3		186.3		186.3
CH(4)	6.36 (d) *2.0*	107.2	6.36 *2.1*	107.2	6.37 *2.0*	107.2	6.37 *2.0*	107.2	6.36 *2.0*	107.2	6.36 *2.0*	107.2
CH(6)	7.18 (d) *2.4*	119.3	7.18 *2.4*	119.3	7.18 *2.4*	119.3	7.18 *2.4*	119.3	7.18 *2.4*	119.3	7.17 *2.4*	119.3
C(7)		153.6		153.6		153.7		153.7		153.7		153.7
CH(8)	7.15 (dd) *8.6, 2.4*	109.7	7.15 *8.6, 2.4*	109.7	7.15 *8.6, 2.4*	109.7	7.15 *8.6, 2.4*	109.7	7.14 *8.6, 2.4*	109.7	7.15 *8.6, 2.4*	109.7
CH(9)	7.82 (d) *8.6*	131.1	7.82 *8.6*	131.1	7.83 *8.6*	131.1	7.83 *8.6*	131.1	7.82 *8.6*	131.1	7.83 *8.6*	131.1

C(11)		148.2		148.2		148.2		148.2		148.2		148.2
C(12)		149.3		149.3		149.3		149.3		149.3		149.3
C(13)		144.3		144.3		144.4		144.4		144.4		144.4
C(14)		131.1		131.1		131.1		131.1		131.2		131.1
COO		171.2		171.2		171.4		171.4		171.4		171.4
OCO*CH₂*			2.62 *7.0*	36.2	2.63 (t) *7.5*	34.4	2.63 *7.5*	34.4	2.63 *7.5*	34.4	2.63 *7.0*	34.4
CO CH₂*CH₂*			1.84 *7.0, 7.4*	18.3	1.79 (tt) *7.5, 7.5*	31.6	1.79 *7.5, 7.5*	24.8	1.79 *7.5, 7.5*	24.8	1.80 *7.0, 7.0*	24.8
CH=CH											5.42-5.34 (2H, m, 9′, 10′)	129.7 (9′), 130.1 (10′)
CH=CH- *CH₂*											2.08-2.02 (4H, m, 8′, 11′)	27.2 (8′), 27.2 (11′)
CH₂-FAC[a]					1.27-1.47 (20 H,	29.0, 28.9, 24.8,	1.47-1.24 (16 H,	22.7, 29.1, 29.2, 29.3, 29.4, 29.6,	1.46-1.25 (32 H,	22.7, 29.1, 29.2, 29.4, 29.4, 29.6,	1.45-1.26 (20 H, m, 17′)	22.7 (17′), 29.0, 29. 29.1, 29.3, 29.5, 29. 29.8 (4′-7′ and 12

					m, 4′-7′)	22.6	m, 4′-11′)	31.9 (4′-11′)	m, 4′-19′)	29.6, 29.7, 29.7, 29.7, 31.9 (4′-19′)		15′), 31.9 (16′)
CH_3	2.38	21.2	1.09 *7.4*	13.6	0.93 *7.0*	14.1	0.94 *7.1*	14.1	0.90 (t) *7.0*	14.1	0.94	14.1

	1g		***1h***		***1i***		***1j***		***1k***	
	δ (H)	δ (C)	δ (H)	δ (C)	δ (H)	δ (C)	δ (H)	δ (C)	δ (H)	δ (C)
CH(1)	7.46 *9.8*	134.8	7.46 (d) *9.8*	134.8	7.47 (d) *9.8*	134.8	7.47 (d) *9.8*	134.8	7.49 *9.8*	134.8
CH(2)	6.89 *9.8, 2.0*	135.2	6.89 (dd) *9.8, 2.0*	135.1	6.90 (dd) *9.8, 2.0*	135.1	6.90 (dd) *9.8, 2.0*	135.1	6.91 *9.8, 2.0*	135.2
C(3)	6.36 *2.0*	186.3		186.3		186.3		186.3		186.3
CH(4)	7.17 *2.4*	107.3	6.36 (d) *2.0*	107.2	6.36 (d) *2.0*	107.2	6.36 (d) *2.0*	107.2	6.38 *2.0*	107.3

CH(6)		119.3	7.16 (d) *2.4*	119.3	7.16 (d) *2.4*	119.4	7.16 (d) *2.4*	119.4	7.32 *2.4*	119.5
C(7)	7.14 *8.6, 2.4*	153.6		153.8		153.8		153.8		153.8
CH(8)	7.82 *8.6*	109.7	7.14 (dd) *8.6, 2.4*	109.7	7.13 (dd) *8.6, 2.4*	109.8	7.13 (dd) *8.6, 2.4*	109.7	7.30 *8.6, 2.4*	109.9
CH(9)		131.2	7.83 (d) *8.6*	131.1	7.83 (d) *8.6*	131.2	7.83 (d) *8.6*	131.1	7.89 *8.6*	131.2
C(11)		148.3		148.2		148.2		148.2		148.3
C(12)		149.4		149.4		149.3		149.3		149.4
C(13)		144.4		144.4		144.4		144.4		144.5
C(14)		131.2		131.1		131.1		131.1		131.2
COO	2.65 (t) *7.0*	33.7 (2′)		174.5		174.1		174.2		164.4
$OCOCH_{(2,1)}(CH_2)_n$	1.88 (3′) *7.0, 7.3*	24.6 (3′)	2.75 (tq) *7.0, 7.0*	39.7	2.58 (dq) *7.7, 7.0*	47.4	2.63 (tt) *7.0, 7.0*	45.9		
$OCOCH_{(2,1)}(CH_2)_n$	5.52-5.33	130.6,129.4,128.7,	1.84 (3′)	33.3	1.80 (dt)	31.6	1.83-1.74	32.4		

	(8H, m, 5′,6′,8′,9′, 11′,12′, 14′,15′)	128.5,128.4,128.0, 127.8,127.5 (5′,6′,8′,9′, 11′,12′, 14′,15′)	*7.0, 7.0*		*7.4, 7.0*		(2H, m) 1.67-1.59 (2H, m)			
CH=CH	2.88-2.82 (6H, m, 7′, 10′, 13′)	27.3 (7′, 10′, 13′)		-		-		-		
CH=CH-*CH_2*	2.25 (4′, dt) *7.0, 7.3* 1.39-1.28 (6 H, m, 17′-19′)	22.6 (19′), 29.3 (17′), 31.6 (18′), 26.5 (4′), 25.7 (16′)		-		-		-		
CH_2-FAC[a]			1.64-1.58 (2H, m) 1.45-1.39 (2H, m)	29.4 22.6	1.74-1.62 1.46-1.36 (6H)	29.6 25.4 22.6	1.44-1.28 (12H, m)	32.1, 31.7, 29.7, 29.2, 27.5 22.6		

CH_3	0.91 (t) *7.6*	14.1	1.34 (d) *7.2* 0.97 (t) *7.0*	14.0 16.9	1.06 (t) *7.4* 0.97 (t) *7.0*	11.9 14.0	0.96 (t) *7.0* 0.92 (t) *7.0*	14.0 14.1		
o-H_{ar}									8.24 (d) *7.7*	130.4
m-H_{ar}									7.58 (t) *7.7*	128.8
p-H_{ar}									7.72 (t) *7.7*	134.2

^{1}H and ^{13}C NMR spectra of 7-hydroxyresorufinyl-acetate (**1a**)

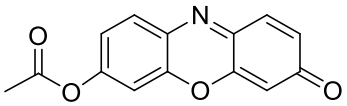

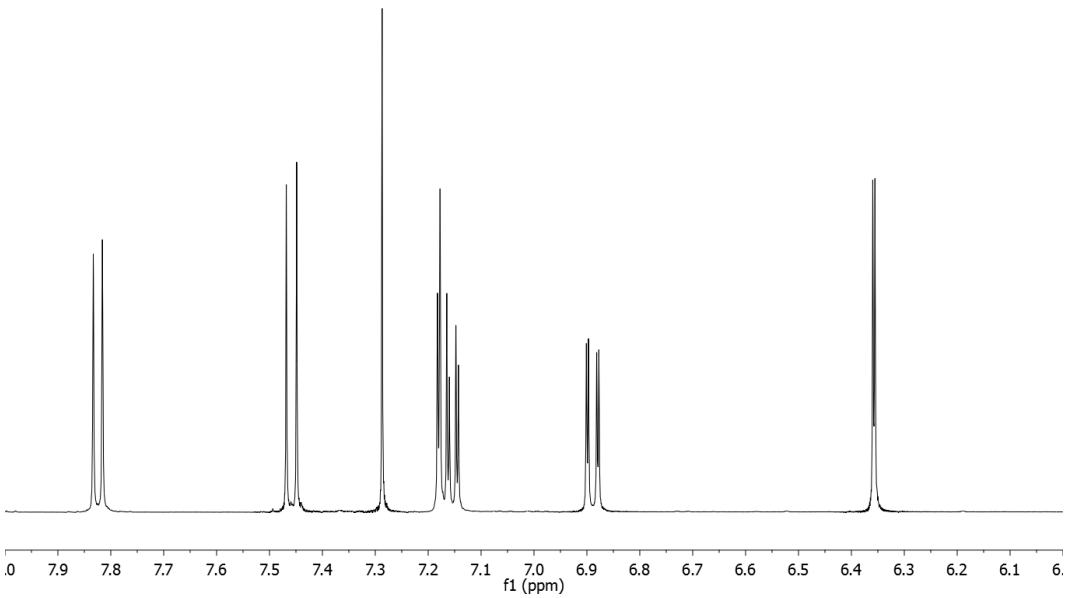

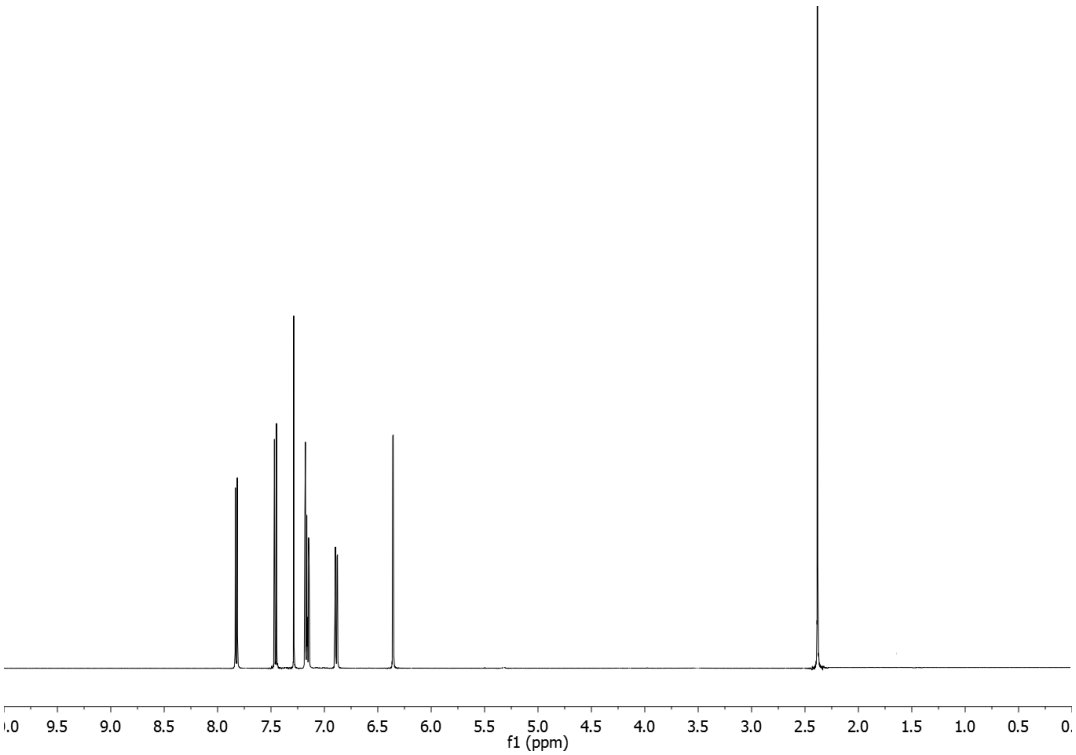

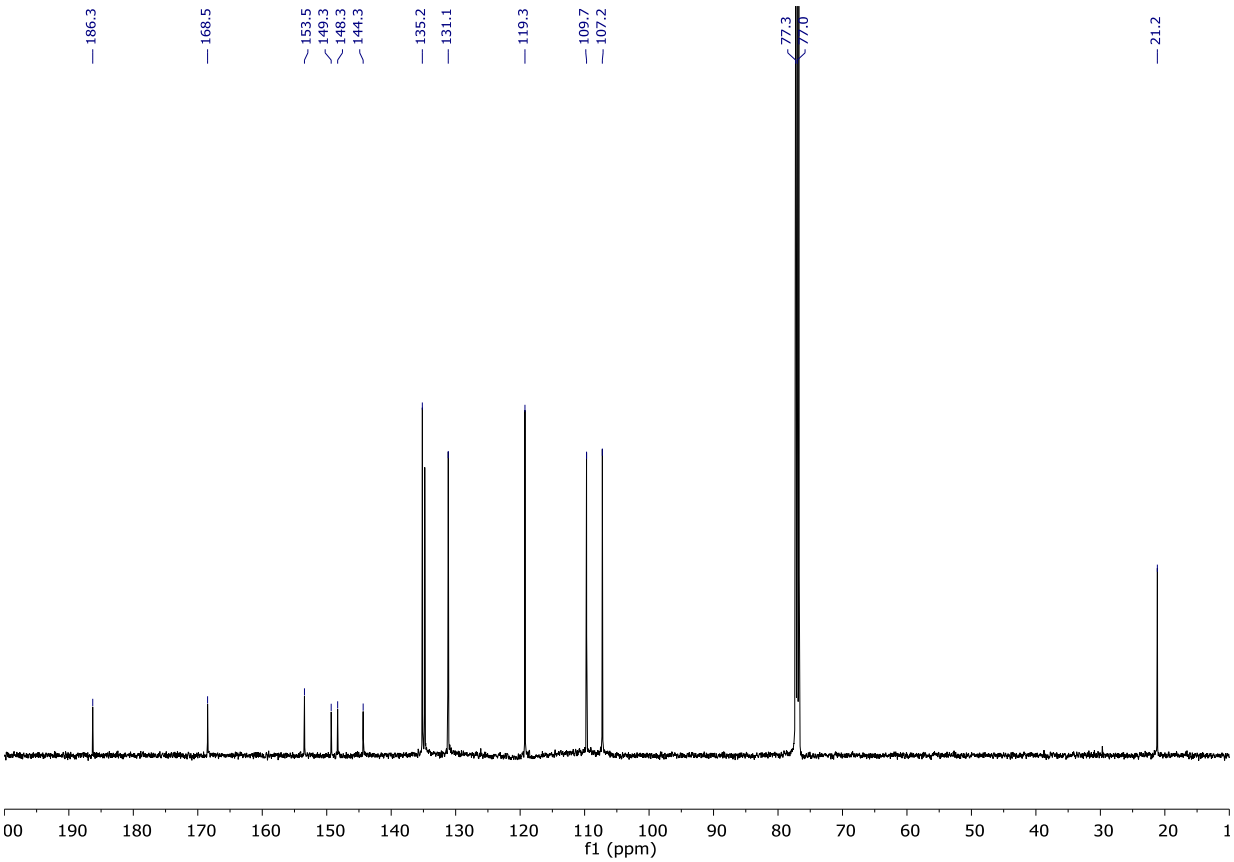
186.3
168.5
153.5
149.3
148.3
144.3
135.2
131.1
119.3
109.7
107.2
77.3
77.0
21.2
f1 (ppm)

^{1}H and ^{13}C NMR spectra of 7-hydroxyresorufinyl-butyrate (**1b**)

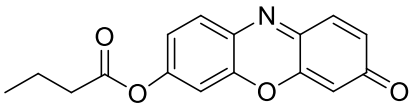

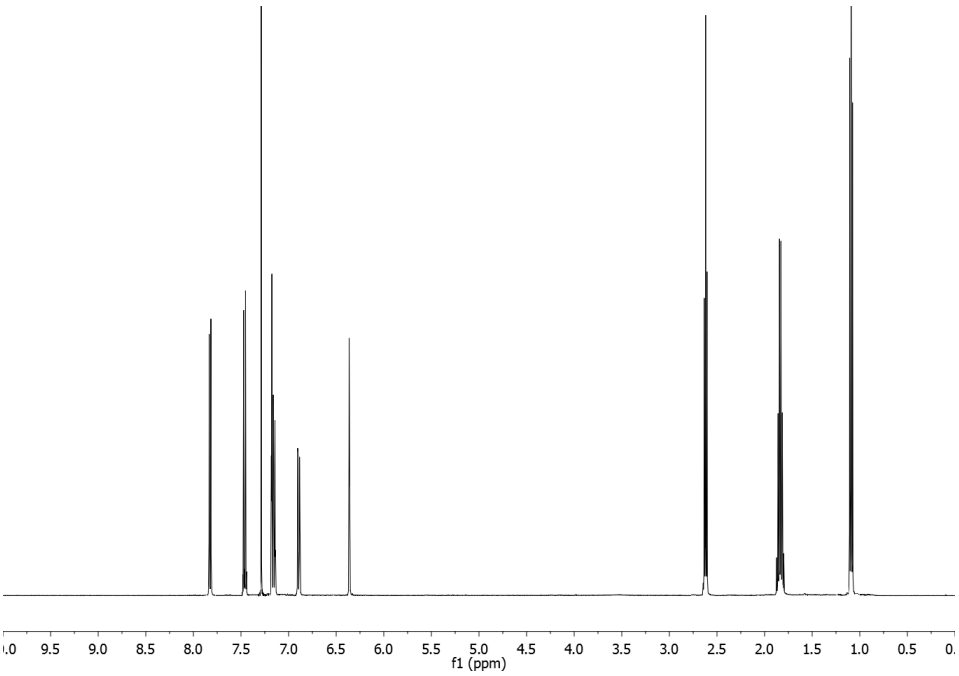

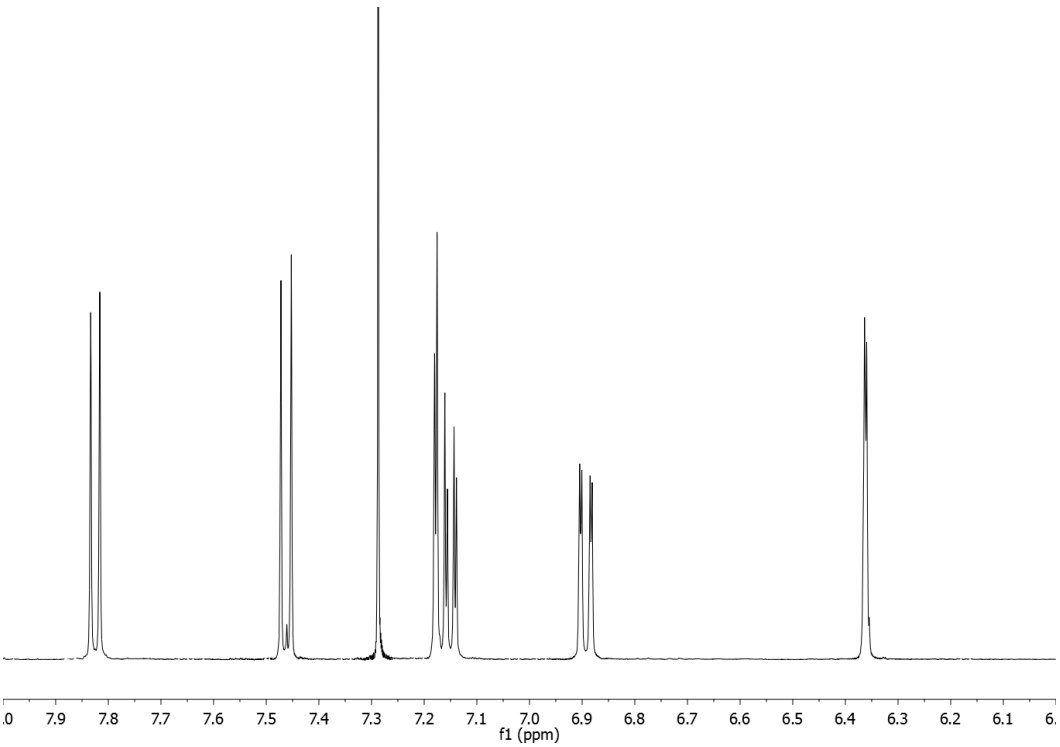

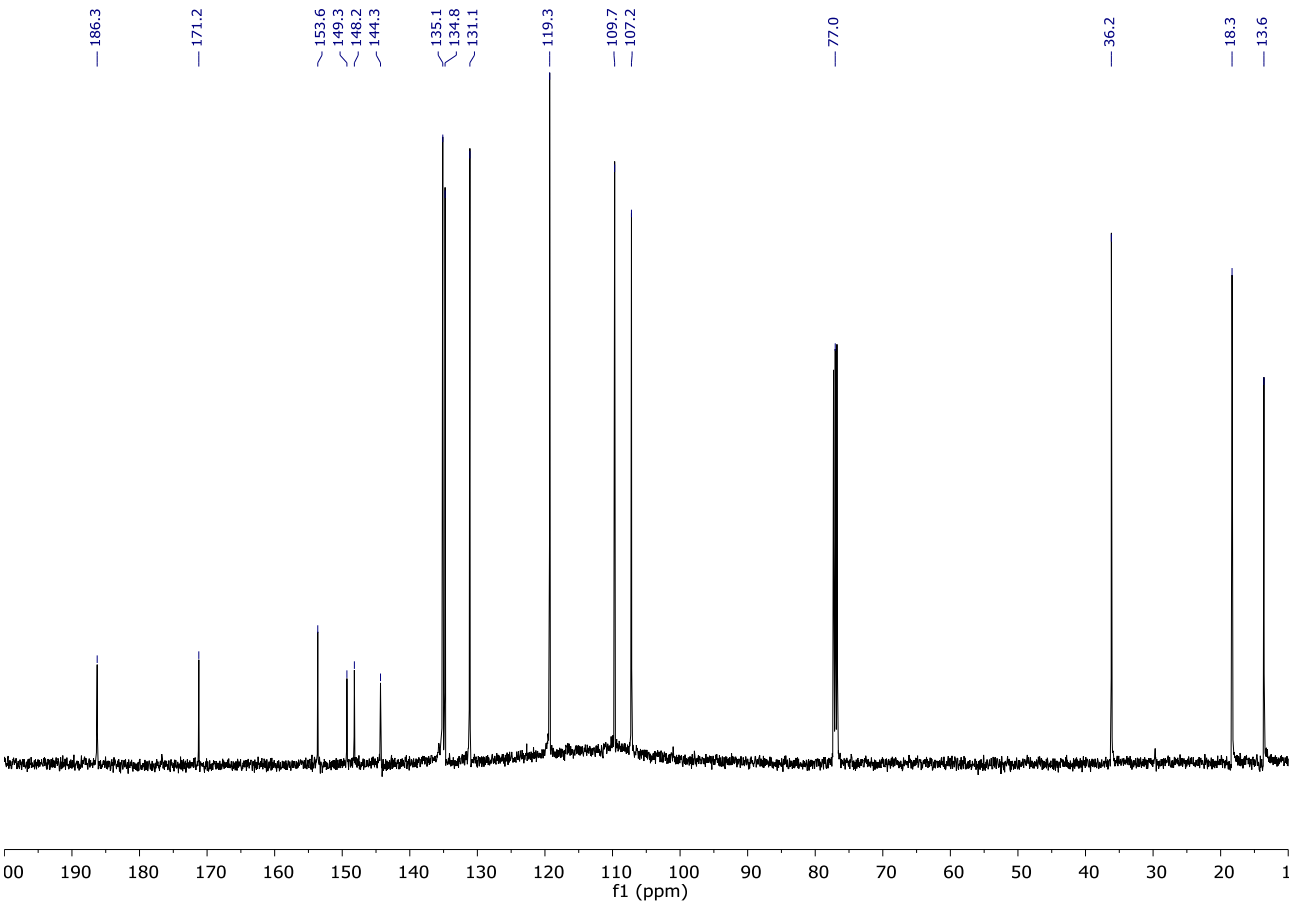
186.3
171.2
153.6
149.3
148.2
144.3
135.1
134.8
131.1
119.3
109.7
107.2
77.0
36.2
18.3
13.6
00 190 180 170 160 150 140 130 120 110 100 90 80 70 60 50 40 30 20 1
f1 (ppm)

^{1}H and ^{13}C NMR spectra of 7-hydroxyresorufinyl-octanoate (**1c**)

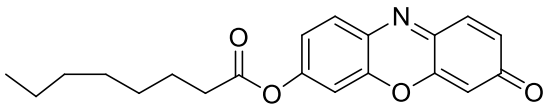

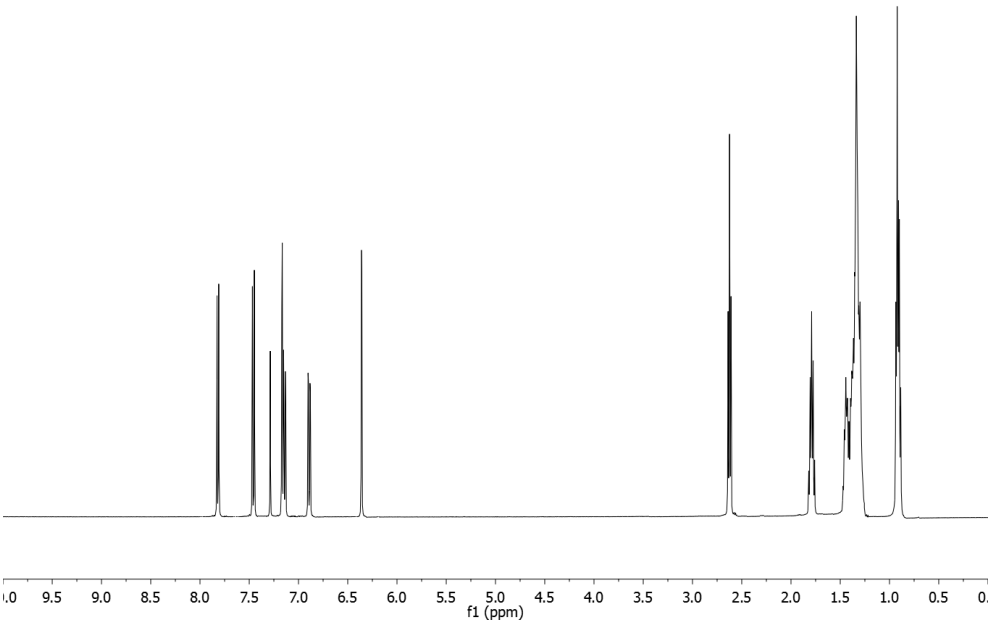

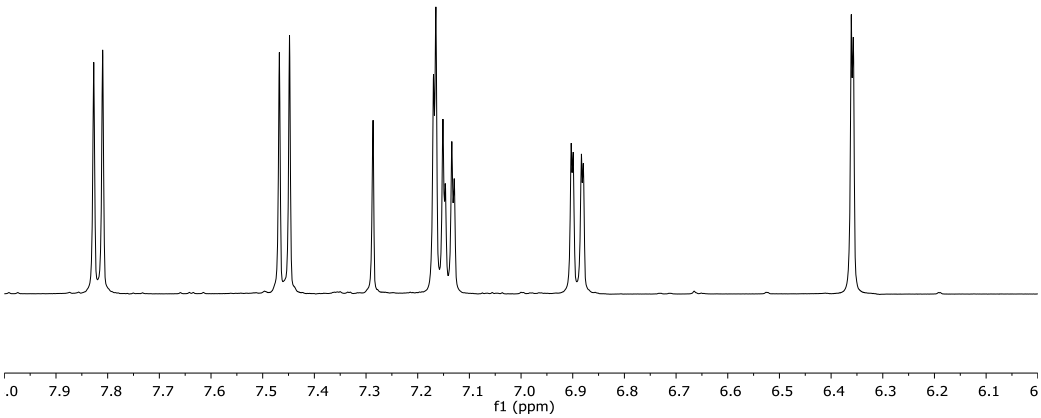

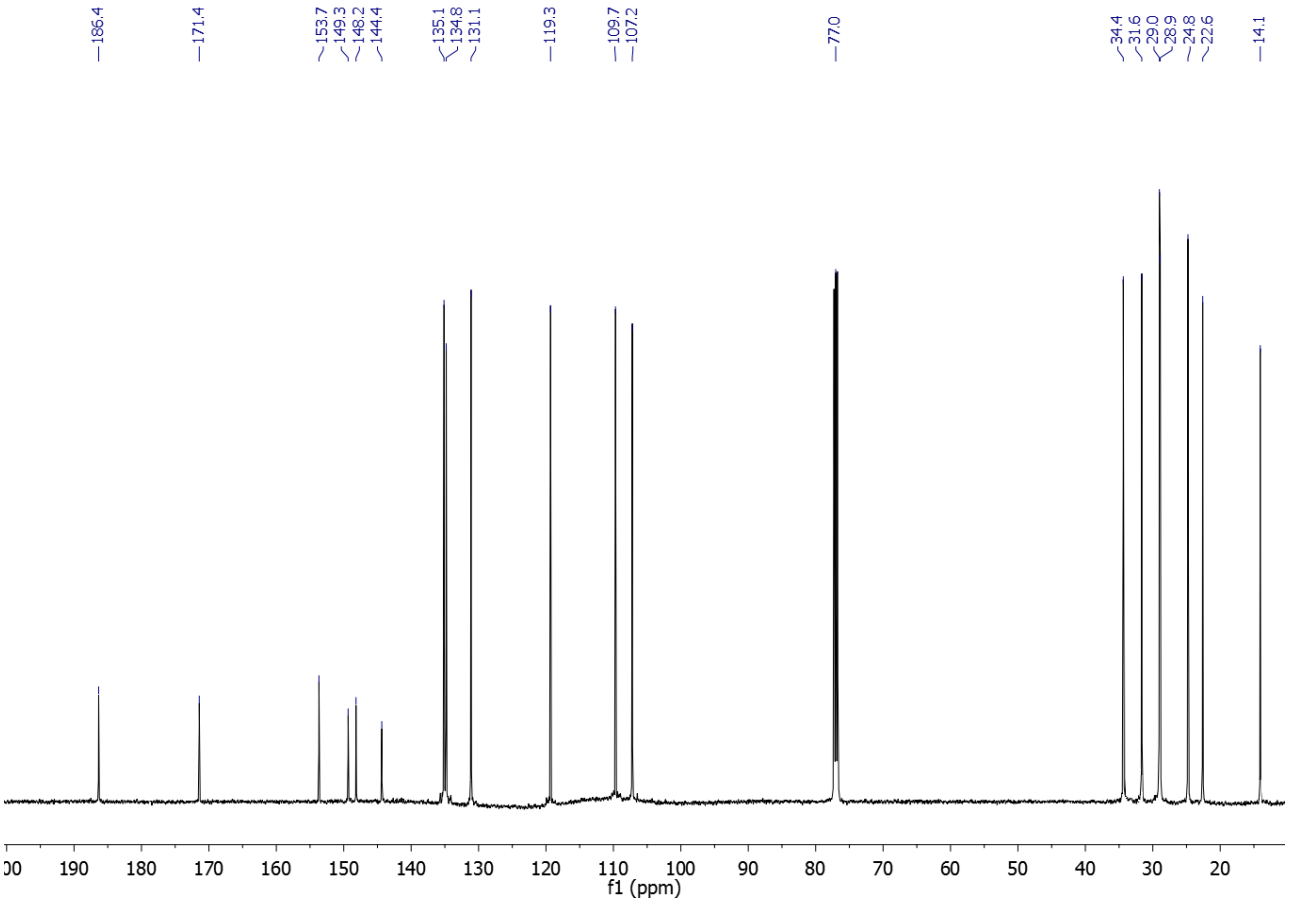
186.4
171.4
153.7
149.3
148.2
144.4
135.1
134.8
131.1
119.3
109.7
107.2
77.0
34.4
31.6
29.0
28.9
24.8
22.6
14.1
00 190 180 170 160 150 140 130 120 110 100 90 80 70 60 50 40 30 20
f1 (ppm)

^{1}H and ^{13}C NMR spectra of 7-hydroxyresorufinyl-laurate (**1d**)

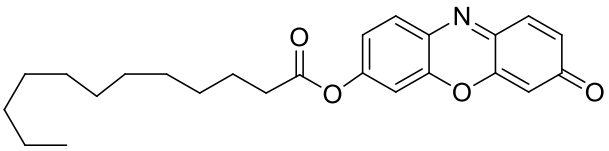

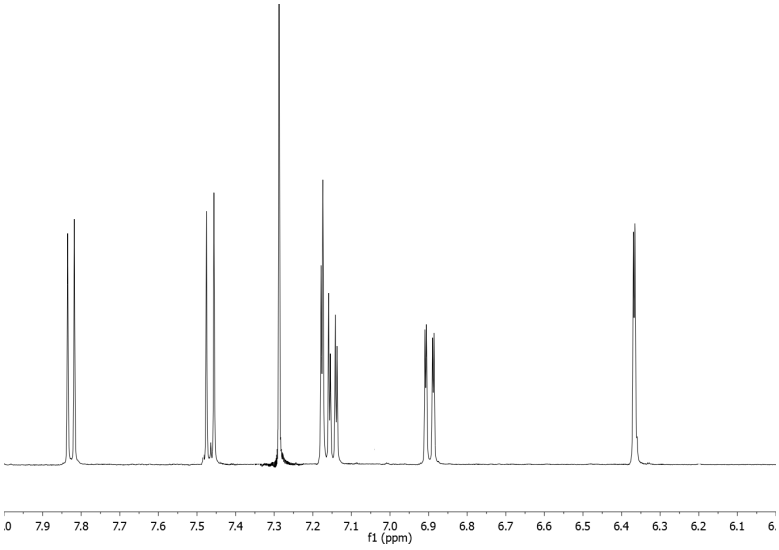

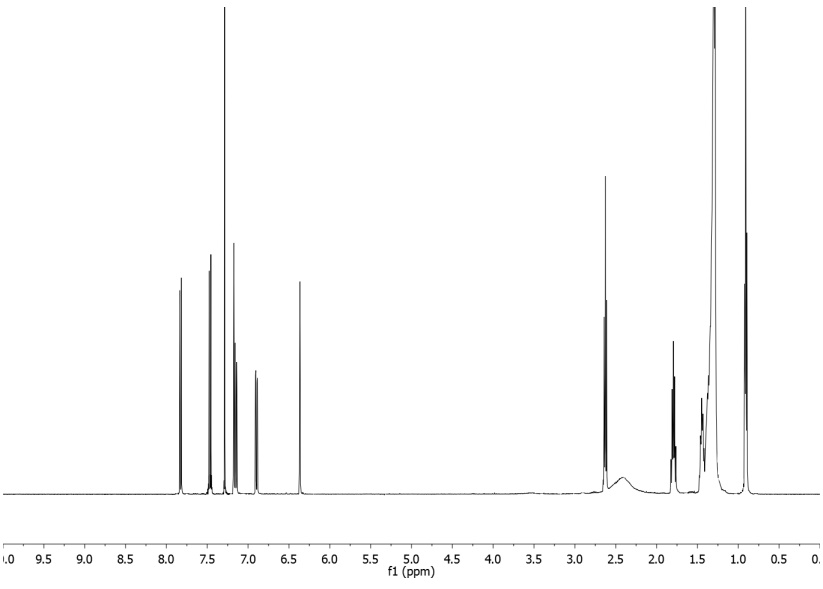

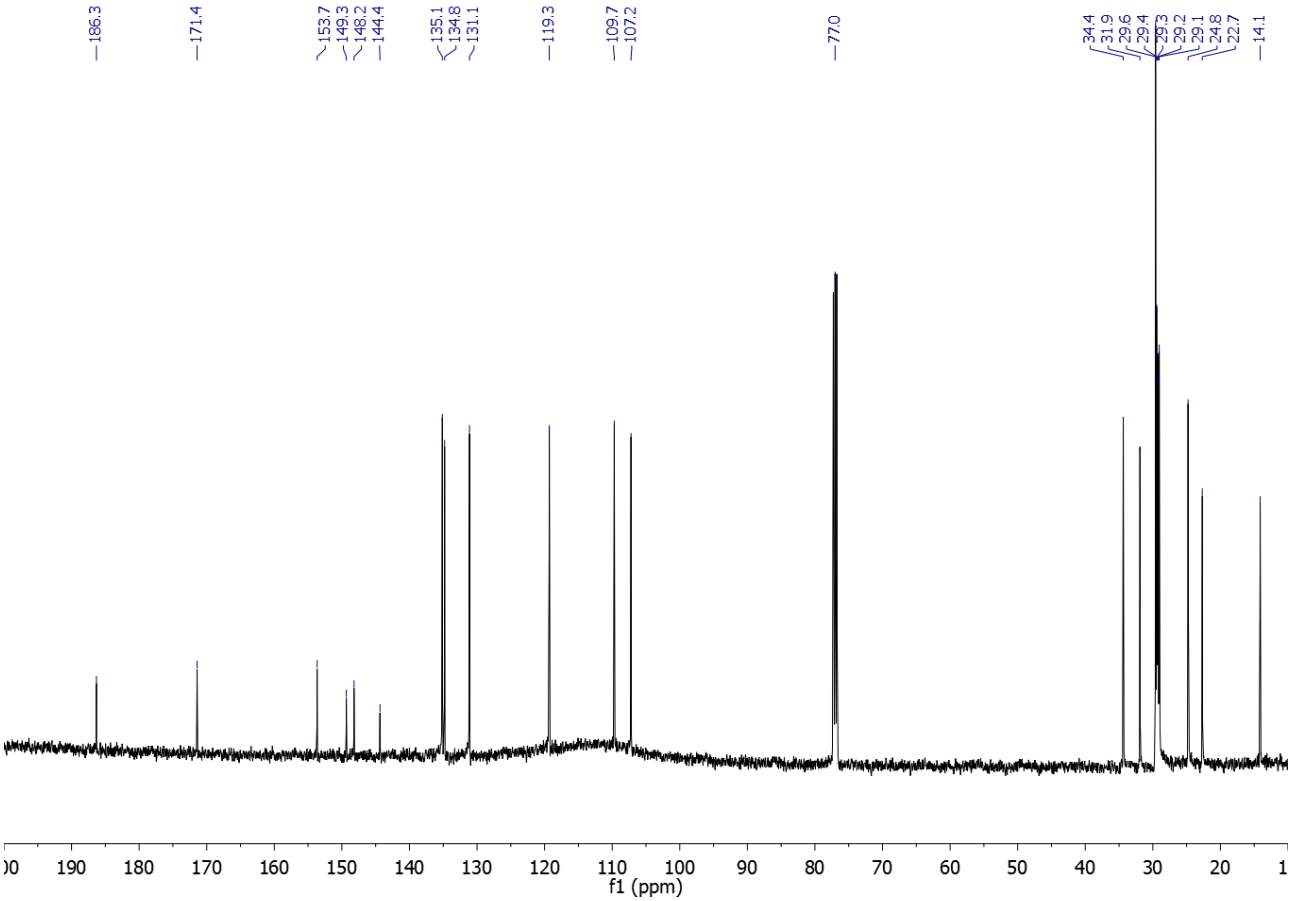
186.3
171.4
153.7
149.3
148.2
144.4
135.1
134.8
131.1
119.3
109.7
107.2
77.0
34.4
31.9
29.6
29.4
29.3
29.2
29.1
24.8
22.7
14.1
190
180
170
160
150
140
130
120
110
100
90
80
70
60
50
40
30
20
f1 (ppm)

^{1}H and ^{13}C NMR spectra of 7-hydroxyresorufinyl-icosanoate(**1e**)

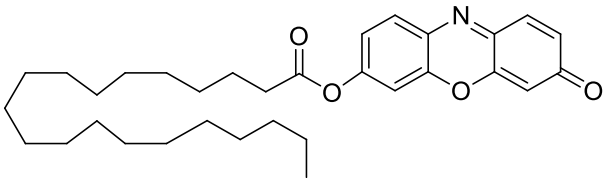

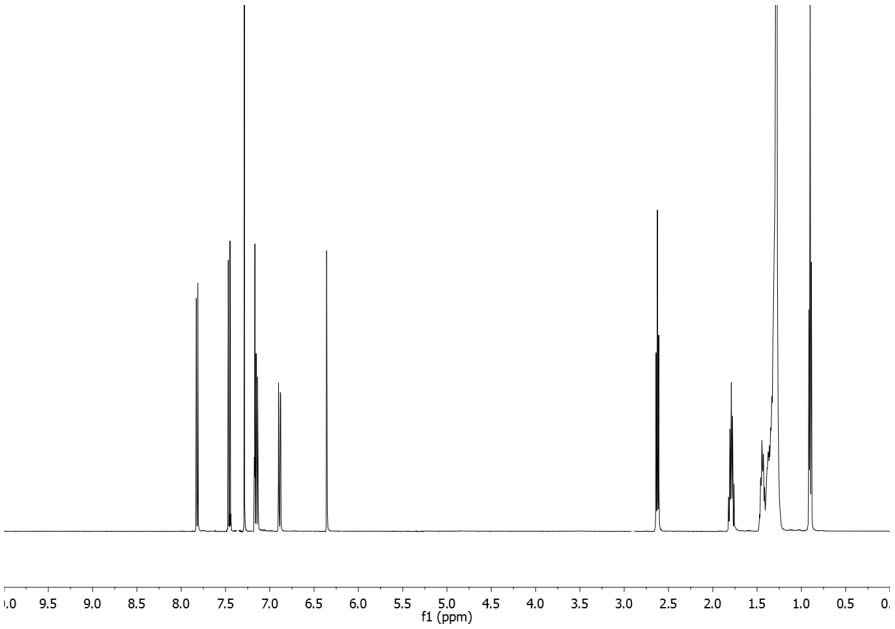

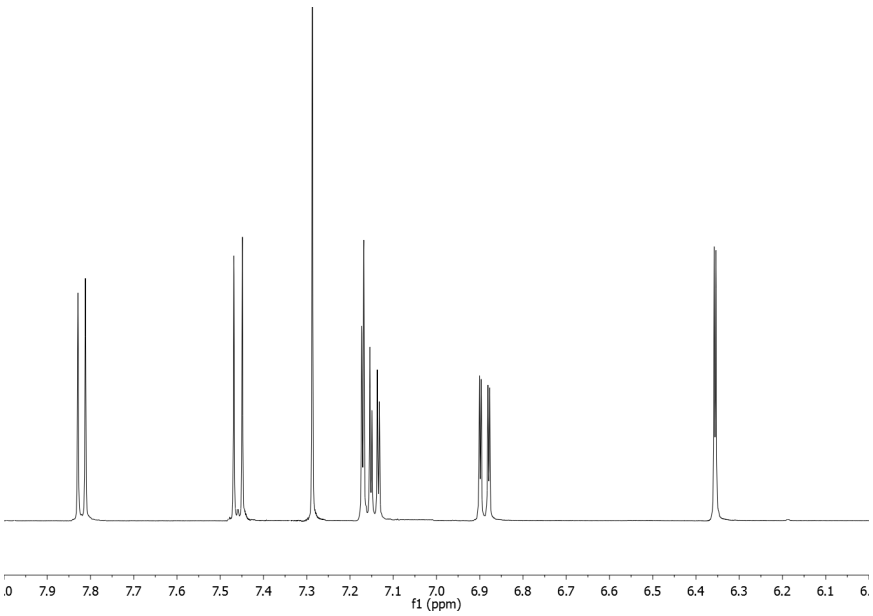

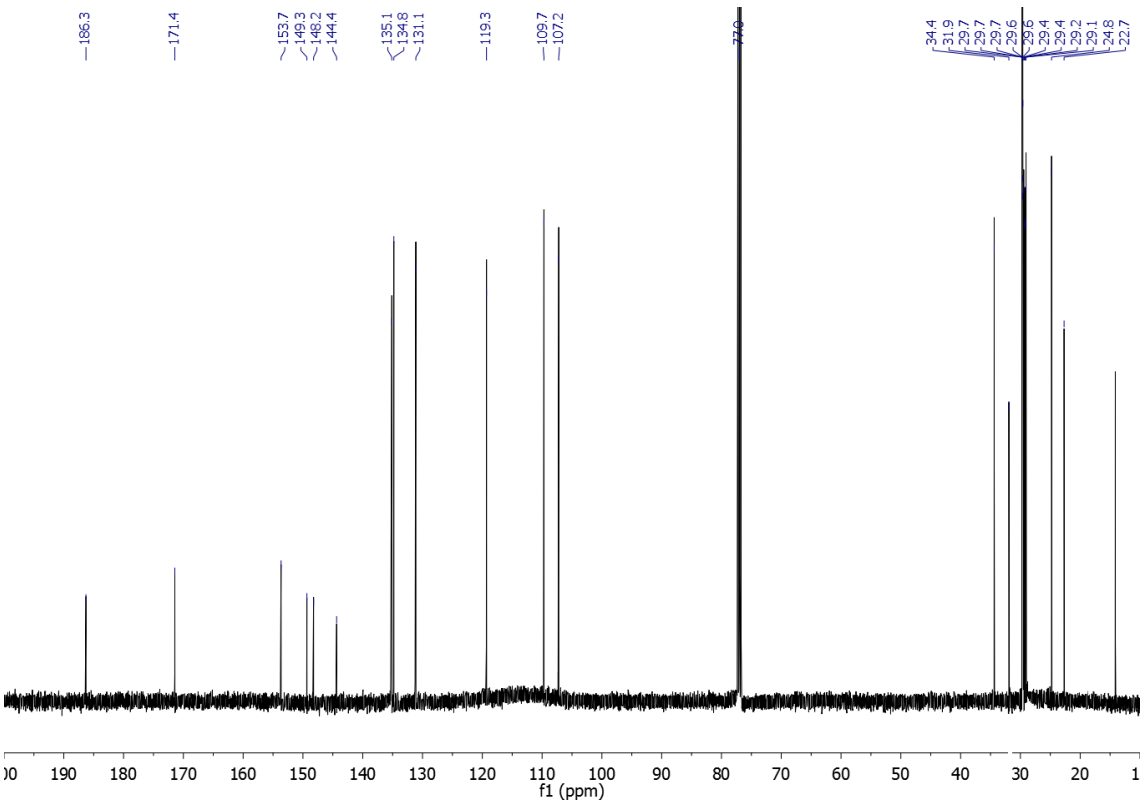
186.3
171.4
153.7
149.3
148.2
144.4
135.1
134.8
131.1
119.3
109.7
107.2
77.0
34.4
31.9
29.7
29.7
29.7
29.6
29.6
29.4
29.4
29.2
29.1
24.8
22.7
190
180
170
160
150
140
130
120
110
100
90
80
70
60
50
40
30
20
f1 (ppm)

^{1}H and ^{13}C NMR spectra of 7-hydroxyresorufinyl-oleate (**1f**)

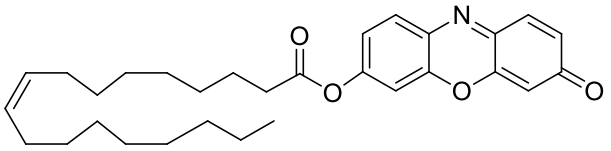

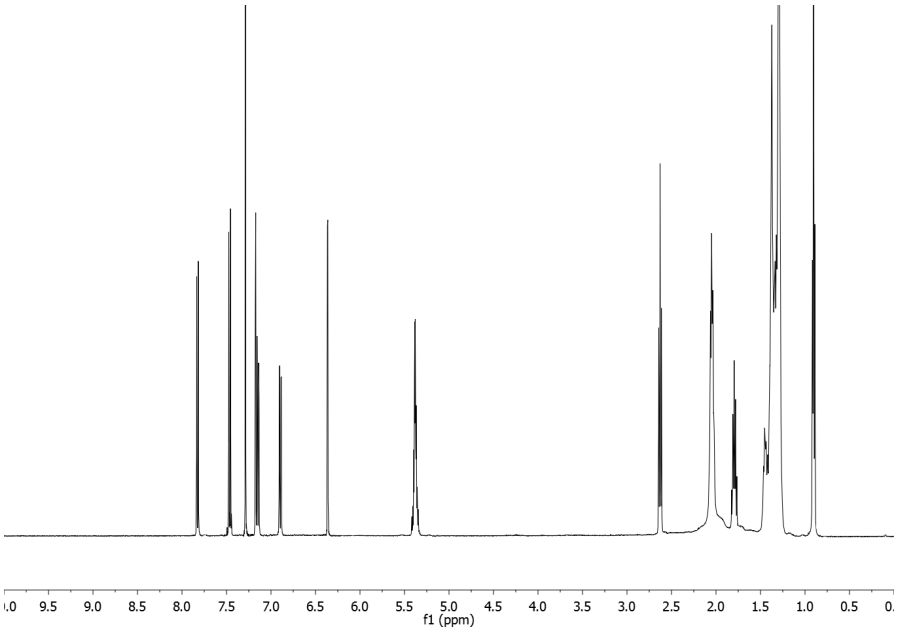

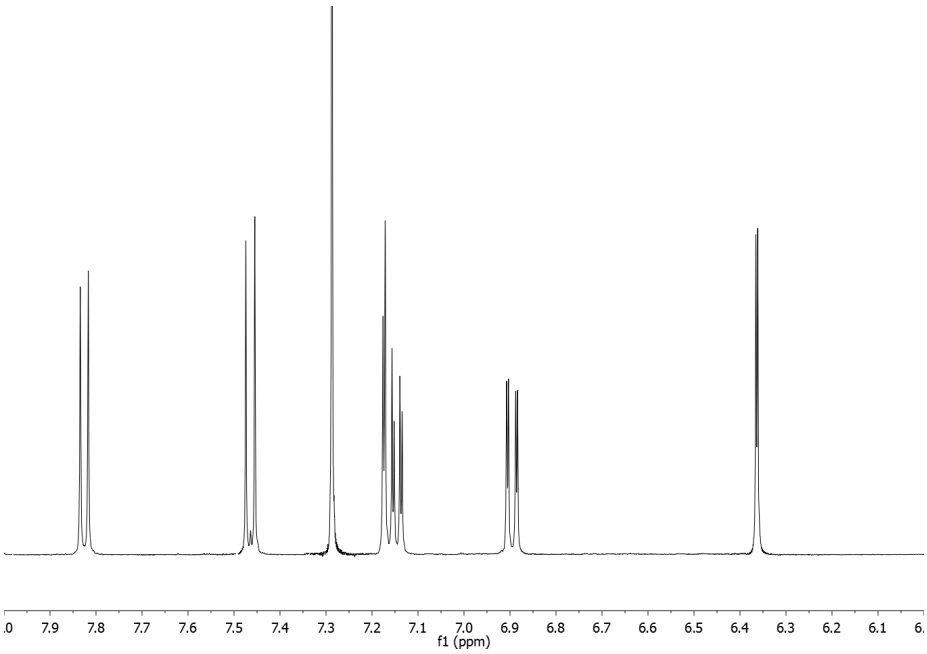

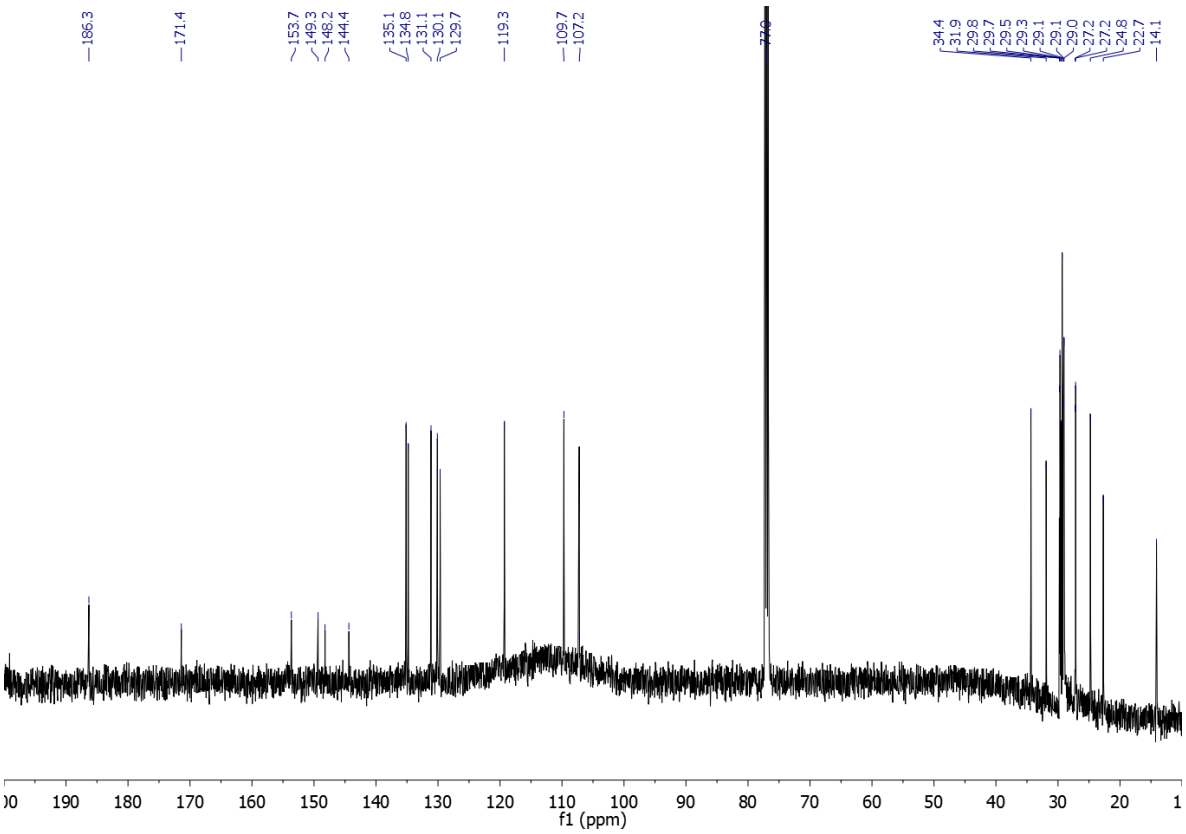
186.3
171.4
153.7
149.3
146.2
144.4
135.1
134.8
131.1
130.1
129.7
119.3
109.7
107.2
77.0
34.4
31.9
29.8
29.7
29.5
29.3
29.1
29.1
29.0
27.2
27.2
24.8
22.7
14.1
190
180
170
160
150
140
130
120
110
100
90
80
70
60
50
40
30
20
f1 (ppm)

^{1}H and ^{13}C NMR spectra of 7-hydroxyresorufinyl-2-methylhexanoate (**1h**)

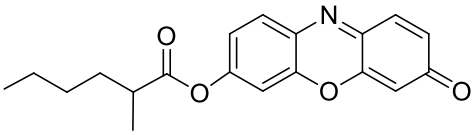

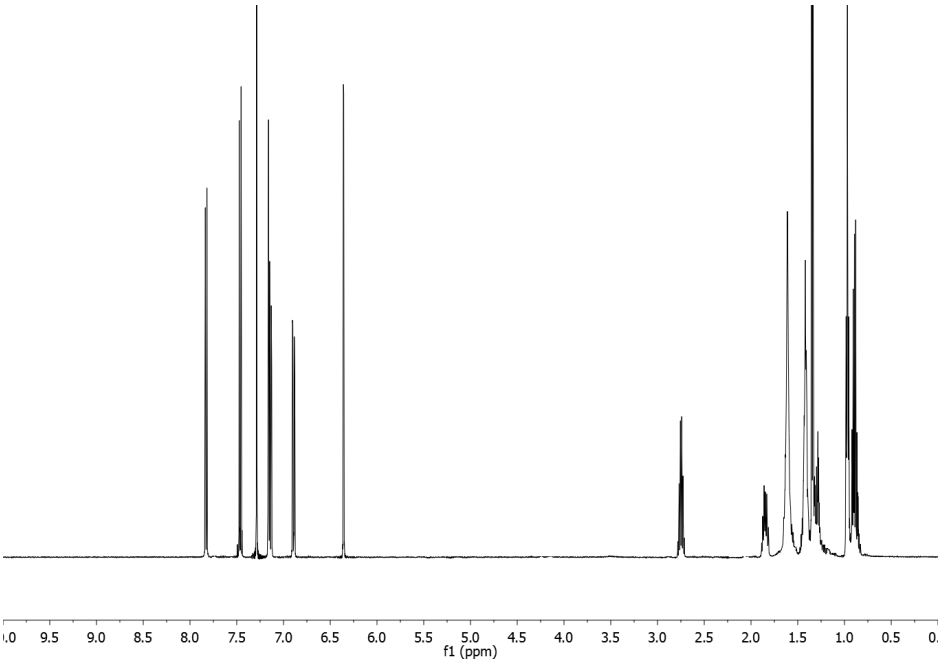

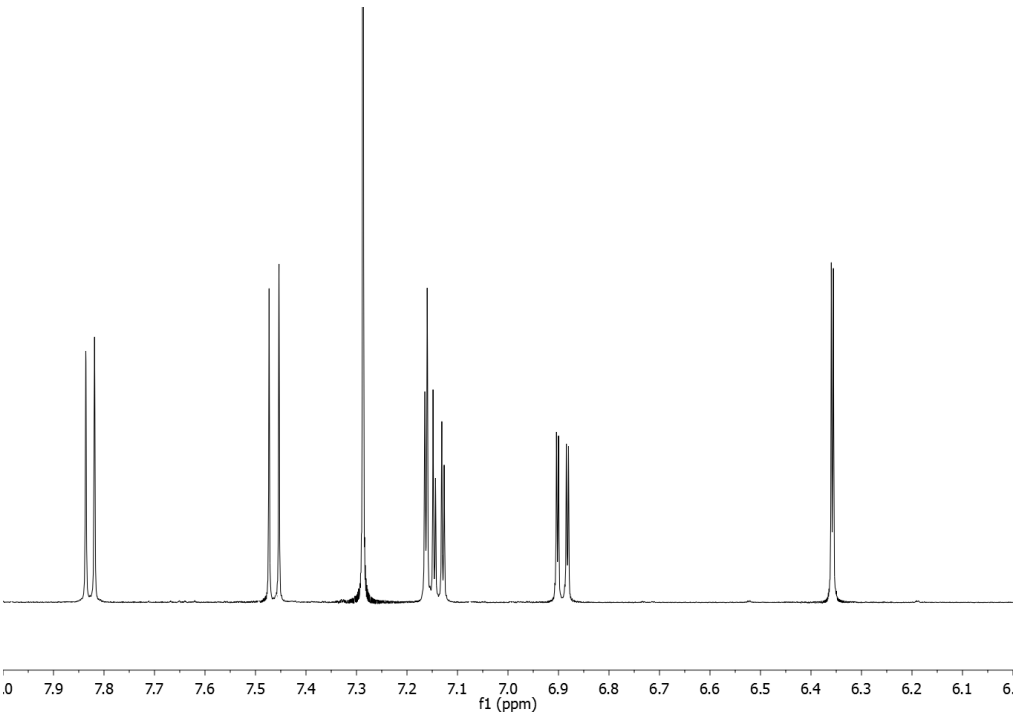

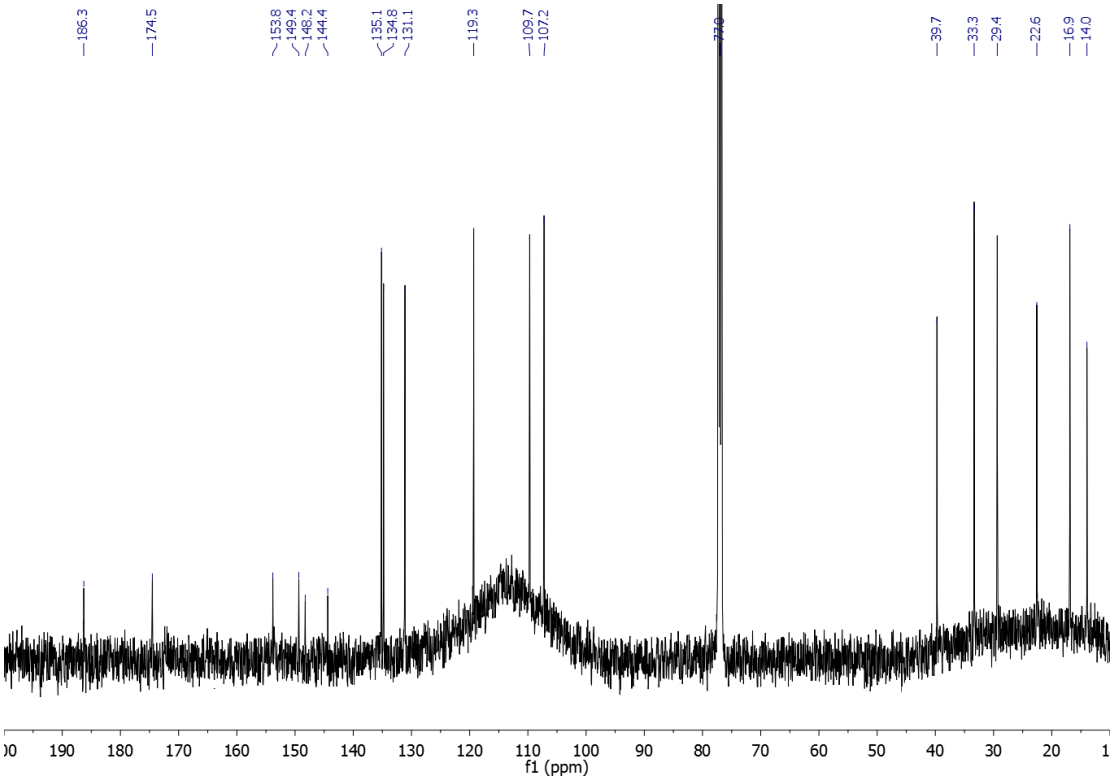
186.3
174.5
153.8
149.4
148.2
144.4
135.1
134.8
131.1
119.3
109.7
107.2
77.0
39.7
33.3
29.4
22.6
16.9
14.0
f1 (ppm)

^{1}H and ^{13}C NMR spectra of 7-hydroxyresorufinyl-2-ethylhexanoate (**1i**)

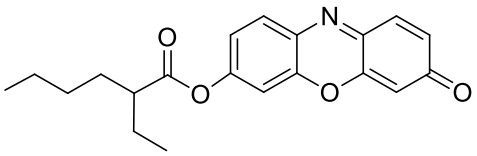

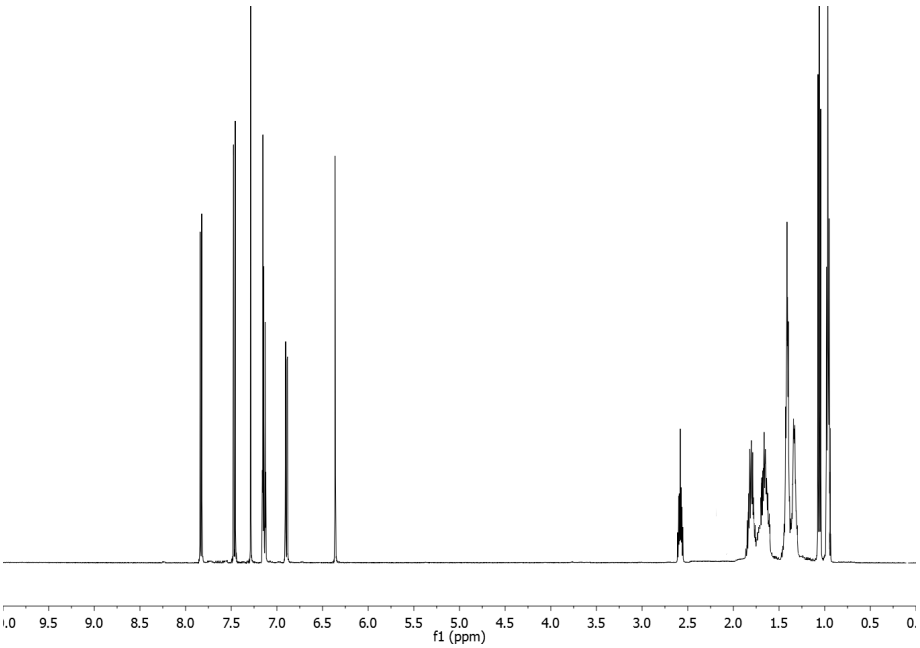

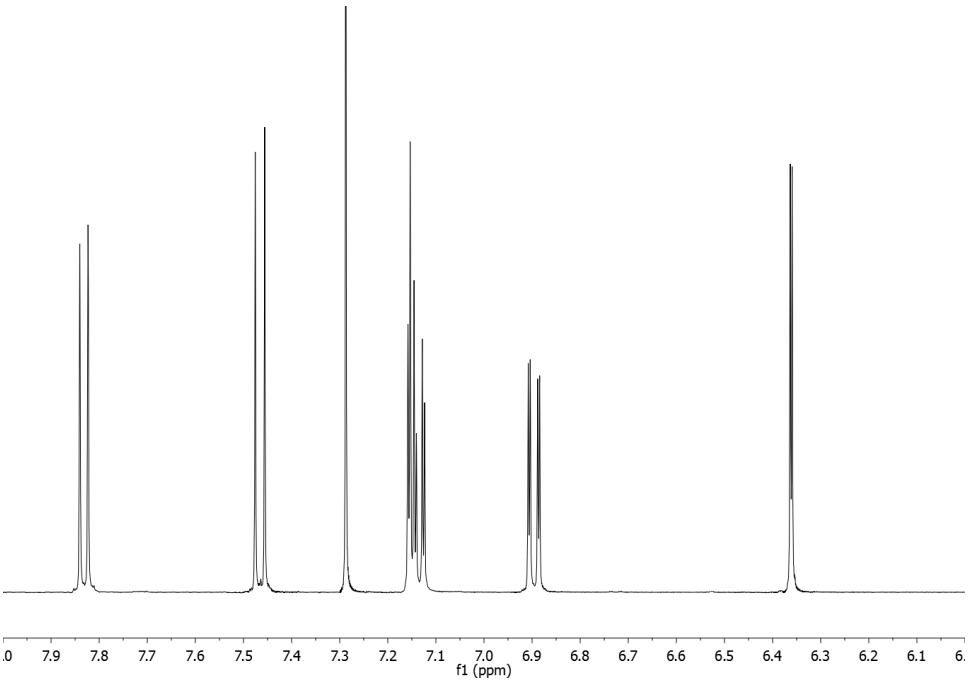

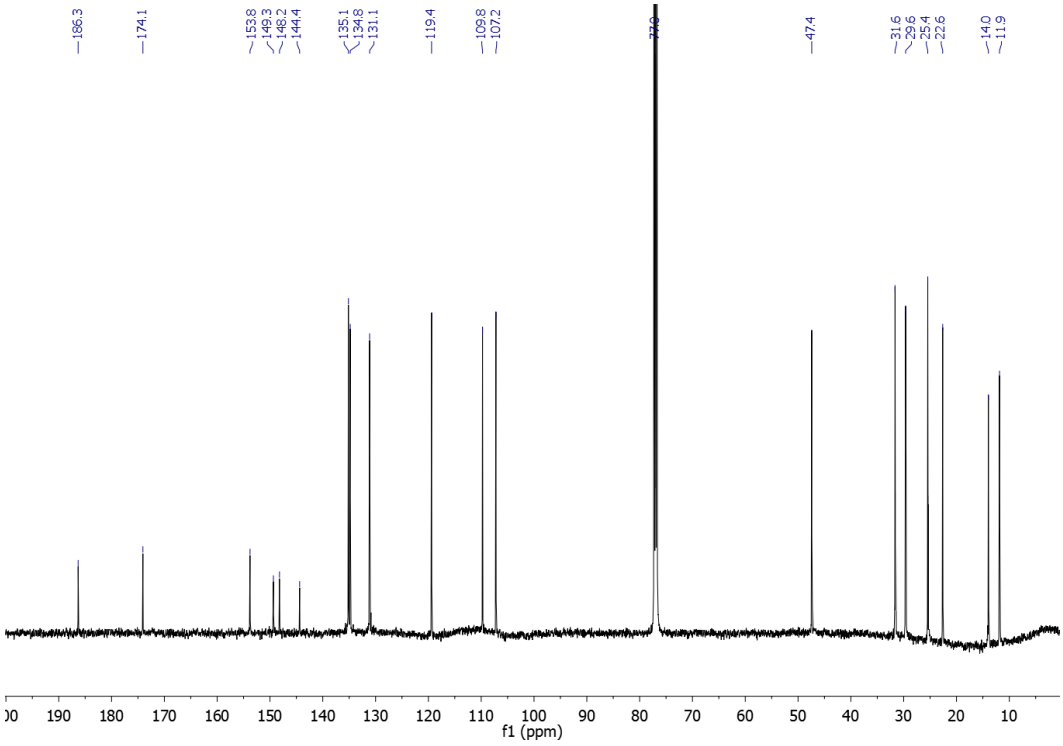
186.3
174.1
153.8
149.3
148.2
144.4
135.1
134.8
131.1
119.4
109.8
107.2
77.0
47.4
31.6
29.6
25.4
22.6
14.0
11.9
190
180
170
160
150
140
130
120
110
100
90
80
70
60
50
40
30
20
10
f1 (ppm)

^{1}H and ^{13}C NMR spectra of 7-hydroxyresorufinyl-2-butyloctanoate (**ij**)

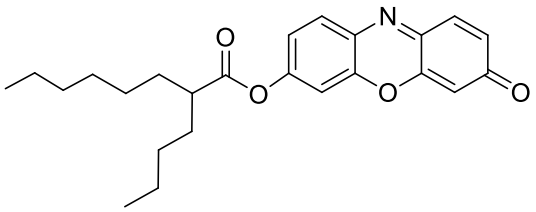

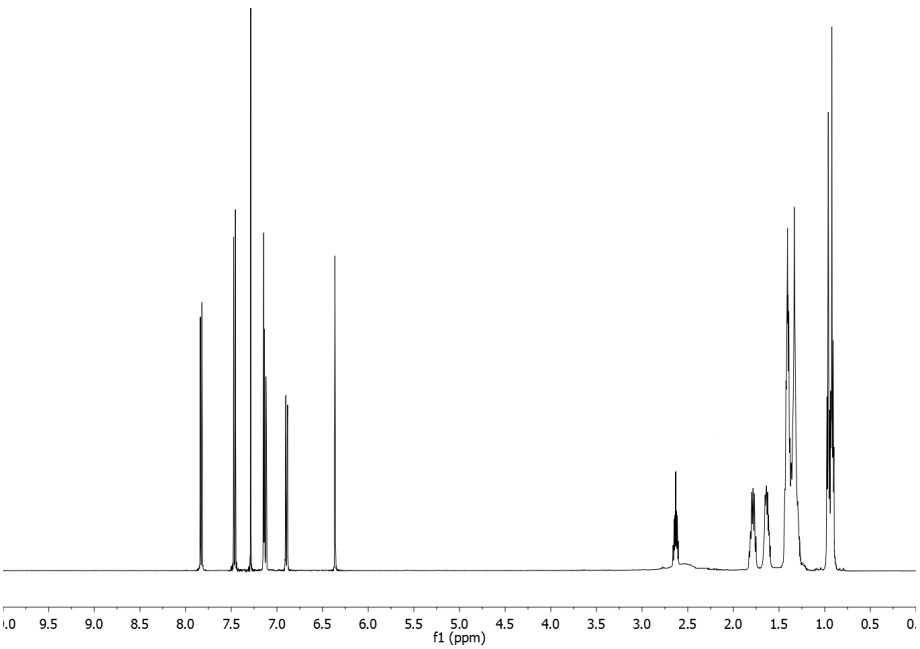

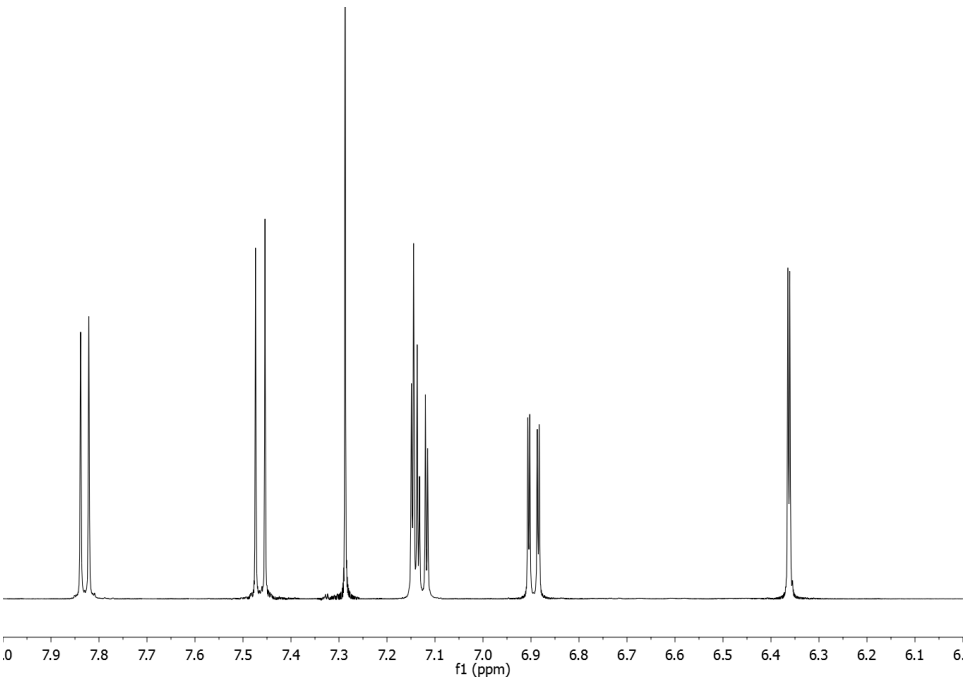

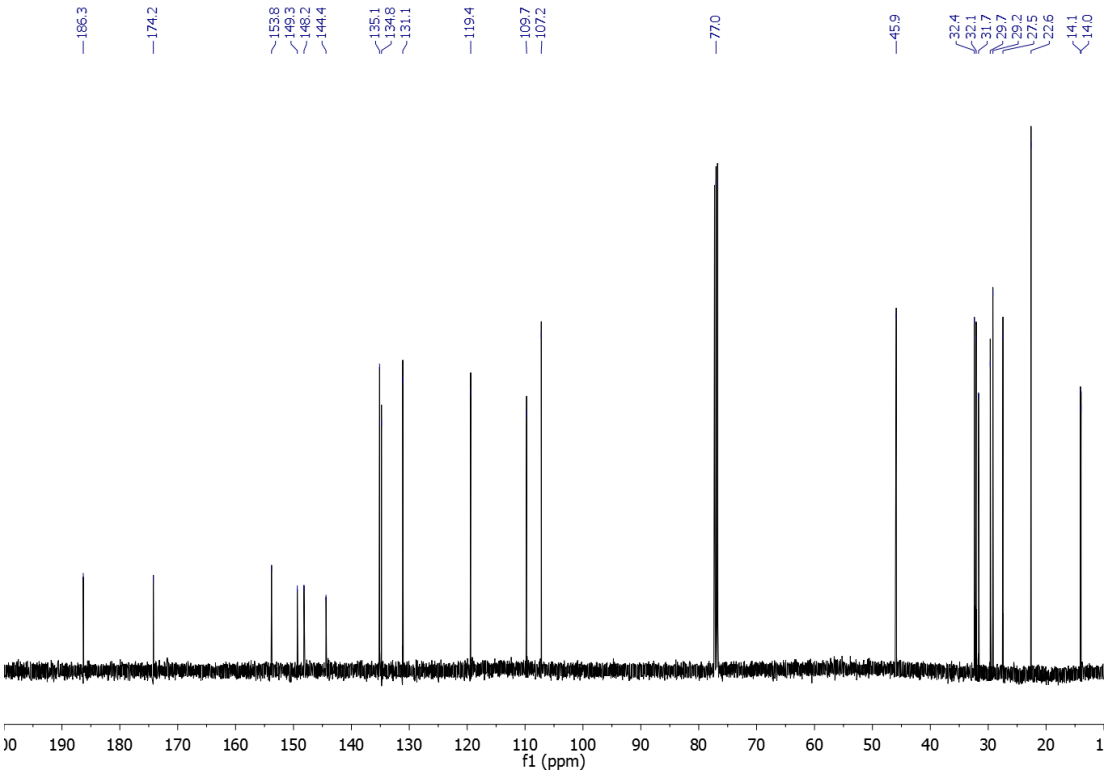
186.3
174.2
153.8
149.3
148.2
144.4
135.1
134.8
131.1
119.4
109.7
107.2
77.0
45.9
32.4
32.1
31.7
29.7
29.2
27.5
22.6
14.1
14.0
190
180
170
160
150
140
130
120
110
100
90
80
70
60
50
40
30
20
f1 (ppm)

H and ^{13}C NMR spectra of 7-hydroxyresorufinyl-2-benzoate (**1k**)

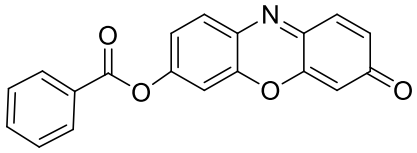

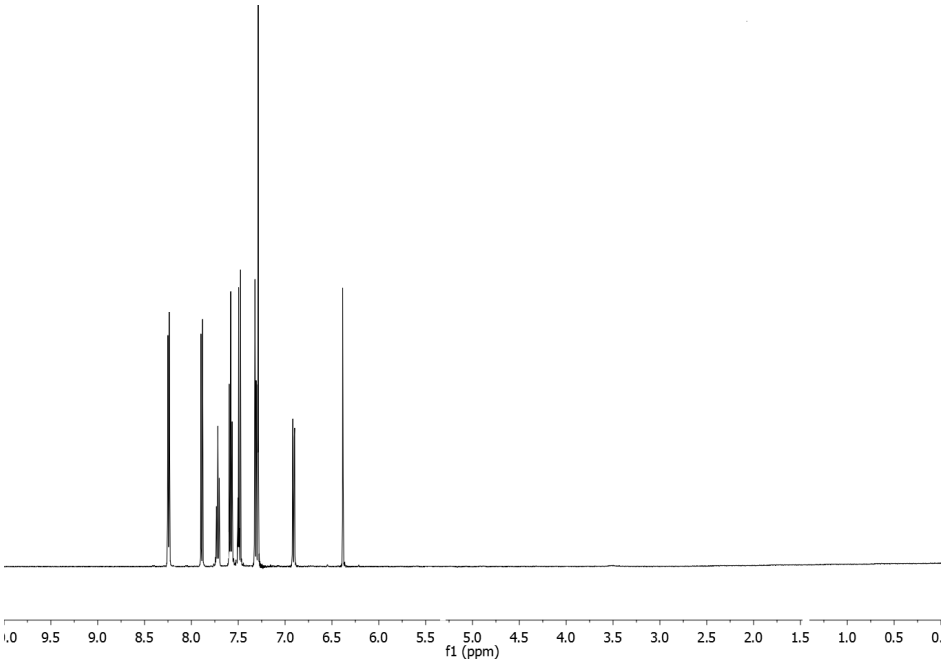

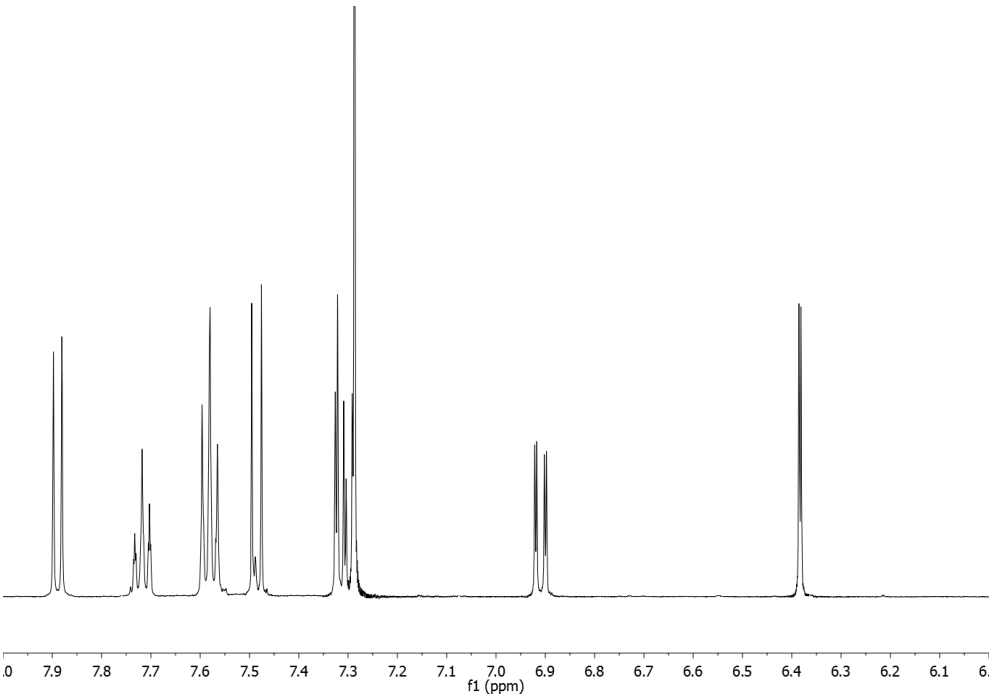

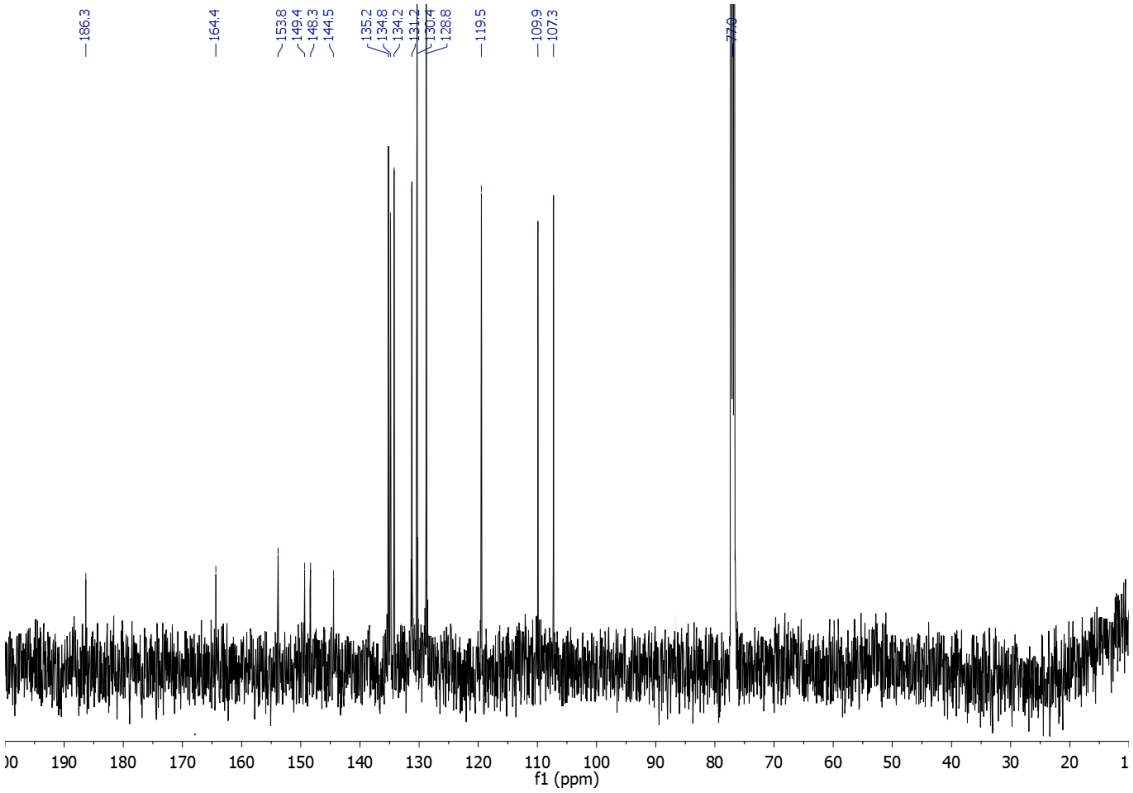
186.3
164.4
153.8
149.4
148.3
144.5
135.2
134.8
134.2
131.2
130.4
128.8
119.5
109.9
107.3
77.0
f1 (ppm)

^{1}H and ^{13}C NMR spectra of 7-hydroxyresorufinyl-arachidonate (7-HRA, **1g**)

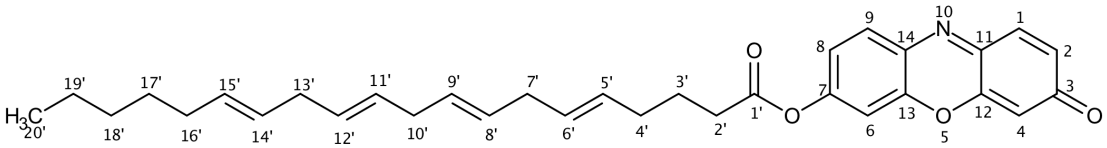

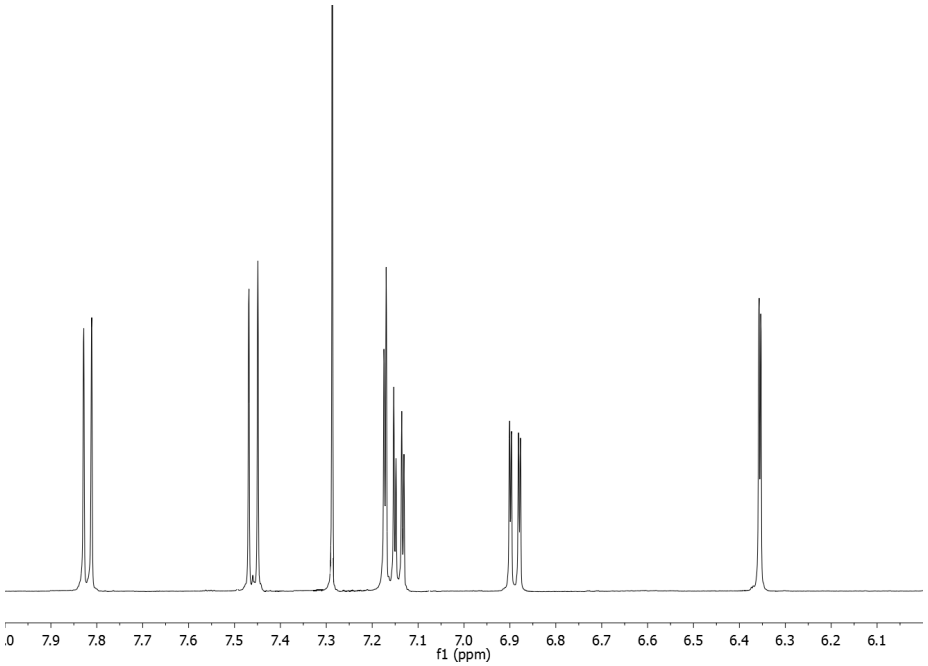

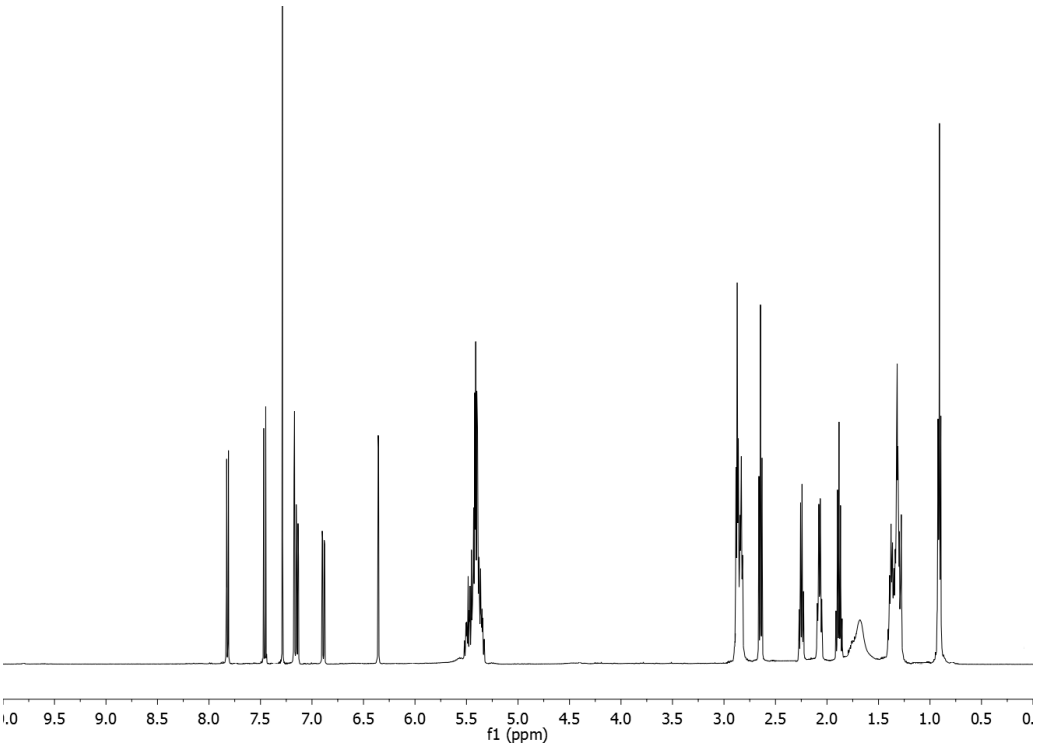

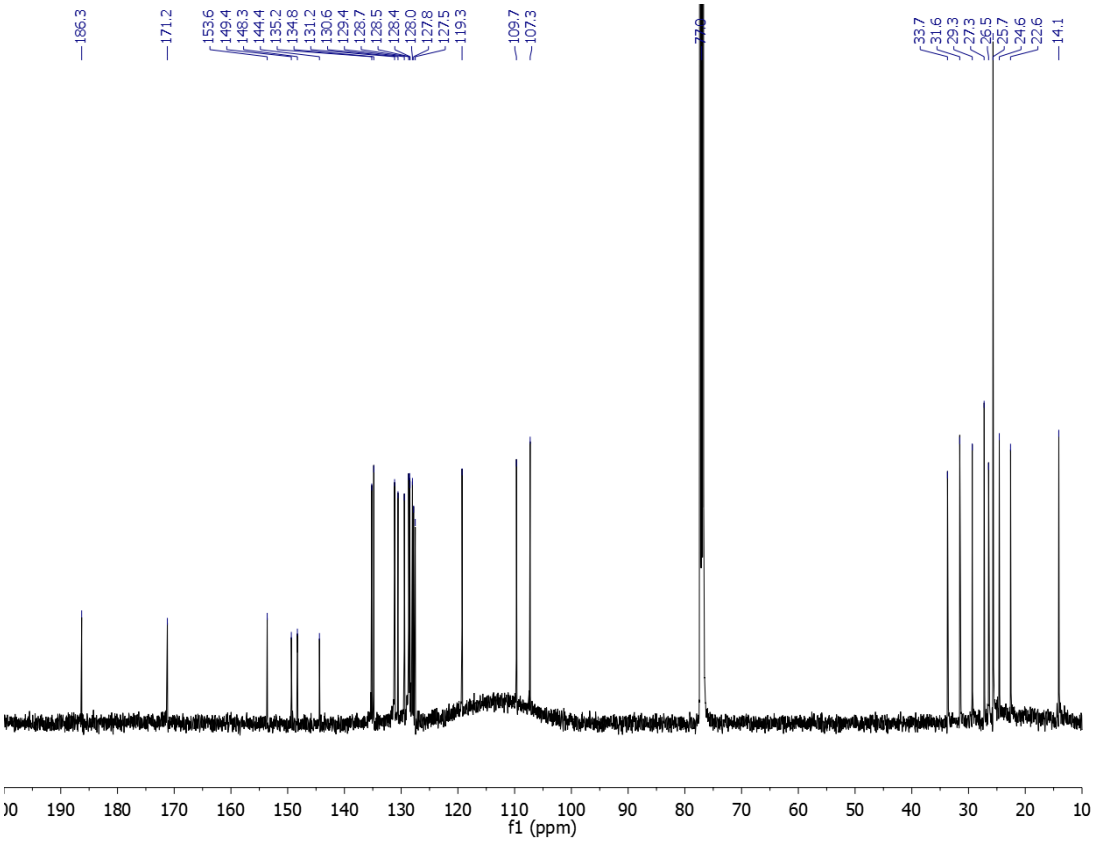
186.3
171.2
153.6
149.4
148.3
144.4
135.2
134.8
131.2
130.6
129.4
128.7
128.5
128.4
128.0
127.8
127.5
119.3
109.7
107.3
77.0
33.7
31.6
29.3
27.3
26.5
25.7
24.6
22.6
14.1
f1 (ppm)

^{1}H and COSY spectra of arachidonoyl luciferin (ArLuc)

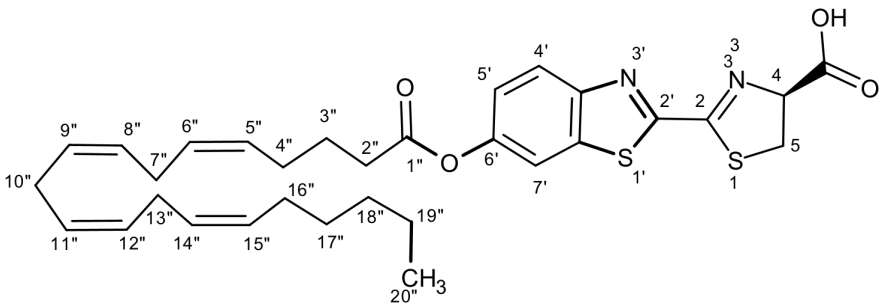

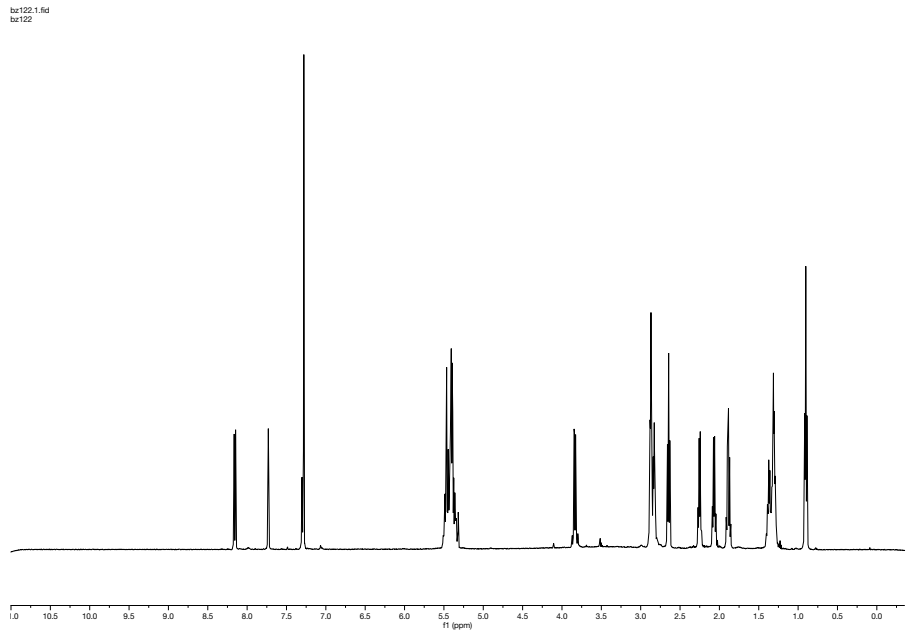

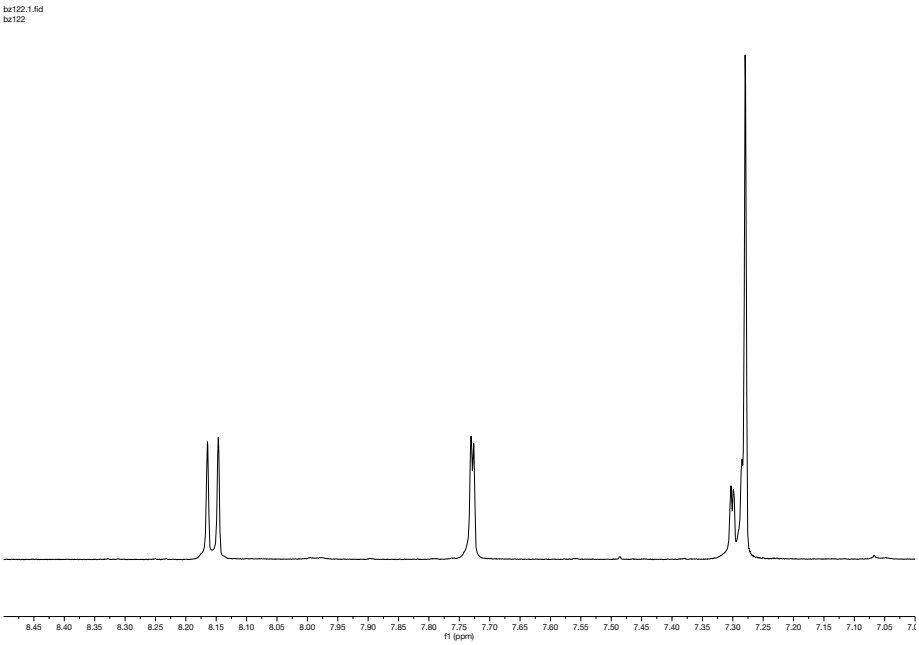

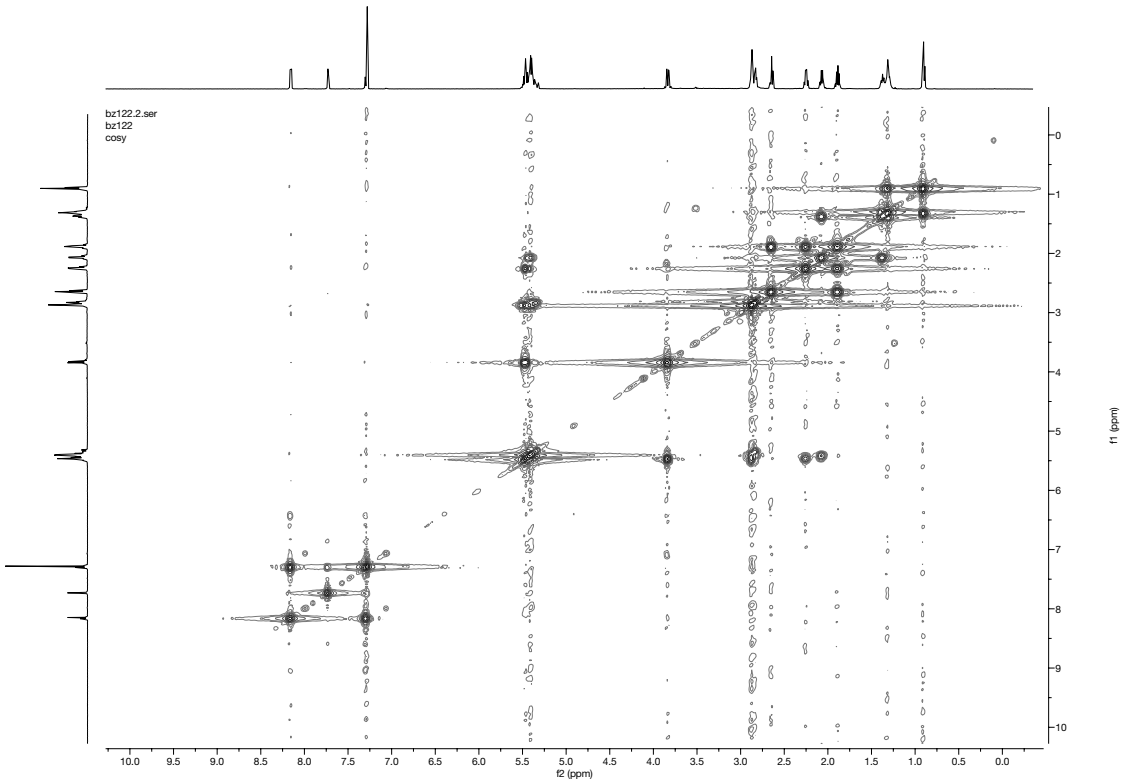
bz122.2.ser
bz122
cosy
f2 (ppm)
f1 (ppm)